Modeling *Ab Initio* Quantum Dynamics in Complex Systems through Multi-Scale Embedding

Andrew Wildman

A dissertation
submitted in partial fulfillment of the
requirements for the degree of

Doctor of Philosophy

University of Washington

2021

Reading Committee:

Xiaosong Li, Chair

David Masiello

Stefan Stoll

Program Authorized to Offer Degree:

Chemistry

University of Washington

Abstract

Modeling *Ab Initio* Quantum Dynamics in Complex Systems through Multi-Scale Embedding

Andrew Wildman

Chair of the Supervisory Committee:
Professor Xiaosong Li
Department of Chemistry

Quantum dynamics underpin almost all methods that chemists have to interrogate molecules – spectroscopy is inherently time-dependent, and reactions occur with nuclear motion. At the same time, the environment surrounding a molecule can have drastic impacts on its properties, and understanding these impacts is a central goal in almost all fields of chemistry, from biochemistry to materials science. More often than not, the actual system of interest is in contact with a system that is of less interest, whether that be a solvent, a protein backbone, or a substrate, and this interaction can drastically modify the observed molecular behavior. Treating the whole system as accurately as possible requires an excess of computational power, since the cost of accurate quantum chemical calculations scale quickly with system size. Classical embedding approaches can circumvent this high computational cost by describing the environment with an approximate, coarser model. The goal of this dissertation is to develop time-dependent quantum chemical methods that interface with classical embedding approaches in a dynamic way. The first chapter sets up the theoretical preliminaries of single Slater determinant wavefunctions and their corresponding Hamiltonians. The second chapter details the classical embedding theories and their time independent interfaces to the Hamiltonians from chapter one. The third chapter describes the development of a time-dependent mixed quantum mechanical and molecular mechanical method

and its application. The fourth chapter extends this development to include nonequilibrium propagation of degrees of freedom in the molecular mechanics environment. The fifth chapter discusses the development of a quantum nuclear dynamics method using the nuclear electronic orbital approach and the same real-time formalism as presented in chapter 1. The sixth chapter embeds this real-time nuclear electronic orbital approach inside a classical polarizable continuum model and investigates the change on the predicted time independent and time dependent properties.

TABLE OF CONTENTS

LIST OF FIGURES

GLOSSARY

DFT: Density Functional Theory

HF: Hartree-Fock

LR: Linear Response

MM: Molecular Mechanics

MMPOL: Polarizable Molecular Mechanics with an induced dipole formalism

ω-MMPOL: Frequency dependent variant of polarizable molecular mechanics with an induced dipole formalism

NEO: Nuclear Electronic Orbital

PCM: Polarizable Continuum Model

RT: Real-Time

SCF: Self-Consistent Field

TDSE: Time-dependent Schrödinger Equation

ACKNOWLEDGMENTS

Graduate study is as much of a personal struggle as it is a scientific one. I am blessed to have been supported both academically and personally by so many wonderful people over the course of my study, and I would like to thank them all.

First and foremost, I would like to thank my advisor, Prof. Xiaosong Li. Your creativity and enthusiasm for science inspire me day after day. You tolerated my many explorations of topics far away from what I was supposed to be researching at the time, and I greatly appreciate it. Perhaps more than anything, I thank you for your consideration for and understanding of issues that happen outside of my graduate studies. I honestly don't know what graduate school would have been like if I did not have you as an advisor, but I don't think it could have been better. Thank you.

I would also like to thank all the fantastic scientists that I have worked along with in the Li group. I am deeply grateful to those postdocs that I have worked with closely – Thank you to Greta Donati who helped me immensely with getting my feet on the ground with research, and thank you Luning Zhao for challenging and helping me right until the end. I am thankful for the mentorship and support I received from the older graduate students when I first started out: thank you to Patrick Lestrange, David Lingerfelt, Josh Goings, and David Williams-Young. I also had the wonderful opportunity to learn from and be challenged by those students and postdocs that joined the group right before and right after me; thank you to Joe Kasper, Lauren Koulias, Hang Hu, Chad Hoyer, Andrew Valentine, Tianyuan Zhang, and surely others that I have left out. Finally, I am so lucky to have joined the group with two of the most talented and supportive people I know: thank you to Torin Stetina and Ryan Beck. The last few years have been tough, but you have made it so enjoyable both

through helping me grow as a scientist and through our camaraderie and “2021 vision.”

Thank you to all those at UW that have supported me outside of my research group. Thank you in particular to the fellow officers of the UW RCC, and especially Sarah Alamdari and Luke Gibson. Thank you to Nam Pho and Prof. Jim Pfaendtner as well. I have been fortunate to work with many researchers outside of UW as well, and I have learned so much from all of them. Thank you to Prof. Benedetta Mennucci, Prof. Aurora Clark, Carolyn Pierce, Kevin Rosso, and Ernesto Martinez-Baez.

Thank you to my friends Chris, Elliot, Mateo, Greg, Kevin, and the many others I have not listed here. All of your friendship and fun have helped me to relax and turn off “grad school brain” when I needed to most.

Thank you to my family for your endless support, and my parents Karen and Pete in particular. I would never have made it without your encouragement and advice. Thank you to Rachel for being a fantastic co-parent and helping me raise Michael even through the trials of graduate school. Finally, thank you to Michael. You don’t know it, but your curiosity and energy feed my own. You bring me back to what is important when I get too caught up when times get tough.

DEDICATION

To Michael and my parents

PREFACE

Advancement of scientific knowledge and methods comes from a collaboration of many scientists, and the developments presented in this work is no exception. To clarify my contributions to each project, I will describe the focus of each chapter and my contributions to each work.

Chapter 1 presents some preliminary quantum mechanical theoretical frameworks that are the foundations for the developments presented in later chapters. In particular, the basics of Hartree-Fock and Kohn-Sham theory are presented, and the direct propagation of these theories in time is discussed.

Chapter 2 presents the basics of quantum/classical multiscale embedding theories. Understanding both these theories and the previous chapter will provide a solid foundation for the developments presented in the next few chapters.

Chapter 3 describes the development of a time-dependent propagation technique that couples real-time time dependent Hartree-Fock and density functional theory with a polarizable molecular mechanics method. Both Dr. Greta Donati and I implemented the interface between the polarizable molecular mechanics model and the real-time propagation of a quantum system, and ran the case studies. Dr. Stefano Capresecca, Prof. Filippo Lipparini, and Prof. Benedetta Mennucci provided the code for the internal energy terms for the polarizable molecular mechanics model. All collaborators were essential to developing the theory used in this work.

Chapter 4 extends the previously developed model into a non-equilibrium description of the environment polarization. Prof. Xiaosong Li provided the motivation for the project and the general form of the model. I provided the conception and implementation of the

specific theoretical model, and I gathered the data for the case studies. The code framework developed by the collaborators during the work in the previous chapter was essential to this extension.

Chapter 5 develops a real-time time dependent form for the nuclear electronic orbital approach. All collaborators developed the theoretical model, and Dr. Luning Zhao and I implemented the model in the ChronusQuantum electronic structure package. Dr. Luning Zhao collected the data for the case studies, and I implemented a visualization technique for the model.

Chapter 6 embeds the previously developed real-time time-dependent nuclear orbital approach into a polarizable continuum model. I developed the theory, implemented the interface, and collected the data for this chapter. The framework developed by the previous chapter was essential to this extension as well.

Chapter 1
THEORETICAL BACKGROUND

In the first two chapters, I will review the relevant theory used in subsequent chapters to develop dynamical embedded systems. The focus of this chapter is to present the background of time-dependent Hartree-Fock (HF) and Kohn-Sham density functional theory (KS-DFT).

1.1 Hatree-Fock and Kohn-Sham Theory

The central equation that governs all of quantum mechanics (assuming a pure state in a closed system) is the Time Dependent Schrödinger Equation (TDSE).

$$i\frac{\partial}{\partial t}\left|\Psi(t)\right\rangle = \hat{\mathcal{H}}(t)\left|\Psi(t)\right\rangle \tag{1.1}$$

Here, $|\Psi(t)\rangle$ is the wavefunction of the total quantum system whose dynamics are generated by the Hamiltonian operator, $\hat{\mathcal{H}}(t)$. In this work, atomic units (in which the reduced Planck constant, elementary charge, Bohr radius, and rest mass of the electron are unity) are used unless specifically noted otherwise. The goal of quantum chemical theories is to solve the TDSE (or the Time Independent Schrödinger Equation – TISE) for $|\Psi\rangle$ when given a form for $\hat{\mathcal{H}}$. Before developing some solutions to the TDSE, let us address the typical approaches for solving the TISE. For an isolated molecular system in the non-relativistic limit, the Hamiltonian has the following form:

$$\begin{aligned}\hat{\mathcal{H}} = &-\sum_A \frac{1}{2M_A}\nabla^2_{\boldsymbol{R}_A} - \sum_i \frac{1}{2}\nabla^2_{\boldsymbol{r}_i} \\ &+ \frac{1}{2}\sum_A\sum_{B\neq A}\frac{Z_A Z_B}{|\boldsymbol{R}_A - \boldsymbol{R}_B|} - \sum_A\sum_i \frac{Z_A}{|\boldsymbol{R}_A - \boldsymbol{r}_i|} + \frac{1}{2}\sum_i\sum_{j\neq i}\frac{1}{|\boldsymbol{r}_i - \boldsymbol{r}_j|}\end{aligned} \tag{1.2}$$

where the indices A, B run over nuclei, and the indices i, j run over electrons; $\boldsymbol{R}_A$, M_A, Z_A are the coordinate, mass, and charge of nucleus A, and $\boldsymbol{r}_i$ is the coordinate of electron i.

Typically, systems of interest to chemists consist of many quantum particles – the electrons are of particular interest when investigating properties of molecules, and the quantum nature of nuclei can be significant during dynamical processes. For this section, we will focus on the electronic problem only, treating the Hamiltonian with the Born-Oppenheimer approximation, though later we will discuss a model that treats nuclei quantum mechanically as well. Due to the many-body nature of the systems of interest, the Hamiltonian operator generates a Hilbert space spanned by many-body basis states, and the ultimate solution of the TDSE can be expressed as a linear combination of these many-body states. This gives rise to the many families of correlated methods in quantum chemistry, (configuration interaction, coupled cluster, density matrix renormalization group, *etc.*) but as these theories are not used for the development in later chapters, we will not discuss them further here.

Instead, it can be convenient to consider an approximate Hamiltonian operator that only considers the interaction between a particle and the average field created by the other particles. This Hamiltonian generates a space spanned by orthogonal single-particle states, $|\phi\rangle$, referred to as orbitals. The total molecular wavefunction corresponding to this non-interacting Hamiltonian would then be a simple product of these orbitals, but in order to satisfy the antisymmetry that wavefunctions must exhibit upon permutation of fermions, the product must be antisymmetrized. The antisymmetrized product of orbitals is referred to as a Slater determinant.

The mean field Hamiltonian referred to above is the Hamiltonian that governs the Hartree-Fock procedure. The Hatree-Fock procedure obtains the best possible approximation to the many-body wavefunction $|\Psi\rangle$ given by a single Slater determinant. This procedure can be derived by minimizing the energy subject to the constraint that orbitals remain orthogonal, but as that has been derived elsewhere[2], we will only present the results here.

The Fock operator $\hat{f}$ gives an eigenvalue equation for a single orbital

$$\hat{f}\,|\phi_i\rangle = \epsilon_i\,|\phi_i\rangle \tag{1.3}$$

where the eigenvalue ϵ_i is called the orbital energy. The Fock operator is given by

$$\hat{f} = \hat{h} + \hat{J} + \hat{K} \tag{1.4}$$

where $\hat{h}$ collects the kinetic energy and nuclear attraction terms, and $\hat{J}$, $\hat{K}$ are given by their action on an orbital.

$$\hat{J}\phi_i(\boldsymbol{r}_1) = \sum_j \left[\int \frac{\phi_j^*(\boldsymbol{r}_2)\phi_j(\boldsymbol{r}_2)}{|\boldsymbol{r}_1 - \boldsymbol{r}_2|} d\boldsymbol{r}_2\right] \phi_i(\boldsymbol{r}_1) \tag{1.5}$$

$$\hat{K}\phi_i(\boldsymbol{r}_1) = \sum_j \left[\int \frac{\phi_j^*(\boldsymbol{r}_2)\phi_i(\boldsymbol{r}_2)}{|\boldsymbol{r}_1 - \boldsymbol{r}_2|} d\boldsymbol{r}_2 \phi_j(\boldsymbol{r}_1)\right] \tag{1.6}$$

Since the Fock operator is dependent on all orbitals in the system, the Fock operator must be applied for each orbital considered.

Practically, the theory above must be put into a finite basis suitable for computation. Typically in molecular calculations, this is a basis of contracted Gaussian functions that resemble atomic orbitals, although for this section the specific choice of basis is not important. That said, we will refer to this as the "atomic orbital" (AO) basis with the understanding that other bases may be used without loss of generality. With a given basis, one can expand the orbitals in said AO basis.

$$\phi_i(\boldsymbol{r}) = \sum_\mu c_{i,\mu}\chi_\mu(\boldsymbol{r}) \tag{1.7}$$

where χ_μ is the basis function μ and $c_{i,\mu}$ is the contraction coefficient for orbital i and basis function μ. The benefit of this expansion is that the integrals required for the computation of the Fock operator can be computed analytically in the given basis. This gives rise to a finite basis Fock matrix, expressed in the AO basis

$$\mathbf{F} = \mathbf{T} + \mathbf{V} + \mathbf{J} + \frac{1}{2}\mathbf{K} \tag{1.8}$$

where the integral matrices ($\mathbf{T}$,$\mathbf{V}$,$\mathbf{J}$,$\mathbf{K}$) have elements of

$$T_{\mu\nu} = \frac{-1}{2}\int \chi_\mu^*(\boldsymbol{r})\nabla^2\chi_\nu(\boldsymbol{r})d\boldsymbol{r} \tag{1.9}$$

$$V_{\mu\nu} = -\sum_A \int \chi_\mu^*(\boldsymbol{r})\frac{Z_A}{|\boldsymbol{r}-\boldsymbol{R}_A|}\chi_\nu(\boldsymbol{r})d\boldsymbol{r} \tag{1.10}$$

$$J_{\mu\nu} = \sum_{\lambda\kappa}\int\int \frac{\chi_\mu^*(\boldsymbol{r}_1)\chi_\nu(\boldsymbol{r}_1)\chi_\lambda^*(\boldsymbol{r}_2)\chi_\kappa(\boldsymbol{r}_2)}{|\boldsymbol{r}_1-\boldsymbol{r}_2|}d\boldsymbol{r}_2 d\boldsymbol{r}_1 P_{\lambda\kappa} \tag{1.11}$$

$$K_{\mu\nu} = \sum_{\lambda\kappa}\int\int \frac{\chi_\mu^*(\boldsymbol{r}_1)\chi_\kappa(\boldsymbol{r}_1)\chi_\lambda^*(\boldsymbol{r}_2)\chi_\nu(\boldsymbol{r}_2)}{|\boldsymbol{r}_1-\boldsymbol{r}_2|}d\boldsymbol{r}_2 d\boldsymbol{r}_1 P_{\lambda\kappa} \tag{1.12}$$

where we have introduced the one particle reduced density matrix in the original basis, given by

$$P_{\mu\nu} = \sum_i^N c_{i,\mu}c_{i,\nu}^* \tag{1.13}$$

and the summation only runs over the number of occupied orbitals. As a shorthand, we will express integrals over the AO basis functions as brakets over the AO indices. (*e.g.* $T_{\mu\nu} = \langle\mu|\nabla^2|\nu\rangle$)

Ultimately this recasts the Fock operator eigenvalue equations into a generalized Fock matrix eigenvalue equation

$$\mathbf{FC} = \mathbf{SC}\boldsymbol{\epsilon} \tag{1.14}$$

Where $\boldsymbol{C}$ is the matrix that collects the AO basis to orbital contraction coefficients and $\boldsymbol{S}$ is the overlap integral matrix between the AO basis functions.

Due to the mean-field nature of the Fock operator, no electron-electron correlation is captured through Hartree-Fock theory. The correlation methods mentioned above can use the Hartree-Fock state as a reference to generate the many-body states required to perform fully correlated calculations, capturing the electron correlation neglected through HF. Another approach that is often used to approximately capture electron correlation is the Kohn-Sham variant of density functional theory (KS-DFT, referred to in this work simply as DFT). In brief, KS-DFT uses orbitals as intermediate objects to evaluate the one-body and coulomb contributions to the Hamiltonian, but uses a functional of the density to capture electron

correlation and occasionally electron exchange. Because KS-DFT and HF share many of the same objects due to the use of orbitals, we can write a generalized matrix eigenvalue equation for KS-DFT that is nearly identical to eq. (1.15).

$$\mathbf{F}^{KS}\mathbf{C} = \mathbf{SC}\boldsymbol{\epsilon} \tag{1.15}$$

where $\mathbf{F}^{KS}$ is the Kohn-Sham matrix, given by

$$\mathbf{F}^{KS} = \mathbf{T} + \mathbf{V} + \mathbf{J} + \mathbf{V}_{xc}[\boldsymbol{P}] \tag{1.16}$$

$\mathbf{V}_{xc}$ is the exchange-correlation potential in KS-DFT. It is important to note that both HF and KS-DFT are theories that use a single Slater determinant as their wavefunction ansatz, so development of new approaches on top of these methods can often be general across both HF and DFT.

1.2 Real-Time Dynamics

With the theory developed for the TISE, we now move towards the solution of the TDSE. In general, the TDSE can be solved either in the time domain or the frequency domain. Methods that solve the TDSE in the frequency domain rely on analysis of residues coming from infinitesimal perturbations. Because these methods look at the *response* of the wavefunction to infinitesimal perturbations, they are referred to as response theory. In contrast, methods that solve the TDSE in the time domain are referred to as real-time or propagated methods. Solving the TDSE in the time domain circumvents the truncation of response theory, allowing for descriptions of non-linear events or coupling to strong fields, and is the starting point for many non-adiabatic electron-nuclear dynamics.

Because the development in the later parts of this work uses the real-time formalism of HF and DFT, we will present it briefly here. If a single Slater determinant is used to describe $|\Psi(t)\rangle$, as in HF or DFT, the TDSE can be rewritten for each non-interacting molecular orbital, ϕ_i

$$i\frac{\partial}{\partial t}\phi_i(t) = \hat{f}(t)\phi_i(t) \tag{1.17}$$

Typically, computations are not done in the orbital basis. Instead, the time dependence of the orbitals is moved to the contraction coefficents.

$$\phi_i(t) = \sum_\mu c_{i,\mu}(t)\chi_\mu \tag{1.18}$$

This allows one to express eq. (1.17) as a matrix equation over contraction coefficents

$$i\frac{\partial}{\partial t}\mathbf{C}(t) = \mathbf{FC} \tag{1.19}$$

A more powerful approach is instead to use the generalization of the TDSE to density matrices, known as the Liouville-von Neummann equation.

$$i\frac{\partial}{\partial t}\rho(t) = [\hat{\mathcal{H}}(t), \rho(t)] \tag{1.20}$$

$$\rho_{ij} = p_{ij} \left|\phi_i(t)\right\rangle \left\langle\phi_j(t)\right| \tag{1.21}$$

where p_{ij} is the probability of finding a particle in a superposition of pure state i and j. For a HF or DFT wavefunction, ρ corresponds to the one particle reduced density matrix, (1RDM) and in the ground state orbital basis, it is the identity matrix for all occupied orbitals and 0 elsewhere. In general, the 1RDM can be expanded in any orthonormal basis, leading to

$$i\frac{\partial \mathbf{P}(t)}{\partial t} = [\mathbf{F}(t), \mathbf{P}(t)] \tag{1.22}$$

This is the typical working equation for real-time HF or DFT. If the 1RDM is expressed in a non-orthonormal basis, factors of the basis function overlap appear on both sides.

The solution of both Equation (1.19) and Equation (1.22) requires sophisticated numerical integration algorithms to ensure stability and preservation of the symmetries of the Hamiltonian. A detailed discussion of these points is not required for the developments later in this work, but interested readers can find discussions in references 3 and 4.

Chapter 2

CLASSICAL EMBEDDING THEORIES

With the theory for solving the TDSE established, we now move on to presenting the theory surrounding classical embedding theories. These theories are essential to capturing important physics in systems too large to model with a single quantum mechanical level of theory.

2.1 Theoretical Approaches to Modeling Environments

In principle, the most accurate methods for modeling molecular systems in an environment are to model the entire system quantum mechanically (QM). In practice, this treatment is computationally intractable, so many theoretical models and computational algorithms have been developed to treat these systems approximately while preserving the accuracy on the prediction of observables of interest. While computationally intractable, beginning discussion of these approximate models from the fully-quantum mechanical picture allows one to see the approximations that are made in the process. We will start our discussion by considering the Hamiltonian of the fully quantum mechanical system in the Born-Oppenheimer approximation and separating terms by subsystem.

$$\hat{\mathcal{H}}^{Total}(r^H, R^H; r^L, R^L) = \hat{\mathcal{H}}^H(r^H, R^H) + \hat{\mathcal{H}}^L(r^L, R^L) + \hat{\mathcal{V}}^{int}(r^H, R^H, r^L, R^L) \tag{2.1}$$

Here, the coordinate r denotes electronic degrees of freedom, R denotes nuclear degrees of freedom, and $\hat{\mathcal{H}}^X(r^X, R^X)$ is the Hamiltonian of the non-interacting subsystem X. We have labeled one subsystem as H for a "high" level of theory with high accuracy applied to it and the other as L for a "low" level of theory with a lower accuracy.

Embedding approaches can be organized in a hierarchy of models that approximate the terms $\hat{\mathcal{H}}^L$ and $\hat{\mathcal{V}}$ in order to make the overall problem more computationally efficient while

sacrificing some accuracy. The key to applying embedding approaches correctly is to select the most efficient model that preserves the essential characteristics of the interactions between the subsystems. The embedding hierarchy can be considered by the levels of approximations that are made at each step:

1. **Full QM**: No approximation is made beyond those of the quantum mechanical method employed. These are sometimes referred to as "supermolecule" models.

2. **QM-in-QM**: $\hat{\mathcal{H}}^L$ is treated at a different level of quantum mechanical theory. The interaction can be treated as an embedding potential [5, 6] or the low level system can be projected out of the orbital space.[7] All degrees of freedom are still accounted for; these methods are generally useful when one wants to apply a high level of *ab initio* electronic structure theory to only a portion of a system, but still needs to describe the environment quantum mechanically.

3. **QM-in-explicit**: At this level, the electronic degrees of freedom are replaced by electrostatic multipoles and polarizabilities. Nuclear degrees of freedom are still included. Because of the removal of electronic degrees of freedom, $\hat{\mathcal{H}}^L$ is generally parameterized using experimental or *ab initio* data. $\hat{\mathcal{V}}^{int}$ typically only consists of Coulombic interactions. These methods are useful when long-range Coulombic interactions dominate the interaction between subsystems, but orientation of the environment is still important, *e.g.* ordered environments such as protein active sites or hydrogen bonding between the subsystems. [1]

4. **QM-in-implicit**: Both the nuclear and electronic degrees of freedom are accounted for in an indirect way. The most common approach, the Polarizable Continuum Model, (PCM) treats the response of the environment as purely through polarization - the environment is described as a typically uniform dielectric. These approaches can be extremely affordable as they implicitly account for averaging over an ensemble of ther-

modynamically accessible structures, but this comes at the cost of being unable to model specific interactions with the environment. [8]

2.2 Atomistic (QM-in-Explicit) Electrostatic Models

In explicit models, approximations to $\hat{\mathcal{H}}^L$ and $\hat{\mathcal{V}}^{int}$ are made to approximate the electronic degrees of freedom by a few electrostatic objects. Arguably the most commonly known atomistic model, molecular mechanics (MM), approximates the operators above with "bonding" and "non-bonding" terms. The form of these bonding and non-bonding terms differ between implementations, referred to as "force fields." Although there are many force fields available which perform best for different systems, the prototypical bond-based force field potential expression is formulated as

$$\begin{aligned}\hat{\mathcal{H}}^L \approx & \frac{1}{2}\sum_b k_b(r_b - r_{0b})^2 + \frac{1}{2}\sum_a k_a(\theta_a - \theta_{0a})^2 + \frac{1}{2}\sum_d k_d(1+\cos(n_d\phi_d + \delta_d)) \\ & + \frac{1}{2}\sum_{i,j}\left[V_{LJ}(R_i^L, R_j^L) + V_{coul}(R_i^L, R_j^L)\right] \end{aligned} \tag{2.2}$$

The first three terms in Equation (2.2) correspond to the bonded terms — the first is a harmonic potential that runs over bonds, the second is a harmonic potential that runs over angles, and the third is a sinusoidal potential that runs over dihedral angles. The last two terms are non-bonding. V_{LJ} is a standard Lennard-Jones 6-12 potential, and V_{coul} is the Coulombic interaction between partial charges located on each atom. The specifics of all terms other than the Coulombic term are unimportant for the further developments in this work because Coulombic interaction is also the term that couples the quantum mechanical and molecular mechanical subsystems in QM/MM embedding.

$$\hat{\mathcal{V}}^{int} \approx \frac{1}{2}\sum_i\sum_j \frac{-q_j}{|r_i^H - R_j^L|} + \frac{1}{2}\sum_i\sum_j \frac{Z_i q_j}{|R_i^H - R_j^L|} \tag{2.3}$$

Because the term $\hat{\mathcal{V}}^{int}$ only involves one electronic coordinate, it is typically easy to account for in *ab initio* quantum chemistry methods, as it represents a perturbation to the

one-electron Hamiltonian. For example, in Hartree-Fock (HF) or Density Functional Theory (DFT), the embedded Fock matrix in the atomic orbital basis is

$$\mathrm{F}_{\mu\nu} = \mathrm{F}^0_{\mu\nu} - \sum_i \langle\mu| \frac{q_j}{|r_i^H - R_i^L|} |\nu\rangle \tag{2.4}$$

Here, $\mathbf{F}^0$ is the unperturbed Fock matrix. The approximation that the interaction between the molecular mechanical and quantum mechanical systems can be captured by point charges interacting with the electronic density is simple yet crude, so many force fields improve on this term.

One improvement to the Coulombic interaction between the subsystems is to carry out the multipolar expansion of the charge density in the molecular mechanical region. A general formalism for coupling arbitrary multipoles through interaction tensors is given by chapter 3 of reference 9. The addition of these multipoles to the interaction part of the overall Hamiltonian only requires electric potential integrals and their derivatives at each multipolar site. Increasing the multipolar expansion on each site can provide a more sophisticated description of the charge density in MM molecules, but it neglects any effect that any external (QM) charge density has on the MM charge density, *i.e.* polarization. Recent studies [10, 1, 11] have shown the importance of including polarization in molecular mechanical models in general. Polarization is particularly important for time-dependent QM/MM embeddings, since the polarization of the solvent represents electronic reorganization, which occurs on the same time scale as *ab initio* electronic dynamics or excitation processes.

Many different models to capture polarization have been developed, including fluctuating charge models,[12] induced dipole based molecular mechanics,[1, 10] (MMPol) the effective fragment potential, [13] Drude oscillator models, [14] and the polarizable embedding model.[15] In this work, we will focus primarily on the induced dipole family of models. For induced dipole based models in a static field, the charge density of each site is expanded as a multipolar expansion, and then each multipole is expanded in orders of external electric field strength. Assuming that induced multipoles higher than the dipole will have negligible contributions to the charge density change compared to induced dipoles, one can neglect the

expansion of high-order multipoles with respect to electric field. The only terms left are the induced dipole, $\boldsymbol{\mu}_i^{ind}$, expanded in terms of electric field.

$$\boldsymbol{\mu}_i^{ind} = \boldsymbol{\alpha}_i \boldsymbol{E} + \boldsymbol{\beta}_i \boldsymbol{E}^2 + \boldsymbol{\gamma}_i \boldsymbol{E}^3 + \dots \tag{2.5}$$

where $\boldsymbol{\alpha}$ is the standard rank-2 dipole polarizability tensor, $\boldsymbol{\beta}$ is the rank-3 hyperpolarizability, and $\boldsymbol{\gamma}$ is the rank-4 second hyperpolarizability. Typically, the hyperpolarizabilities are neglected and $\boldsymbol{\alpha}$ is approximated to be isotropic, [16] leading to

$$\boldsymbol{\mu}_i^{ind} = \alpha_i \boldsymbol{E} \tag{2.6}$$

For QM/MM systems, the form of $\boldsymbol{E}$ can be broken down more explicitly

$$\boldsymbol{\mu}_i^{ind}(\rho^H) = \alpha_i \left(\boldsymbol{E}_{static} + \boldsymbol{E}(\rho^H) + \boldsymbol{E}_{ext} + \sum_{j \neq i} T_{ij} \boldsymbol{\mu}_j^{ind} \right) \tag{2.7}$$

where ρ^H is the total (electronic and nuclear) charge density in the QM region. The first electric field contribution comes from all static multipoles, the second comes from the QM charge density, the third is any other external external field, such as that coming from an experiment, and the final contribution is the field from all other induced dipoles. The induced dipole-induced dipole interactions are calculated through the interaction tensor T_{ij} which may be the bare dipole-dipole interaction tensor,[9] or it may be a damped interaction tensor in order to prevent overpolarization.[17] From Equation (2.7), it is apparent that the induced dipoles are dependent on the electronic density. This dependence is the origin of the mutual polarization that can be accounted for in QM/polarizable MM embedding schemes.

The presence of induced dipoles contributes to both the internal MM energy term and the interaction operator between systems. With the additional term due to induced dipoles, the internal MM energy is now given by

$$\hat{\mathcal{H}}^L \approx H^{L,static} + \frac{1}{2} \sum_i \boldsymbol{\mu}_i \cdot \boldsymbol{E}^L(R_i) \tag{2.8}$$

Here, $H^{L,static}$ includes all the terms from Equation (2.2), and $\boldsymbol{E}^L(R_i)$ is the electric field from static multipoles and other induced dipoles at polarizable site i. The interaction term

now reads as

$$\hat{\mathcal{V}}^{int} \approx \hat{\mathcal{V}}^{int,static} + \frac{1}{2}\sum_i \boldsymbol{\mu}_i \cdot \boldsymbol{E}^H(R_i) \tag{2.9}$$

where $\hat{\mathcal{V}}^{int,static}$ includes all terms from Equation (2.3) and $\boldsymbol{E}^H(R_i)$ is the electric field from nuclei and the electron density in the quantum mechanical region at polarizable site i.

2.3 Dielectric (QM-in-Implicit) Electrostatic Models

Rather than describe the environment explicitly, it can be convenient to assume polarization of the environment dominates the interaction between the environment and the system of interest. In this case, one can substitute the configurational degrees of freedom in the environment for a general description of the environment as a dielectric medium in which the quantum mechanical system is placed. When the environment of interest can be described as an isotropic dielectric, the problem maps onto Poisson's equation for electrostatics. Namely,

$$\nabla \cdot [\epsilon(r)\nabla\Phi(r)] = -4\pi\rho(r) \tag{2.10}$$

Where $\epsilon(r)$ is the position dependent electric permittivity, $\Phi(r)$ is the electric potential, and $\rho(r)$ is the charge density. Continuum models can be also be used when the surrounding environment is composed of ionic solutions, anisotropic dielectrics, or other metal surfaces, in which case Equation (2.10) is substituted for the appropriate differential equation, and the corresponding Green's function is used to solve the problem. In this article, we will focus on solving the standard problem presented by Equation (2.10). For a uniform, non-ionic environment, $\epsilon(r)$ may be represented by

$$\epsilon(r) = \begin{cases} 1 & r \in \text{cavity} \\ \epsilon & r \notin \text{cavity} \end{cases} \tag{2.11}$$

Because of the explicit boundary defined by the cavity, the effect of Equation (2.10) may be captured by representing the polarization of the dielectric as a fictitious charge distribution on the dividing boundary. The potential in Equation (2.10) is then represented as a sum

over the *ab initio* charge density and this charge distribution.

$$\Phi(r) = \int \frac{\rho(r')}{|r - r'|} dr' + \int_\Gamma \frac{\sigma(s)}{|r - s|} ds \tag{2.12}$$

where Γ is the cavity surface, and $\sigma(s)$ is the surface charge at s.

The surface charge $\sigma(s)$ is the solution to the equation

$$\left[2\pi \frac{\epsilon + 1}{\epsilon - 1} I - \hat{D} \right] \hat{S}\sigma(s) = -(2\pi I - \hat{D}) \int \frac{\rho(r)}{|r - s|} dr \tag{2.13}$$

This formulation of PCM is often referred to as the Integral Equation Formalism (IEF) PCM. Other PCM formulations, such as the Conductor-like Screening Model (COSMO) or the dielectric PCM (DPCM) formulation, are specializations of the IEF-PCM formalism. Here we have introduced the integral operators S and D which are defined as

$$\hat{S}\sigma(s) = \int_\Gamma \frac{\sigma(s')}{|s - s'|} ds' \tag{2.14}$$

$$\hat{D}\sigma(s) = \int_\Gamma \sigma(s') \frac{\partial}{\partial n_{s'}} \frac{1}{|s - s'|} ds' \tag{2.15}$$

n_s is the normal vector to the surface at s. The physical interpretation of $\hat{S}$ is simple — it represents the field at the surface from the charge elsewhere on the surface. The physical interpretation of $\hat{D}$ is more difficult — one could say that it represents the "integral of the normal field" on the surface. Perhaps a more intuitive way to regard $\hat{D}$ is to describe it as the adjoint of the operator $\hat{D}^*$ which is the electric field normal to the surface. For more information on these operators, see references 18 and 19.

Practically, solving for $\sigma(s)$ typically requires discretization of the surface, and assigning each surface element an area a_i and charge, q_i, assuming that the surface charge will remain constant across the element for sufficiently small areas. The definition of q_i is then

$$q_i = \sigma(s_i) a_i \tag{2.16}$$

This discretization forms a basis in which $\hat{S}$ and $\hat{D}$ can be expressed, transforming Equation (2.13) into a matrix equation.

$$\left[2\pi \frac{\epsilon + 1}{\epsilon - 1} \mathbf{A}^{-1} - \mathbf{D} \right] \mathbf{Sq} = -\left(2\pi \mathbf{A}^{-1} - \mathbf{D} \right) \mathbf{V} \tag{2.17}$$

The matrix forms of $\hat{S}$ and $\hat{D}$ are given by

$$S_{ij} = \begin{cases} \frac{1}{|s_i - s_j|} & i \neq j \\ k\sqrt{\frac{4\pi}{a_i}} & i = j \end{cases} \tag{2.18}$$

$$D_{ij} = \begin{cases} \frac{(s_i - s_j)\cdot n_j}{|s_i - s_j|^3} & i \neq j \\ k\frac{\sqrt{4\pi a_i}}{2R_I} & i = j \end{cases} \tag{2.19}$$

where R_I is the radius of the sphere on which the surface element resides. $\mathbf{A}$ is the diagonal surface element area matrix, and $\mathbf{V}$ is the electric potential arising from the QM region.

Once the surface charges are solved for a given QM electronic density, the coupling between the QM and PCM regions that approximates $\hat{\mathcal{V}}^{int}$ from Equation (2.1) is simply

$$\hat{\mathcal{V}}^{int} \approx \sum_i q_i \int \frac{\rho(r)}{|r - s_i|} dr \tag{2.20}$$

This can be cast into the appropriate basis, depending on the quantum mechanical model used. For example, in Hartree-Fock or Density Functional Theory, this is a contribution to the Fock or Kohn-Sham matrix that can be expressed in the AO basis.

$$\mathrm{F}_{\mu\nu} = \mathrm{F}^0_{\mu\nu} - \sum_i q_i \left\langle \mu \left| \frac{1}{|r - s_i|} \right| \nu \right\rangle \tag{2.21}$$

While this expression looks like the non-polarizable MM contribution to the Fock matrix in Equation (2.4), the values of the charges, q, themselves depend on the electron density. This creates a mutual QM/environment dependence similar to polarizable MM, meaning that the surface charge must be solved in parallel with the electronic density for SCF or electron dynamics procedures.

2.4 Considerations for Choosing Continuum or Discrete Environments

The primary and defining difference between implicitly and explicit environments is the manner in which they perform configurational sampling. Continuum approaches implicitly integrate over all configurational degrees of freedom, which can give an accurate description

of the system-environment interactions, provided that these interactions may be described in an "average" manner. Whenever the interaction between the environment and system of interest is strongly dependent on relative orientation, such as in the case of solute-solvent hydrogen bonding, an explicit environment is necessary. The drawback to atomistic models is that the configurational sampling must now be done explicitly, often over hundreds or more structures. This sampling is not trivial — not only does it now require many more quantum mechanical calculations, care must also be taken while generating the configurations over which to sample in order to ensure an unbiased and accurate ensemble average. Nevertheless, atomistic descriptions are necessary if one requires more accurate results than continuum approaches provide.

An ever more popular approach is to combine the methods in order to minimize the computational cost of configurational sampling while also allowing for some specific system-environment interactions. These "layering" methods are no more theoretically challenging than either of the methods on their own. The challenge lies primarily in their implementation rather than their conception. The electrostatic objects in each model contribute to the energy and polarization of each other simply by additional terms in the potential or fields of Equation (2.7) and Equation (2.17). Layered models may also be used to compose any variety of environmental description within another. A common use is to embed a quantum mechanical region inside of a polarizable explicit environment, and then embed that entire system within a non-polarizable explicit environment. [11] Another, more technically challenging, use of layered models is to use multiple models for different sections of a heterogeneous environment, such as a molecule on a plasmonic nanoparticle in solution. [20]

Finally, especially when performing dynamics calculations, one must consider what response (*e.g.* orientational, vibrational, electronic) is desired from the environment. Non-polarizable explicit methods offer no environmental response to quantum dynamics, polarizable explicit methods only capture electronic response, and implicit methods primarily capture orientational response. More discussion of these points is given in the following section.

2.5 Embedded Real-Time Dynamics

The time-dependent Schrödinger equation (TDSE) governs all spectroscopy and dynamics of a quantum mechanical system.

$$i\frac{\partial\Psi(t)}{\partial t} = \hat{\mathcal{H}}(t)\Psi(t) \tag{2.22}$$

Embedded quantum mechanical systems are no different, so the use of standard techniques to solve the TDSE also apply to mixed quantum/classical systems. Chapter 1 discusses the solution techniques for the TDSE, so here we will only discuss the contributions from the environment. It is worth noting here that static perturbations, *i.e.* those that do not depend on the electronic density, will not contribute to changes to the theory or working equations of the TDSE. The effect of embedding schemes such as non-polarizable molecular mechanics on time-dependent properties is simply to provide a static field in which to solve the TDSE, and any time-dependent response of the environment is neglected.

For polarization-including embedding methods, polarization terms that are induced by a time-dependent electronic density are themselves time-dependent.

$$\mathbf{H}(t) = \mathbf{H_0}(t, \mathbf{P}(t)) + \mathbf{V}(\mathbf{P}(t)) \tag{2.23}$$

For explicit embedding models that include induced dipole polarization, the additional polarization term is given by

$$V_{\lambda\nu}^{dipole}(\mathbf{P}(t)) = -\frac{1}{2}\sum_{p} \langle\lambda| \frac{\mu_p(\mathbf{P}(t)) \cdot (\mathcal{R}_p - \mathbf{r})}{|\mathbf{r} - \mathcal{R}_p|^3} |\nu\rangle \tag{2.24}$$

where

The time dependence of the polarization terms originates entirely from the time dependence of the induced dipoles. For induced dipole, explicit embedding models, the simplest and most common treatment of the time dependence of the induced dipoles is to neglect the frequency dependence of the polarizability. Because induced dipole models attempt to capture electronic polarization, not configurational polarization, this approximation often

performs well. Specifically, the "static polarizability" approximation holds when the excitations of the environment lie far away from the dominant frequencies arising from the time dependent quantum region. Within this approximation, the governing equation for the induced dipoles is the same as Equation (2.7) with the time-dependent electronic density.

For PCM, the treatment of the time dependence of the induced surface charges is more complicated, since the dielectric permittivity captures both configurational and electronic polarization. Typically, the polarization of the cavity is separated into two terms: a "slow" polarization and a "fast" polarization. The slow polarization term is kept fixed for the duration of the simulation, whereas the fast polarization is allowed to come to equilibrium at each time step. Early models separated the polarization of the cavity into configurational (slow) and electronic (fast) components. [21] Later models separated the polarization of the cavity into inertial (slow) and dynamic (fast) components. [22, 8] This scheme differs from the first by including electronic polarization that is induced by the configurational polarization in the inertial (slow) component, rather than the electronic (fast) component. Practically, however, this is simply an implementation difference. Both models give rise to the same *total* potential on the quantum mechanical system and give rise to the same changes in properties of the system of interest. [23] A more detailed discussion of the difference between these models can be found in reference 8.

In a similar manner to the explicit solvation models, the frequency dependence of the dielectric permittivity is typically neglected after the polarization separation scheme is chosen. The fast polarization is then solved by substituting the optical dielectric constant for the static dielectric constant in the PCM working equations. Once the fast component of the cavity polarization is determined, the time dependent potential acting upon the quantum mechanical system is then

$$\mathrm{V}_{\mu\nu}^{PCM}(\mathbf{P}(t)) = -\sum_i (q_i^{slow} + q_i^{fast}(\mathbf{P}(t))\langle\mu|\frac{1}{|r-s_i|}|\nu\rangle \tag{2.25}$$

Chapter 3

ELECTRONIC DYNAMICS WITHIN AN EQUILIBIRIUM POLARIZABLE QM/MM MODEL

Mixed Quantum Mechanical and Molecular Mechanical (QM/MM) simulations have been increasing in popularity, since they allow for an inexpensive description of a chemical environment (such as a protein) around a system of interest (such as an active site). However, traditional molecular mechanical models in which the charge distribution of molecules is a sum over static monopoles have often been shown to be too simplistic for many applications. This is especially the case when performing quantum dynamics calculations, since the response of the environment is completely neglected. Polarizable molecular mechanics methods have been developed to overcome this limitation, but prior to this work, no implementation of *ab initio* real-time quantum dynamics within polarizable molecular mechanics models had been developed. In this chapter, the theoretical framework for the real-time dynamics of a polarizable QM/MM system is given, and the application to a couple of systems of interest is shown. The work presented in this chapter has been adapted with permission from Donati, G., Wildman, A., Caprasecca, S., Lingerfelt, D.B., Lipparini, F., Mennucci, B. and Li, X., 2017. Coupling real-time time-dependent density functional theory with polarizable force field. The Journal of Physical Chemistry Letters, 8(21), pp.5283-5289. Copyright 2017, American Chemical Society.

3.1 Motivation

One of the most widely-employed techniques for calculating linear absorption spectra of molecular systems, the linear response time-dependent density functional theory (LR-TDDFT)[24, 25, 26, 27], relies on the application of response theory to a ground-state 'reference' wave

function. The response function is expressed as a series expansion in orders of the perturbation strength, so high-order terms and explicit electronic dynamics are inaccessible under this approach. Alternatively, one may directly solve the time-dependent Schrödinger equation to simulate the photoexcitation dynamics using the real-time TDDFT approach.[28, 29, 30, 31, 32] This method not only incorporates all higher order terms ignored by any level of response theory,[33] but it also opens the door to a time-resolved description of the changes in the system's electronic structure affected by the environment, disentangling the potentially diverse effects of system-environment interactions following electronic excitation.

The environment acts as an external perturbation to the system, causing deviations in its temporal evolution with respect to that of an equivalent isolated system. Interactions between the system and the environment as they mutually evolve in time cause properties of the system to depend (in potentially non-obvious ways) on the environmental degrees of freedom. The environment can not only impose changes in the system's conformation through steric interactions [34, 35], it can also significantly alter the system's electronic structure via noncovalent interactions leading to changes in the system's response to electromagnetic fields [36, 37, 38] (i.e. spectroscopic properties) and chemical reactivity.[39, 40, 41, 42]

A wide variety of theoretical models have been proposed to capture the essential aspects of the system-environment interactions while reducing the large number of degrees of freedom required to describe the environment. Among such approaches, continuum solvation models treat the environmental degrees of freedom implicitly, sacrificing any atomistic description thereof. The combination of continuum models and QM descriptions of the system has shown to give an accurate description of system-environment interactions, in all the cases where the latter can be represented in terms of an average effect.[43, 44, 8, 45] However, an atomistic description of the environment becomes necessary when the change in the system's properties are the result of specific system-environment interactions which strongly depend on the relative orientation and distance between the two (e.g. solute-solvent hydrogen bondings).[46] To preserve the atomistic nature of the environment, hybrid models were devised in which the system electronic degrees of freedom are treated quantum mechanically (QM), while the

environment is described at a classical level (often through molecular mechanics (MM)). [47, 48, 49] The most common examples of hybrid QM/MM models include the effect of the classical environment on the QM system using fixed point charges to represent the environment atoms. This "electrostatic" embedding approach has shown to capture the large part of the environment effects, but obviously it cannot model any mutual polarization between the system and its environment. To overcome this limitation, in recent years hybrid QM/MM models have been generalized to include a "polarizable" embedding. Many approaches for including the polarization of the system by its environment (and *vice versa*) have been explored, including the so-called "Effective Fragment Potential Method"[50, 51], "induced dipoles"[52, 1, 53, 54, 55], "fluctuating charges"[56, 57, 58, 59], and Drude oscillator-based models[14]. In this chapter, the induced dipole formulation of polarizable MM (MMPol) is employed to describe the the environment degrees of freedom, while the system degrees of freedom are treated quantum mechanically via the time-dependent self consistent field approach.

In particular, the QM/MMPol formulation is here extended to RT-TDDFT for computations of spectroscopic quantities and simulations of the electronic dynamics of chemical systems embedded in a large polarizable force field. LR-TDDFT calculations on QM/MMPol systems have already been performed and validated in previous works to simulate electronic spectra of (supra)molecular systems in complex environments.[52, 11, 60, 61, 62]. Very recently, an example of the extension of MM polarizable embeddings to RT-TDDFT has been presented within the software deMon2k that relies on auxiliary fitted densities.[63]

3.2 Theoretical Approach

The time-dependent electronic degrees of freedom of the quantum subsystem are modeled with the RT-TDDFT approach,

$$i\frac{d\mathbf{P}(t)}{dt} = [\mathbf{K}(t), \mathbf{P}(t)] \tag{3.1}$$

where $\mathbf{K}$ and $\mathbf{P}$ are the Kohn-Sham/Fock and density matrices in the orthonormal basis, respectively. Equation (4.10) is integrated using the modified midpoint unitary transformation (MMUT) approach, a second order "leap-frog" style algorithm,[28, 64, 29, 65]

$$\begin{aligned}
\mathbf{P}(t_{k+1}) &= \mathbf{U}(t_k) \cdot \mathbf{P}(t_{k-1}) \cdot \mathbf{U}^{\dagger}(t_k) \\
\mathbf{U}(t_k) &= \mathbf{C}(t_k) \exp\left[-i2\Delta t\ \boldsymbol{\lambda}(t_k)\right] \mathbf{C}(t_k) \\
\boldsymbol{\lambda}(t_k) &= \mathbf{C}^{\dagger}(t_k) \cdot \mathbf{K}(t_k) \cdot \mathbf{C}(t_k)
\end{aligned} \tag{3.2}$$

where $\mathbf{C}$ and $\boldsymbol{\lambda}$ are the eigenvectors and eigenvalues of the Kohn-Sham/Fock matrix.

To describe the many-electron dynamics embedded in a polarizable force field, one needs to integrate the mutual interaction and polarization between the TDDFT and MMPol subsystems during the reaction dynamics.

The interaction between the polarizable environment and the quantum system is introduced via a density-dependent operator, $\mathbf{V}^{\mathrm{MMPol}}$, in the Kohn-Sham/Fock matrix,

$$\mathbf{K}'(t) = \mathbf{K}'_{\mathbf{0}}(t, \mathbf{P}'(t)) + \mathbf{V}^{\mathrm{MMPol}}(\mathbf{q}, \boldsymbol{\mu}(\mathbf{P}'(t))) \tag{3.3}$$

where $\mathbf{K}'_{\mathbf{0}}$ is the perturbation-free Hamiltonian matrix for the QM region. Note that primed notations reference corresponding matrices in non-orthogonal atomic orbital basis.
$\mathbf{V}^{\mathrm{MMPol}}(\mathbf{q}, \boldsymbol{\mu}(\mathbf{P}'(t)))$ is the time-dependent interaction potential induced by the MM charges and induced dipoles $\boldsymbol{\mu}(t)$ from the MMPol region. This perturbation term represented in the atomic basis $(\lambda, \nu, ...)$ takes on the following form,[52, 1]

$$\begin{aligned}
V^{\mathrm{MMPol}}_{\lambda\nu} = &- \sum_i \langle\lambda| \frac{q_i}{|\mathbf{r} - \mathcal{R}_i|} |\nu\rangle \\
&- \sum_p \langle\lambda| \frac{\mu_p(\mathbf{P}'(t)) \cdot (\mathcal{R}_p - \mathbf{r})}{|\mathbf{r} - \mathcal{R}_p|^3} |\nu\rangle
\end{aligned} \tag{3.4}$$

where we use $\mathcal{R}$ and $\mathbf{R}$ to indicate nuclear coordinates in the MM and QM regions, respectively. The bra-ket notation implicitly integrates over the electronic degrees of freedom $\mathbf{r}$. We also use the index p and p' to label the polarizable sites in the MM region.

During the time-evolution of the quantum electronic dynamics, the Kohn-Sham/Fock matrix (eq. (4.11)) is computed on-the-fly at every time step by including the time-dependent

perturbing potential (eq. (4.12)) arising from the induced MM dipoles $\mu_p(\mathbf{P}'(t))$. The time-dependence of the MM dipoles $\mu_p(t)$ arises from the fact that the dipoles are computed as the linear response to the electric field produced by the MM charges and time-dependent QM density, by solving the following linear system of equations

$$\begin{aligned}\boldsymbol{\mu}_p(t) = \boldsymbol{\alpha}_p(\mathbf{E}_p(\mathbf{P}'(t)) + \sum_{p' \neq p} S^{(3)}_{pp'} \frac{\boldsymbol{\mu}_{p'}(t)}{|\mathcal{R}_{pp'}|^3} \\ - \sum_{p' \neq p} S^{(5)}_{pp'} \frac{3\mathcal{R}_{pp'}(\mathcal{R}_{pp'} \cdot \boldsymbol{\mu}_{p'}(t))}{|\mathcal{R}_{pp'}|^5})\end{aligned} \tag{3.5}$$

where $\boldsymbol{\alpha}_p$ is the static polarizability tensor at MM site p. $S^{(3)}_{pp'}$ and $S^{(5)}_{pp'}$ are screening factors depending on the MM topology which are introduced to avoid overpolarization effects.[66, 17, 67] $S^{(3)}_{pp'}$ and $S^{(5)}_{pp'}$ parameters used in the following case studies are tabulated in the Supplementary Information. In this work, we only consider static polarizabilities of the environment. This is a reasonable and useful approximation for cases where the electron field generated by the QM region is much slower than that from the MM region.

In eq. (3.5), we have assumed that the electronic degrees of freedom of the environment, modelled here by the induced dipoles, respond instantaneously to the electric field produced by the time-dependent electronic density of charge $\rho(\mathbf{r}, t)$ at each polarizable site p:

$$\begin{aligned}\mathbf{E}_p(\mathbf{P}'(t)) &= \sum_{i \neq p} q_i \frac{\mathcal{R}_p - \mathcal{R}_i}{|\mathcal{R}_p - \mathcal{R}_i|^3} \\ &+ \sum_i Z_i \frac{\mathcal{R}_p - \mathbf{R}_i}{|\mathcal{R}_p - \mathbf{R}_i|^3} \\ &+ \int \rho(\mathbf{r}, t) \frac{\mathcal{R}_p - \mathbf{r}}{|\mathcal{R}_p - \mathbf{r}|^3} d\mathbf{r}\end{aligned} \tag{3.6}$$

In addition, we assume that the process of geometrical relaxation (reorientation) of the environment happens at a slower timescale than the one investigated, and therefore we keep the positions of the MM atoms frozen.

3.3 Case study 1: Coumarin

The first case study is the solvatochromic dye coumarin 153[68, 69, 70, 71, 72, 73, 74, 75, 76, 77], a member of a class of molecules widely employed as sensitizers in solar cells.[78] The RT-TDDFT/MMPol electronic dynamics of the coumarin 153 dye in methanol solvent are simulated to resolve the absorption spectrum. All the calculations were performed by employing the PBE0[79] hybrid functional with the 6-31G(d) basis set.[80, 81] Coumarin 153 was placed in a box of 175 methanol molecules and a schematic picture is given in fig. 3.1.[82, 83]

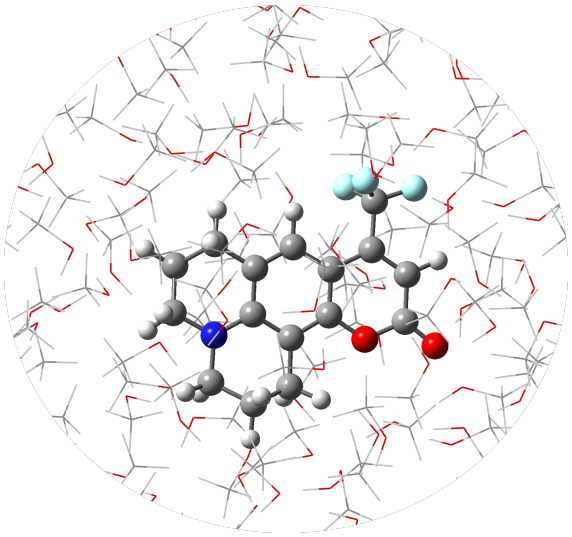

Figure 3.1: Schematic picture of coumarin 153 in methanol solution. The QM region is shown in a ball and stick representation while the MMPol region is shown in a line representation.

The solvation box was previously equilibrated using the Amber parm99SB force field.[84, 85, 86] LR-TDDFT and RT-TDDFT calculation were performed at QM/MMPol theory level in order to obtain absorption spectra that include solute/solvent mutual polarization. The real-time dynamics simulations were performed for 15 fs with an electronic time step of ∼0.25 attoseconds. The external electric field employed to perturb the system had an intensity of 0.0001 a.u., low enough to allow a linear approximation of the system response to the

perturbation. The external field was applied only for the first step of the dynamics and then turned off for all the rest of the simulation. The spectrum from RT-TDDFT simulations was obtained by using the Padé approximant of the Fourier transform. This approach has been shown to accelerate the convergence of the Fourier transform, allowing for shorter simulation timescales.[87, 65, 88, 89] Isotropic static atomic polarizabilities derived by Wang and co-workers were employed. The Amber linear model, already employed for protein simulations performed at QM/MMPol theory level,[1, 61] was used for the screening factors.[67] Dipole-dipole, charge-dipole and charge-charge interactions are taken into account depending on the connectivity, and 1-2 and 1-3 bonded neighbors are excluded. Because a polarizable MM scheme was used, the set of partial charges of the non-polarizable Amber force field could not be employed in the calculations. So, a new set of partial charges was derived [90] according to the chosen polarization model. All calculations were performed with a modified version of the development version of the Gaussian software.[91]

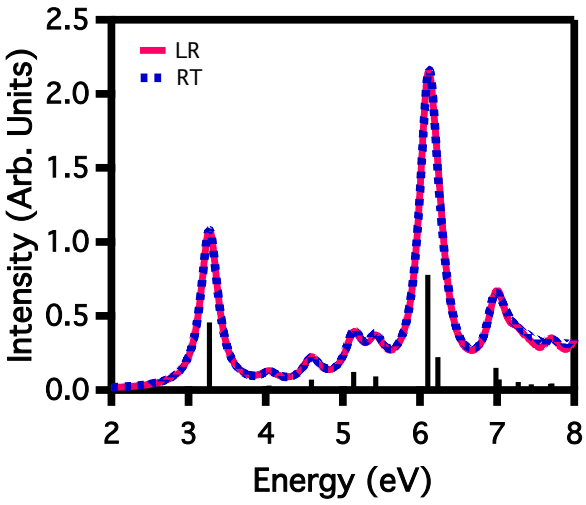

Figure 3.2: Absorption spectrum of coumarin 153 in methanol solution computed with LR- and RT-TDDFT/MMPol methods. Oscillator strengths from the LR-TDDFT calculation are also shown as black sticks.

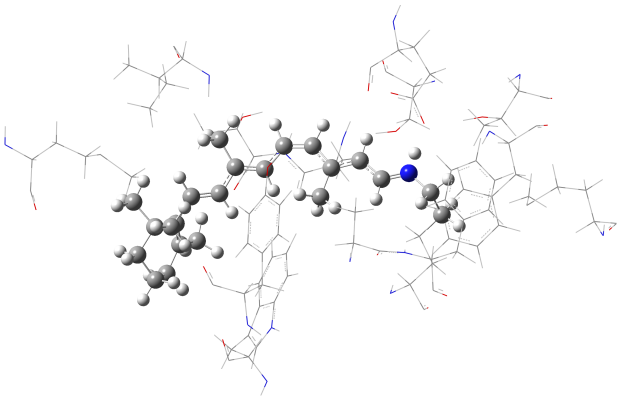

Figure 3.3: Schematic picture of 11-*cis* retinal protonated Schiff base in a shell of residues from bovine rhodopsin. The QM region is shown in a ball and stick representation and the MMPol region is shown in a line representation. The chromophore is covalently bonded to the Lys296 residue. The free valency created on C_δ by the division of the QM and MM regions was capped with a hydrogen link atom. See Ref. 1 for details in the partitioning scheme.

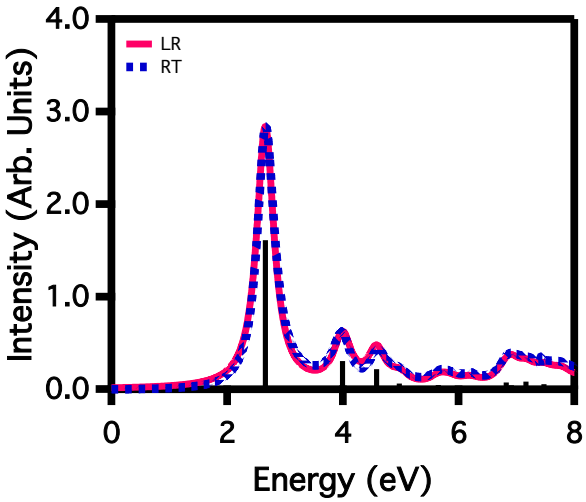

Figure 3.4: Absorption spectrum of RPSB in bovine rhodopsin calculated with LR- and RT-TDDFT/MMPol. Oscillator strengths from the LR-TDDFT calculation are shown as black sticks.

The spectrum of coumarin in methanol calculated using the Padé transformation from 15 fs of RT-TDDFT dynamics is shown in fig. 3.2. Two absorption peaks dominate the spectrum, one peak centered at 3.27 eV and the other at 6.12 eV; the more energetic peak is about twice as intense as the first. In order to validate the developed method, the absorption spectrum is compared to the LR-TDDFT calculation coupled with the same MMPol approach. Figure 3.2 shows that the LR- and RT-TDDFT spectra are in excellent agreement.

3.4 Case study 2: Rhodopsin

The coumarin model system provides good support for the validity of this model in the case of a solute/solvent system. However, simulating a heterogeneous environment such as that provided by a protein is much more challenging. In order to test the RT-TDDFT/MMPol method developed in this work, the 11-*cis* retinal protonated Schiff base (RPSB, fig. 3.3) in bovine rhodopsin residues was investigated. Simulations were carried out at the CAM-B3LYP[92]/6-31G(d)[80, 81] level of theory. The structure was obtained from a cluster analysis of frames extracted from QM/MM molecular dynamics (MD) trajectories where the QM part was treated within DFT using the PBE exchange-correlation functional (see Ref. 11 for the details).

The interactions with the surrounding residues strongly affect the optical properties of the chromophore. Even small changes in the conformations of residues can significantly shift the absorption.[93] Including mutual polarization between the environment and RPSB is required in order to accurately recover the excitation energies,[93] and because RPSB undergoes a *cis/trans* photoisomerization,[94, 95, 96, 97] accurate descriptions of the early-time electron dynamics are essential for understanding this process. The comparison between the LR- and RT-TDDFT for RPSB are shown in fig. 3.4. Again, the spectra show excellent agreement, with all of the peaks showing the same positions and relative intensities between methods. It is also informative to investigate the dynamics of the net dipoles in both the QM and MM regions. As can be seen in fig. 3.5, the net dipole in the MM region shows anti-oscillatory behavior compared to that in the QM region. Because the dipoles are being propagated

instantaneously with the perturbed electronic density, this behavior is expected; the dipoles are responding to the changing electronic density by aligning to the lowest energy position - against the dipole in the QM region.

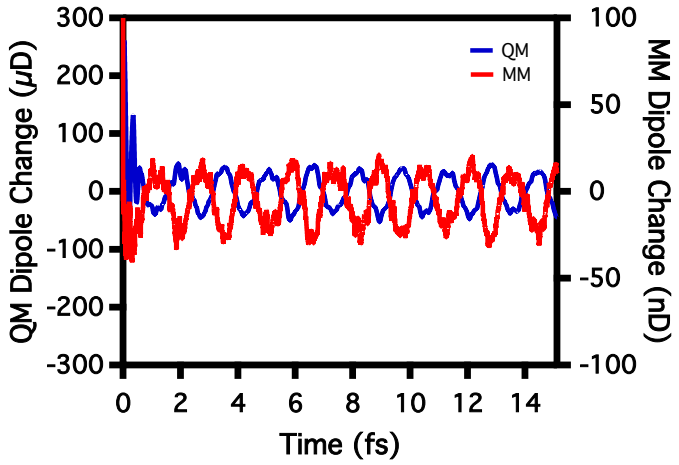

Figure 3.5: Evolution of the net dipole in both the QM and MMPol region. Note the different scales on left and right axes.

We conclude the discussion by commenting about the nature of the response of the environment included in the present RT-TDDFT formulation.

Polarizable embeddings introduce a specificity which is not present in non-polarizable embeddings. [98, 99, 100, 101] When we consider an electronic excitation in the QM subsystem, the electronic component of the environment response (here represented by the induced dipoles) can be determined by either the corresponding transition density or the change in the electronic density between ground and excited state. The former response is accounted for in a LR-TDDFT approach while the latter requires going beyond the standard TDDFT formulation and calculating the relaxation of the electronic density upon excitation. To account for this State-Specific (SS) term within a TDDFT framework, different approximations have been proposed.[102, 75, 103, 55] The simplest one is a perturbative correction to the excitation energy which is calculated in terms of the interaction between the change

Method	Energy (eV)
LR/Vacuo	2.4775
LR/MMPol	2.6581
RT/MMPol	2.6647
cLR/MMPol	2.7635

Table 3.1: First excitation energy of RPSB calculated with different TDDFT formulations.

in the electronic density and the corresponding change in the electronic component of the environment polarization. Such an approach (commonly known as corrected LR, or cLR) was originally proposed for PCM,[102] but it has been more recently extended to the induced dipole formulation of polarizable MM,[55] and it is also used here (table 3.1).

The setup of the real time simulation, i.e., the system in the ground state is perturbed with a very short pulse and then left to evolve, is consistent with the assumptions made in LR-TDDFT. Consequently, the RT-TDDFT results match the LR-TDDFT ones, while the state-specific (SS) corrected shift is larger. This discrepancy is of particular interest for understanding the different regimes modeled by the LR and SS approach. Since a complete consensus on how to describe excited states of solvated (or embedded) systems using classical polarizable models has not yet been achieved, we expect the RT formalism to be able to provide clearer insights into how to properly describe the response of environment to excited state dynamics. A detailed investigation of these aspects will be object of a future communication.

3.5 Summary

Real-time TDDFT is coupled with a polarizable QM/MM model, connecting the propagation of a wave function with the mutual polarization between the QM system and the environment. The proposed method was successfully validated by comparing the spectrum calculated by

both this method and LR-TDDFT of two completely different systems: a solvatochromatic dye in methanol solution and a chromophore in its protein environment.

Until now RT-TDDFT simulations of solvated systems or protein environments were either based on computationally expensive full quantum mechanical time-dependent theory or coupled with the mean-field time-dependent polarizable continuum model. With the time-dependent mutual polarization approach introduced in this work, the coupled RT-TDDFT and polarizable force field approach holds the potential to accurately probe the ultrafast non-equilibrium interaction between both the solvent and solute degrees of freedom and a chromophore embedded in its protein environment.

Chapter 4

NONEQUILIBRIUM ENVIRONMENT DYNAMICS IN A FREQUENCY-DEPENDENT POLARIZABLE EMBEDDING MODEL

Up to this point, we have only considered a model which allows the environment to respond instantaneously to changes in the electronic density. This is not realistic, since the polarization response in the environment is also due to electronic motion, so the polarization should move on the same time scale as the quantum mechanical electronic motion. In this chapter, a model that accounts for these time scales is developed by using a frequency-dependent polarizability in the molecular mechanical region. The work in this chapter was adapted with permission from Wildman, A., Donati, G., Lipparini, F., Mennucci, B. and Li, X., 2018. Nonequilibrium environment dynamics in a frequency-dependent polarizable embedding model. Journal of Chemical Theory and Computation, 15(1), pp.43-51. Copyright 2019 American Chemical Society.

4.1 Motivation

A fully quantum mechanical treatment of chemical systems interacting with their environment is still a computationally unfeasible approach. Because of that, approximate methods are commonly used where quantum and classical methods are applied to the two different components of the whole system. Among them, hybrid quantum mechanics/molecular mechanics (QM/MM) methods[47, 48, 49, 104, 105, 106] are particularly successful mostly due to the fact that they keep an atomistic description of the environment. Within this framework, the chemical system of interest is treated at the selected QM level of theory whereas the environment is described through a given MM force field.

Early QM/MM models ignored the direct influence of the MM region on the QM description (this scheme is generally denoted as mechanical embedding), but currently, almost all the applications of these methods account for this influence through electrostatics (electrostatic embedding). More recently, mutual polarization effects have been added through polarizable embedding schemes. Within this framework, a variety of methods have been proposed so far. Some strategies are based on a "fragmentation" approach where the full system is divided into fragments, some QM level is selected to calculate the wave function, energy, and properties of each fragment in the field of the others, and finally the results from the fragment calculations are combined to predict the same properties for the whole. Well known examples of this strategy are the effective fragment method (EFP),[107] and the explicit-polarization method (X- Pol)[108] A less expensive formulation uses parameters for describing the classical polarizable subsystems either using "induced dipoles," [109, 52, 110, 111] "fluctuating charges," [56, 57, 58] and Drude oscillators [14]. In particular, in the induced dipole formulation of polarizable MM (from now on indicated as MMPol), each classical polarizable site is described through a fixed charge (or a multipolar expansion) and a polarizability.

A typical application scenario for MMPol methods is the modeling of solvatochromic effects in solvated or embedded molecules. [112, 113, 55, 15, 114, 115] The MMPol description can be used in such a case to describe the shift of the absorption (or emission) frequencies and the change in intensities due to the presence of an environment. Notably, MMPol models are able to capture not only the modifications induced by the environment on the electronic structure of the chromophore, but also the way the environment responds to such a change. A standard assumption in these models is that the polarization of the environment can respond instantaneously to changes in the electron density of the chromophore (neglecting the possible relaxation of its geometry and configuration around the chromophore, due to a much slower time scale). From an experimental point of view, this instantaneous polarization response corresponds to a scenario where the environment is transparent at the absorption frequencies of the chromophore. A reasonable assumption in such a case is that the environment polarization responds with a frequency-independent (i.e. static) polarizability.

This is, of course, an approximation, as the polarizability of the environment does indeed depend on the frequency. In the case that the environment absorbs light at much higher frequencies than the system of interest (sometimes called the "non-resonance" condition), this approximation is fully justified.[116] However, the optical response of the environment is fast, but not instantaneous, and retardation and relaxation effects can be expected on a very short time scale. Furthermore, a much more dramatic effect can be observed if the environment can become resonant with the external field or with the excitation of the chromophore. Such a regime can either correspond to the environment itself absorbing light, or with it exhibiting global oscillation modes that have a similar frequency to the chromophore absorption one. An example of the latter scenario is given by metal nanoparticles, which have plasmonic modes that can resonate with molecular transition energies, greatly enhancing the molecular response.

While a classical description of an environment that is capable of absorbing light may not be adequate, classical models for plasmonic systems have already been proposed and can be considered well established.[117, 118, 119, 120, 121, 122] In the case of plasmonic systems, the environment may be homogeneous enough to model using continuum approaches, but a molecular mechanical model will allow for the general modeling of complex environments with specific interactions between the subsystems, such as hydrogen bonding. Both the modeling of ultra-fast retardation effects in the environment response and of enhanced spectroscopies, where the enhancement is produced by a nearly resonant interaction of the chromophore with some collective mode of the environment, require the introduction of a frequency dependent MMPol model, referred to here as ωMMPol. Frequency dependent force fields have been previously developed, [123, 124] however these works have only considered a polarizability at specific frequencies and have always been used in conjunction with response theory.

In this work, we pursue a different approach. The goal of this work is to develop a framework for allowing time-propagation of a QM/MMPol system in the cases where the non-resonance condition is not satisfied, and a frequency dependent force field must be considered. First, we will detail the model formalism, then we will validate the method, by

investigating the capability of the ωMMPol model to describe the nearly resonant regime for simple model systems.

4.2 Theory

Previous work [125] has developed a method for performing electron dynamics calculations in a MMPol approach, but made the critical assumption that the polarizability of the MM sites was frequency independent. In other words, the response of the polarizable environment considers only an instantaneous static field perturbation by ignoring the "memory", history or frequency of the perturbation. This assumption holds for systems which fulfill the "non-resonant condition" that the perturbing frequencies are very different than the intrinsic response or the optical excitation frequencies of the environment. This assumption breaks down when the absorption bands of the environment and system of interest overlap as well as when the full spectrum of the system of interest is desired. To properly describe environment response in the presence of near-resonant perturbations, the polarizability must be frequency dependent.

Here we begin with expressing the induced dipoles as a power series in the perturbing field [126, 127]

$$\begin{aligned}\tilde{\boldsymbol{\mu}}(\omega,\omega',\dots) = \boldsymbol{\mu}_0 &+ \tilde{\boldsymbol{\alpha}}(\omega)\tilde{\boldsymbol{E}}(\omega) \\ &+ \tilde{\boldsymbol{\beta}}(\omega,\omega')\tilde{\boldsymbol{E}}(\omega)\tilde{\boldsymbol{E}}(\omega') + \dots\end{aligned} \tag{4.1}$$

where $\tilde{\boldsymbol{\alpha}}(\omega)$ is the frequency-dependent polarizability tensor, which is related to the linear refractive index and is responsible for linear absorption. $\tilde{\boldsymbol{\beta}}(\omega,\omega')$ is the first hyperpolarizability which gives rise to the second-harmonic generation and optical rectification. In this work, we will focus on introducing $\tilde{\boldsymbol{\alpha}}(\omega)$ into the framework of a dipole-based polarizable force field.

The first-order frequency-dependent dipole term in eq. (4.1) is

$$\tilde{\boldsymbol{\mu}}(\omega) = \tilde{\boldsymbol{\alpha}}(\omega)\tilde{\boldsymbol{E}}(\omega) \tag{4.2}$$

Fourier transforming eq. (4.2) and applying the convolution theorem leads to the time-dependent dipole moment formalism,

$$\boldsymbol{\mu}(t) = \int_{-\infty}^{t} \boldsymbol{\alpha}(t - t')\boldsymbol{E}(t')dt' \tag{4.3}$$

Equation (4.3) suggests that the time-dependent dipole moment has a notion of "history," as it depends on the value of the electric field at all previous times.

To deploy eq. (4.3) in the context of a polarizable force field, a time-dependent expression of the polarizability is required. We proceed as follows. Linear response theory can be used to obtain an expression for the frequency-dependent polarizability, which is given by the dipole-dipole linear response function

$$\tilde{\alpha}_{ab}(\omega) = \sum_{n>0} \left\{ \frac{\langle \mathbf{0} | \hat{\mu}_a | \boldsymbol{n} \rangle \langle \boldsymbol{n} | \hat{\mu}_b | \mathbf{0} \rangle}{\omega - \omega_{n0}} - \frac{\langle \mathbf{0} | \hat{\mu}_b | \boldsymbol{n} \rangle \langle \boldsymbol{n} | \hat{\mu}_a | \mathbf{0} \rangle}{\omega + \omega_{n0}} \right\} \tag{4.4}$$

where a and b are Cartesian coordinates. In eq. 4.4, ω and ω_{n0} are the driving frequency of the external perturbation and the resonant frequencies of the perturbed molecular system. In polarizable force fields, isotropic polarizabilities are usually employed. [16] Under such an assumption, eq. (4.4) reduces to

$$\tilde{\alpha}(\omega) = \sum_{n>0} -| \langle \boldsymbol{n} | \hat{\mu} | \mathbf{0} \rangle |^2 \frac{2\omega_{n0}}{\omega^2 - \omega_{n0}^2} \tag{4.5}$$

A time dependent polarizability can then be recovered via Fourier transform

$$\alpha(t) = \sum_{n>0} | \langle \boldsymbol{n} | \hat{\mu} | \mathbf{0} \rangle |^2 \sin(\omega_{n0} t). \tag{4.6}$$

Equation (4.6) is a simple trigonometric polynomial that requires the knowledge of transition dipole moments and resonant frequencies, which are both readily obtainable or parameterized from spectroscopic measurements and/or electronic structure calculations.

In a complex molecular system, the time-dependent dipole moment in eq. (4.3) usually does not have an analytically integrable expression. The complexity arises from the unknown

form of the electric field at each polarizable site. In this work, we discretize the electric field's evolution in time, assuming that over a short interval, it is constant,[128, 30]

$$\begin{aligned}\boldsymbol{E}(t) = \boldsymbol{E}(t_{-\infty}) \\ &+ (\boldsymbol{E}(t_0) - \boldsymbol{E}(t_{-\infty}))\Theta(t - t_0) + \dots \\ &+ (\boldsymbol{E}(t_k) - \boldsymbol{E}(t_{k-1}))\Theta(t_k - t_{k-1})\end{aligned} \tag{4.7}$$

for $t_k \leq t < t_{k+1}$. Inserting $\Delta\boldsymbol{E}_k = \boldsymbol{E}(t_k) - \boldsymbol{E}(t_{k-1})$ into the integral in eq. (4.3), we have

$$\boldsymbol{\mu}(t) = \boldsymbol{\mu}(t_{-\infty}) + \sum_{i=0}^{k} \Delta\boldsymbol{E}_i \int_{t_i}^{t} \alpha(t - t')dt' \tag{4.8}$$

Because the time-dependent polarizability in eq. (4.6) has an easily integrable form, this expression can be simplified to

$$\begin{aligned}\boldsymbol{\mu}(t) = \boldsymbol{\mu}(t_{-\infty}) \\ &+ \sum_{i=0}^{k} \Delta\boldsymbol{E}_i \sum_{n>0} \frac{|\langle \boldsymbol{n}| \hat{\mu} |\boldsymbol{0}\rangle|^2}{\omega_{n0}} (1 - \cos(\omega_{n0}(t - t_i)))\end{aligned} \tag{4.9}$$

Equation (4.9) will serve as the theoretical foundation for introducing the frequency-dependent polarizability into the framework of a polarizable force field, namely ωMMPol. It should be noted that, due to the interest in correctly capturing the optical response of the environment, nuclear motion is currently neglected in ωMMPol, and any vibrational, rotational, and geometric relaxation contributions to environment polarization response will not be captured. This approximation is sufficient for short timescales on which nuclear motion will be small.

In this work, we investigate the effect of a frequency-dependent or non-instantaneous polarizable environment in the form of eq. (4.9) on the electronic dynamics of a simple test system. Understanding the interplay between the time-dependent quantum system and ωMMPol is crucial not only for laying the theoretical groundwork and validation for the proposed ωMMPol, but also for providing physical insight into the non-equilibrium photochemical dynamics.

The time-dependent quantum system is modeled in this chapter with the real-time time-dependent density functional theory (RT-TDDFT), equation for TDDFT.

$$i\frac{d\mathbf{P}(t)}{dt} = [\mathbf{K}(t), \mathbf{P}(t)] \tag{4.10}$$

where $\mathbf{K}$ and $\mathbf{P}$ are the Kohn-Sham/Fock and density matrices in the orthonormal basis, respectively. The perturbation from the MMPol region enters the Hamiltonian matrix in the atomic orbital basis (primed notation) as

$$\mathbf{K}'(t) = \mathbf{K}'_{\mathbf{0}}(t, \mathbf{P}'(t)) + \mathbf{V}^{\mathrm{MMPol}}(\mathbf{q}, \boldsymbol{\mu}(t)) \tag{4.11}$$

Note that, in contrast to previous time dependent polarizable embedding models, the dipoles are explicitly time-dependent rather than dependent on time only through the external field and time-dependent electron density.

The term that couples the electronic dynamics to the environmental dynamics is given by

$$\begin{aligned} V_{\lambda\nu}^{\mathrm{MMPol}} = &- \sum_i \langle\lambda| \frac{q_i}{|\boldsymbol{r} - \boldsymbol{\mathcal{R}}_i|} |\nu\rangle \\ &- \sum_p \langle\lambda| \frac{\boldsymbol{\mu}_p(t) \cdot (\boldsymbol{\mathcal{R}}_p - \boldsymbol{r})}{|\boldsymbol{r} - \boldsymbol{\mathcal{R}}_p|^3} |\nu\rangle \end{aligned} \tag{4.12}$$

where the Greek indices refer to atomic orbitals, $\boldsymbol{r}$ is the electronic coordinate, and $\boldsymbol{\mathcal{R}}$ is the coordinate of a site within the MM region. Equation (4.10) is integrated using the modified midpoint unitary transformation (MMUT) approach, a second order "leap-frog" style algorithm,[28, 64, 29, 65]

$$\begin{aligned} \mathbf{P}(t_{k+1}) &= \mathbf{U}(t_k) \cdot \mathbf{P}(t_{k-1}) \cdot \mathbf{U}^\dagger(t_k) \\ \mathbf{U}(t_k) &= \mathbf{C}(t_k) \exp\left[-i2\Delta t\ \boldsymbol{\lambda}(t_k)\right] \mathbf{C}(t_k) \\ \boldsymbol{\lambda}(t_k) &= \mathbf{C}^\dagger(t_k) \cdot \mathbf{K}(t_k) \cdot \mathbf{C}(t_k) \end{aligned} \tag{4.13}$$

where $\mathbf{C}$ and $\boldsymbol{\lambda}$ are the eigenvectors and eigenvalues of the Kohn-Sham/Fock matrix.

The electric field at any time can be calculated as follows

$$\boldsymbol{E}(t, \boldsymbol{\mathcal{R}}_p) = \sum_{\lambda,\nu} P'_{\lambda\nu}(t) \langle\lambda| \frac{\boldsymbol{\mathcal{R}}_p - \boldsymbol{r}}{|\boldsymbol{r} - \boldsymbol{\mathcal{R}}_p|^3} |\nu\rangle + \sum_{p' \neq p} \mathbf{T}_{pp'} \cdot \boldsymbol{\mu}_{p'}(t) + \boldsymbol{E}_{ext}(t) \tag{4.14}$$

$$+ \boldsymbol{E}_{q,nuc} \tag{4.15}$$

where $\boldsymbol{E}_{q,nuc}$ gathers the electric field from the point charges and nuclei and $\mathbf{T}_{pp'}$ is the dipole relay matrix, defined as

$$\mathbf{T}_{pp'} = S^{(3)}_{pp'} \frac{\mathbf{1}}{|\boldsymbol{\mathcal{R}}_p - \boldsymbol{\mathcal{R}}_{p'}|^3} - 3S^{(5)}_{pp'} \frac{(\boldsymbol{\mathcal{R}}_p - \boldsymbol{\mathcal{R}}_{p'})(\boldsymbol{\mathcal{R}}_p - \boldsymbol{\mathcal{R}}_{p'})}{|\boldsymbol{\mathcal{R}}_p - \boldsymbol{\mathcal{R}}_{p'}|^5} \tag{4.16}$$

where $S^{(3)}_{pp'}$ and $S^{(5)}_{pp'}$ are screening and damping functions that are introduced in the model in order to avoid overpolarization. [66] A complete review of our MMPol implementation can be found in ref. 53.

4.3 A numerical validation

To validate the model and understand the fundamental physical behavior of ωMMPol, we consider a single ωMMPol site driven by a continuous oscillatory external wave with a frequency of $\omega = 0.4746$ a.u. and an amplitude of 0.025 a.u. For these simulations, three values of ω_{n0} for the ωMMPol site were explored: 0.2, 0.45, and 0.6 a.u. (referred to as the driving-above, driving-near, and driving-below resonance cases, respectively). In order to analyze these simulations as different perturbations on the same ground state, the extrapolated polarizability of each polarizable site was set to 5 a.u. by tuning the squared transition dipole moment ($|\langle\boldsymbol{n}|\hat{\mu}|\mathbf{0}\rangle|^2$) to 0.5, 1.125, and 1.5 a.u. for the ω_{n0} equal to 0.2, 0.45, and 0.6 a.u. cases, respectively. These cases were compared to the instantaneous propagation method for reference, and the explicitly propagated cases provide insight into systems that are driven with a frequency above, near, and below the environment's response, respectively.

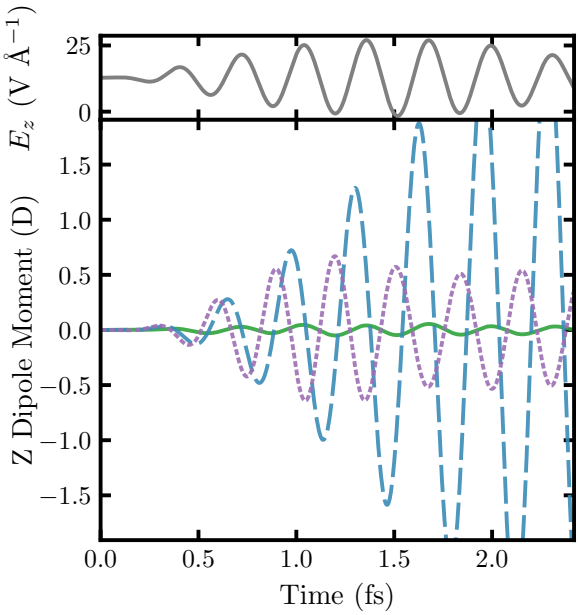

Figure 4.1: Induced dipole response to an external field of 0.4764 a.u. The induced dipoles had fundamental frequencies of 0.2 (green, solid), 0.45 (blue, dashed), and 0.6 (purple, dotted) a.u. The top panel shows the external field (grey).

Figure 4.1 shows the induced dipole's response at the ωMMPol site to an external continuous wave. As a framework for understanding the non-instantaneous response of the induced dipoles in the environment, consider an undamped, driven harmonic oscillator.[129] If the driving force has a higher frequency than the oscillator's fundamental frequency ($\omega > \omega_{n0}$), the oscillator cannot respond quickly enough to the driving force, and nearly no response is expected. Similarly, if the driving force is higher in frequency than the oscillator's fundamental frequency ($\omega < \omega_{n0}$), the oscillator will have enough time to come to equilibrium with the driving force, and a steady state solution is expected to be achieved quickly. For the case where the driving force is near resonance ($\omega \approx \omega_{n0}$), the oscillator is expected to exhibit large response. As can be seen in fig. 4.1, the response of the induced dipole behaves like a driven oscillator; the driving-above-resonance case has little response, the driving-below-resonance case achieves steady state quickly, and the driving-near-resonance case demonstrates a large

response.

When a ωMMPol site is coupled to a time-dependent QM subsystem, the total system will undergo a complex time-evolution due to the time-dependent mutual polarization between the QM and MM subsystems. The goal of TDQM/ωMMPol model is to provide inexpensive, yet sufficiently accurate descriptions of the time-dependent mutual polarization that governs non-equilibrium photophysical processes. The following discussion will focus on the effect of the non-instantaneously responding environment on the quantum electronic dynamics.

One of the simplest and most intuitive test cases in time-dependent quantum mechanics is Rabi oscillations – a phenomenon in two level systems which causes population inversion between states when driven on resonance with the excitation energy. In these simulations, the two-level system is generated by H_2^+ with the minimal STO-3G basis set.[28] Note that because this system is a one-electron doublet state, it does not suffer from the two-electron Rabi frequency shift due to the irrepresentable closed-shell singlet excited states.[28, 130]

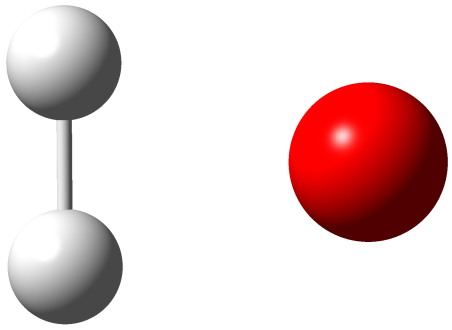

Figure 4.2: (a) H_2^+ (white) with a single polarizable site (red) orthogonal to the bonding axis. (b) H_2^+ in an octahedron of polarizable sites.

The hydrogen nuclei are placed at the ground state bond distance of 1.0603 Å apart. At this bond distance, the resonant $D_0 \rightarrow D_1$ excitation frequency of H_2^+ is 0.4746 a.u. at the TDHF/STO-3G level of theory. A single ωMMPol site was placed 1.5$\times$ the bond distance away from H_2^+ center, shown in fig. 4.2a. The system was perturbed with an external field

with a frequency $\omega = 0.4746$ a.u., in resonance with the optical excitation of H_2^+ quantum subsystem. The amplitude of the field is chosen to be 0.025 a.u., polarized along the bonding axis of H_2^+. Three values of $\omega_{n0} = 0.2, 0.45, 0.6$ a.u. for the ωMMPol site were explored and compared to equilibrium MMPol for reference.

The occupations of the D_0 and D_1 states in each simulation are shown in fig. 4.3. In the absence of frequency-dependent polarizability at the MMPol site (the static case in fig. 4.3a), the Rabi frequency is $\Omega = 0.0273$ a.u. When the fundamental frequency of the ωMMPol site is off-resonant with respect to the driving field (fig. 4.3b and fig. 4.3d), the most noticeable change is a slight speed-up and slow-down of the frequency of population inversion: the frequency of population inversion is 0.0278 a.u. for the driving-above-resonance case and 0.0271 a.u. for the driving-below-resonance case, compared to the static case, with a Rabi oscillation of 0.0273 a.u. When the fundamental frequency of the ωMMPol site is off-resonant with respect to the driving field (both externally and internally), its effect on the QM Rabi oscillations can be understood from perturbation theory, [131, 28]

$$\tilde{\Omega} = \sqrt{|d||E_{eff}| + (\omega - \omega_{n0}^{QM})^2} \tag{4.17}$$

where d and E_{eff} are the transition dipole moment and effective field amplitude, respectively. ω_{n0}^{QM} is the fundamental excitation frequency of the QM system. Equation (4.17) suggests that in the perturbative regime, the observed Rabi frequency depends on the effective field E_{eff} acting on the QM system and the frequency ω of the external driving field. When the ωMMPol is driven by external perturbing waves and internal field from the QM site, it, in return, generates an oscillating field, similar to those observed in fig. 4.1, to polarize the QM site. In other words, the effective field acting on the QM subsystem can be written as

$$E_{eff} = E^{external} + E^{\omega\text{MMPol}} \tag{4.18}$$

where $E^{\omega\text{MMPol}}$ is directly related to the additional polarization potential in eq. (4.12). In order to evaluate the effect of the field originating from the MM region, the normalized z component of the electric dipole of both the QM and MM systems is plotted in fig. 4.4.

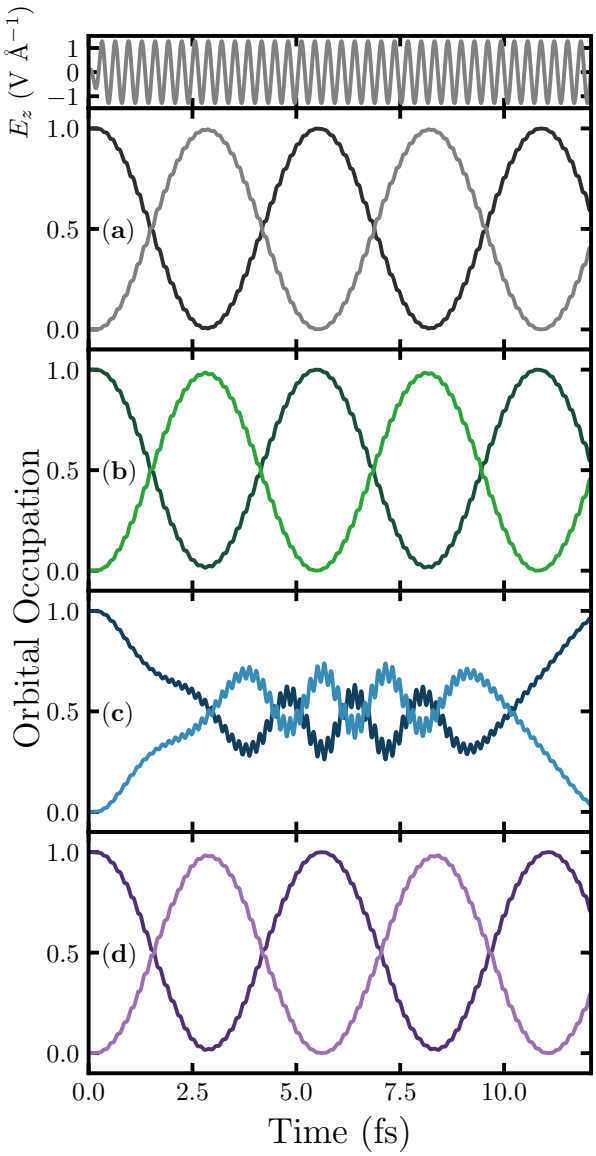

Figure 4.3: Occupations of the first (dark) and second (light) molecular orbitals in H_2^+ for the models with an instantaneous induced dipole (a, grey), and with an induced dipole with fundamental frequencies of 0.2 (b, green), 0.45 (c, blue), and 0.6 (d, purple) a.u. The top panel shows the external field (grey).

Both the off-resonant simulations exhibit primarily the same frequency in both the QM and MM region. In the driving-above-resonance case, the MM dipole oscillates approximately

in phase with the QM dipole. This observation suggests that the field generated by the ωMMPol site strengthens the effective field acting on the QM site, giving rise to a faster Rabi oscillation. For the driving-below-resonance case, the MM dipole oscillates anti-phase with the QM dipole, weakening the effective field and slowing down the Rabi oscillation at the QM site. These analyses validate the proposed TDQM/ωMMPol model in the perturbative regime when the ωMMPol site is off-resonant with respect to the driving field.

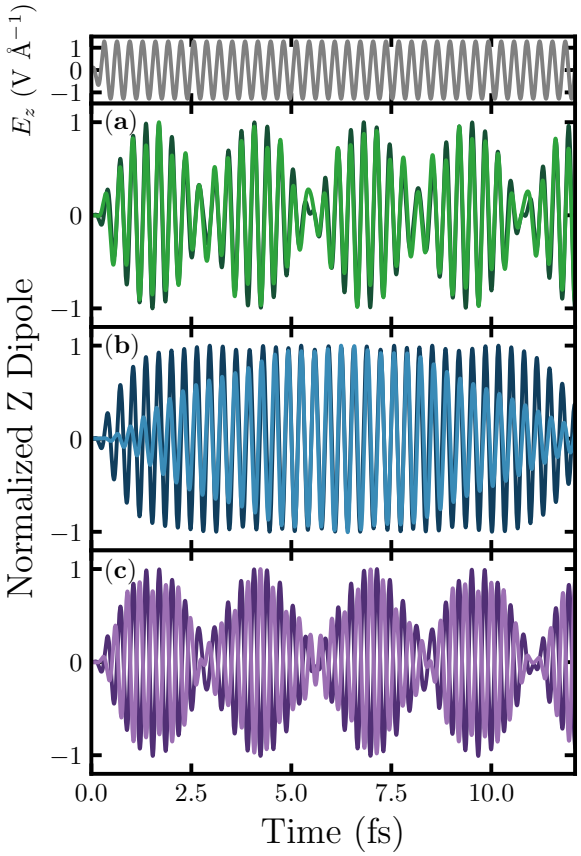

Figure 4.4: Normalized z dipole moment for both the QM (dark) and MM (light) regions the models with an induced dipole with fundamental frequencies of 0.2 (a, green), 0.45 (b, blue), and 0.6 (c, purple) a.u. The top panel shows the external field (grey).

Clearly, the largest modification of Rabi oscillation behavior occurs for the near-resonance

case, where the population never reaches full inversion (fig. 4.3c). This is when the proposed TDQM/ωMMPol model becomes very important for illustrating the photochemical dynamics in the strong non-perturbative, non-equilibrium regime. In the near-resonance case, the time-dependent mutual polarization between the QM and MM regions causes a non-constant phase relationship (fig. 4.4b), which contributes to the the frequency de-tuning term $(\omega - \omega_{n0})$ in eq. (4.17). However, eq. (4.17) with a frequency de-tuning is only applicable in the perturbative regime and can not resolve the destruction of the Rabi oscillation behavior observed in fig. 4.3c.

The electric fields, including terms from both the external perturbation and the ωMMPol region, at the center of H_2^+ is given in fig. 4.5. In terms of amplitude, the field originating from the ωMMPol dipole dominates in the near-resonant case, and is only a small perturbation in the driving-above-resonance case. The amplitude of the driving-below-resonance case has approximately equal contributions from both the MM and external fields. In the near-resonance case, the resonant condition between the QM subsystem and the external field is suppressed by the internal field generated by the ωMMPol site, driving the QM system off resonance. In other words, the polarization from the environment significantly modifies the resonant condition of the QM system.

The test case of a single polarizable site next to H_2^+ provides essential theoretical insight into the underlying interactions between the QM and ωMMPol subsystems, but the power of any QM/MM approach lies in an explicit description of an extended environment. Here we first systematically expand the H_2^+ model through the addition of multiple excitation frequencies and multiple polarizable sites.

Figure 4.6 shows the influence of a polarizable site with all previously mentioned excitation energies (0.2, 0.45, and 0.6 a.u.) and their respective transition dipole moments (0.5, 1.125, and 1.5 a.u.) on the Rabi oscillations of H_2^+. The Rabi oscillations in this case are modified in a similar manner to the near-resonance case above. This result is expected; whenever a perturbation is close to a fundamental frequency of the polarizable site, the response corresponding to that frequency should dominate.

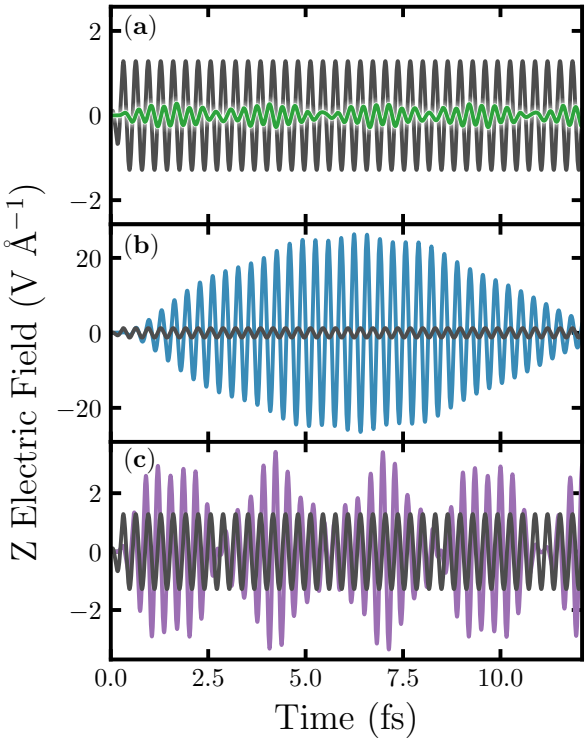

Figure 4.5: z component of the electric field in the center of H_2^+ for the models with fundamental frequencies of 0.2 (a, green), 0.45 (b, blue), and 0.6 (c, purple) a.u. The external field is shown for comparison on each (dark, grey).

Figure 4.7 shows the Rabi oscillations of H_2^+ placed in an octahedron of polarizable sites, each site 1.5× the bond length from the H_2^+ center, shown in fig. 4.2b. As before, the polarizable sites were set to have excitation energies of $\omega_{n0} = 0.2$, 0.45, and 0.6 a.u. Similar to the conclusions in the single polarizable site simulations above, the driven-above and driven-below resonance cases belong to the perturbative regime, but the near-resonant case significantly modifies the resonance condition of the H_2^+, causing a complete destruction of the Rabi oscillations. Specifically, the effect of the driven-above and driven-below resonance cases is simply a modification of the external field. Interestingly, due to the increased number of sites, this modification to the field is large enough to create an incomplete population inversion, which indicates that the effective field is detuned with respect to the resonant

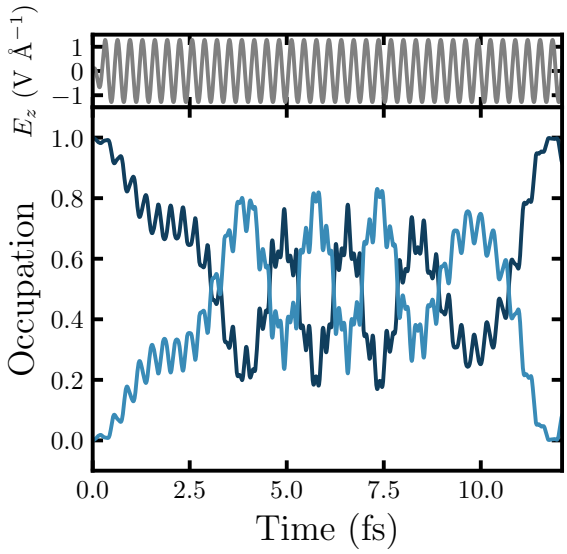

Figure 4.6: Occupations of the first (dark) and second (light) molecular orbitals in H_2^+ next to a polarizable site with fundamental frequencies of 0.2, 0.45, and 0.6 a.u. The top panel shows the external field.

condition of the H_2^+.

4.4 Application to Charge Transfer Dynamics

Solvation is widely known to significantly modify charge transfer processes, and the development of the QM/ωMMPol method enables studying charge transfer processes within a realistically responding environment. Here, we investigate the effects of a ωMMPol environment on the charge transfer dynamics of *para*-nitroaniline (pNA). pNA is widely studied by both theoreticians [132, 133] and experimentalists,[134, 133] and serves as a useful benchmark for novel solvation methods. In this study, we focus on pNA in a tetrachloromethane (CCl_4) solvent. The structure was generated by placing 50 CCl_4 molecules in a 20 Å box surrounding the pNA, [135] then a chemically reasonable structure was obtained by optimizing the structure in an ONIOM framework at the B3LYP/6-31G(d)[136, 137, 81] and UFF[138] level of theory. The resulting structure is given in fig. 4.8. Charges for each of the

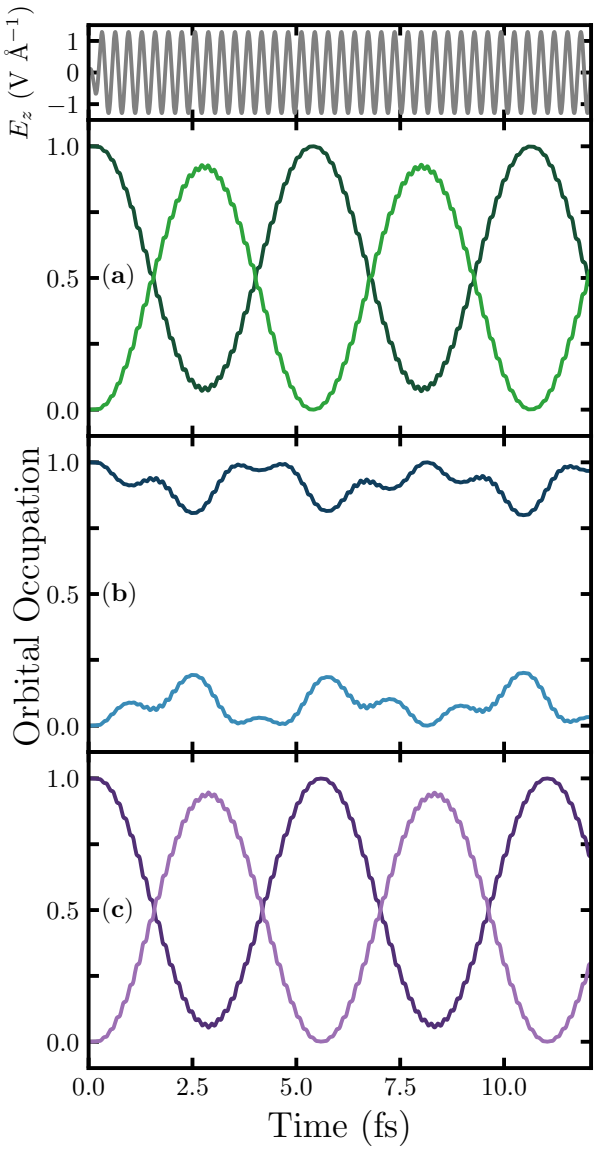

Figure 4.7: Occupations of the first (dark) and second (light) molecular orbitals in H_2^+ in an octahedron of polarizable sites with fundamental frequencies of 0.2 (a, green), 0.45 (b, blue), and 0.6 (c, purple) a.u. The top panel shows the external field (grey).

CCl_4 atoms were obtained from a Mulliken population analysis on an isolated CCl_4 molecule, and the first twenty excited states were used to determine ω_{n0} and the transition dipole mo-

ments. All transition dipole moments were scaled to reproduce the static polarizability when extrapolated to $\omega = 0$. Specifics about this parameterization can be found in the Supporting Information. The pNA was modeled with the 6-31G(d) basis set[81] and B3LYP[136, 137] functional across all simulations.

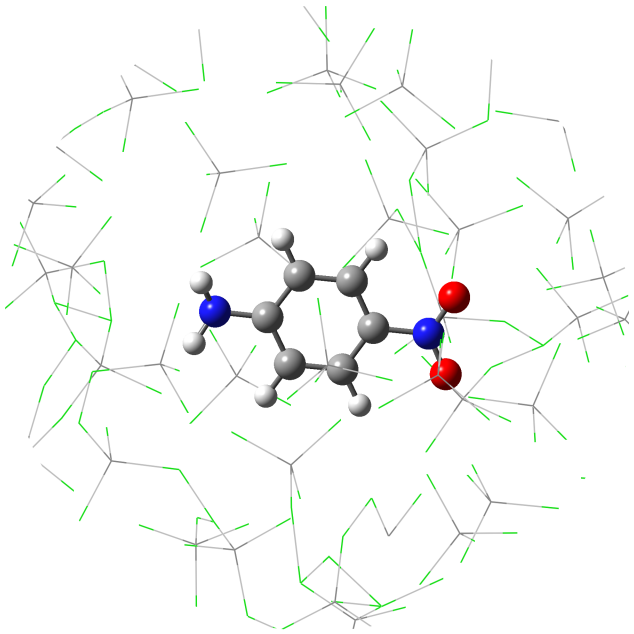

Figure 4.8: Schematic showing *para*-nitroaniline (pNA) solvated by CCl_4. The quantum mechanical region is represented by a ball and stick model, and the ωMMPol region is represented by a wire model.

The charge transfer dynamics within pNA were initialized by promoting an electron from the HOMO to the LUMO, which dominates the charge transfer excited state. The occupation of the HOMO and LUMO are presented in fig. 4.9 for pNA in vacuum, pNA in instantaneously propagated MMPol CCl_4, and pNA in the ωMMPol CCl_4 solvent. The charge transfer dynamics in vacuum are characterized by a rapid decay of the excited state after a single femtosecond, followed by a fractional repopulation of the LUMO at $\sim$2 fs. In contrast, the dynamics within both the instantaneous MMPol and the ωMMPol solvent demonstrate a considerably increased lifetime, since the presence of the polarizable CCl_4

extends the lifetime of the excited state by stabilizing the large dipole moment created by the charge transfer. In the instantaneously propagated solvent, this transition is stabilized to an artificially high degree, due to the rapid response of the environment to any oscillation of electronic density. This artificially high stabilization is strong enough to extend the lifetime of the excited state beyond the time of this simulation. The ωMMPol solvent responds to the modified electron density in a more realistic manner, providing a stabilization of the excited state, but collapsing out of the excited state around 7 fs. This indicates that including the frequency dependent response of the solvent is essential to describing photochemical processes in solution.

4.5 Summary

In this chapter, a method for integrating frequency dependent behavior with polarizable force fields is proposed, namely ωMMPol. This is then coupled with a real-time quantum mechanical method, and the effect of a non-instantaneously responding environment on electronic dynamics is investigated. In all cases, the environment interacts with the QM subsystem through a modification of the effective electric field within the QM subsystem. When the excitation frequencies in the environment are off-resonant with the excitation frequencies of the QM subsystem, the environmental contribution to the effective electric field is on the same order, or smaller, as the external field. In these cases, the frequency dependent environment behaves as an additional perturbation on the QM subsystem. When the excitation energies of the environment is nearly resonant with the excitation energies of the QM subsystem, the environmental response dominates the effective electric field, and can no longer be treated as a small perturbation. In this non-perturbative regime, the mutual interaction between the QM and MM subsystems causes a destruction of the Rabi oscillation behavior by modifying frequency detuning. This destruction is maintained when extending the system towards realistic environmental configurations. The effectiveness of this method to simulating realistic chemical systems is demonstrated by capturing charge transfer dynamics within a solvated system, and the importance of properly describing the frequency dependent response of the

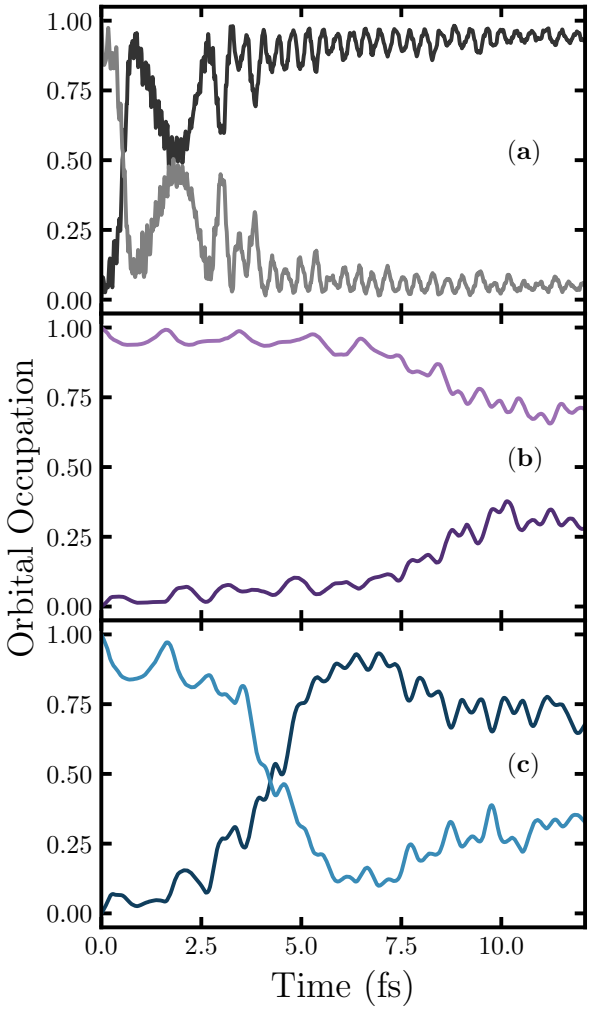

Figure 4.9: HOMO (dark) and LUMO (light) occupation for *para*-Nitroaniline (pNA) after photoexcitation in vacuum (a, gray), in instantaneous MMPol (b, purple), and in ωMMPol CCl_4 (c, blue).

environment is shown by the drastically different dynamics within an instantaneous MMPol solvent and an ωMMPol environment. The model proposed within offers an effective method for investigating time dependent phenomena in complex environments, especially when the response of the primary system and its environment are close in energy.

Chapter 5

AB INITIO NUCLEAR DYNAMICS WITH REAL TIME NUCLEAR ELECTRONIC ORBITAL THEORY

The previous two chapters described quantum dynamics within a frozen-nuclei approximation. This limits the timescales on which those simulations can be relevant, so in this chapter we develop a model that allows some nuclei to move quantum mechanically using the nuclear electronic orbital (NEO) approach. Other approaches to including quantum nuclear motion often treat electrons and nuclei as very separate objects, but the NEO approach is elegant in that it treats both nuclei and electrons on the same footing. This allows us to develop a model for quantum nuclear motion while still using the formalism of real-time propagation. This work was adapted with permission from Zhao, L., Tao, Z., Pavošević, F., Wildman, A., Hammes-Schiffer, S. and Li, X., 2020. Real-Time Time-Dependent Nuclear-Electronic Orbital Approach: Dynamics beyond the Born-Oppenheimer Approximation. The Journal of Physical Chemistry Letters, 11(10), pp.4052-4058.

5.1 Motivation

First-principles simulation of the time evolution of a quantum system is a powerful tool to probe the underlying physical principles of ultrafast, nonequilibrium, and nonadiabatic chemical processes with spatial and temporal resolution unparalleled by most experiments. The exact non-relativistic quantum dynamics formally mandates treatment in the framework of the full time-dependent Schrödinger equation for the entire (electronic plus nuclear) system. This treatment represents a computationally prohibitive prospect for all but the smallest of molecules with a few active electrons.

Various approximations based on the nature of the chemical system of interest have been introduced with the aim of achieving reliable results at lower computational cost. The existing approaches for quantum dynamics rely heavily on semi-classical approximations, in which nuclei are treated as classical particles and/or electronic degrees of freedom are represented by a relatively small number of electronic potential energy surfaces. These methods include Ehrenfest dynamics,[139, 140, 64, 141, 88, 142] surface hopping,[143, 144, 145, 146, 147] *ab initio* multiple spawning,[148, 149, 150, 151] multiconfigurational time-dependent Hartree (MCTDH)[152, 153], and Gaussian wave packet dynamics.[154, 155] However, without treating nuclei fully quantum mechanically, effects such as quantized vibrational states, vibronic coupling, and nuclear tunneling would be difficult to describe, if not impossible. On the other hand, quantum dynamics of electronic degrees of freedom is needed when a molecular reaction is subject to a strong field perturbation or in the strong nonadiabatic regime where electronic adiabatic potential energy surfaces are no longer well-defined.

This chapter aims to introduce a full quantum description of coupled nuclear-electronic dynamics that follows the time-dependent variational principle and treats both electronic and specified nuclear degrees of freedom on equal footing. Such a computational framework will allow for quantum dynamical studies of proton-coupled electron transfer,[156, 157] thermally activated singlet fission,[158, 159] and quantum decoherence.[160, 161] Obtaining fundamental knowledge of these processes could potentially aid the development of artificial photosynthesis,[162] light-harvesting materials,[163] and scalable quantum computers.[164]

A promising and computationally tractable approach is based on the multicomponent nuclear-electronic orbital (NEO) framework, which treats specified nuclei quantum mechanically on the same level as the electrons with molecular orbital techniques.[165, 166, 167, 168] The NEO approach has been implemented in conjunction with methods widely used in electronic structure theory, such as Hartree-Fock (HF),[165] density functional theory (DFT),[168, 169, 170] perturbation theory,[171] coupled-cluster,[172, 173] and multi-reference methods[165] to study coupled nuclear-electronic quantum effects in both ground and excited states.

Quantum mechanical solutions based on the time-independent Schrödinger equation within the NEO framework have been successfully applied to study proton delocalization in the ground state wavefunctions of small molecules.[165, 166, 167, 168, 169, 172] Recently, the NEO approach has been extended to investigate both electronic and proton vibrational excited states with the linear response[174] and equation-of-motion[173] formalisms. While these methodological advances can provide stationary characteristics of combined electronic and protonic quantum mechanical systems, studies of nonequilibrium nonadiabatic processes require the solution of the time-dependent Schrödinger equation.

5.2 Theory

The dynamics of electrons and protons are determined by the time-dependent Schrödinger equation,

$$i\hbar\frac{\partial}{\partial t}\Psi_{\mathrm{NEO}}(\boldsymbol{x}^{\mathrm{e}},\boldsymbol{x}^{\mathrm{p}};t)=H(\boldsymbol{x}^{\mathrm{e}},\boldsymbol{x}^{\mathrm{p}};t)\Psi_{\mathrm{NEO}}(\boldsymbol{x}^{\mathrm{e}},\boldsymbol{x}^{\mathrm{p}};t) \tag{5.1}$$

in which $\boldsymbol{x}^{\mathrm{e}}$ and $\boldsymbol{x}^{\mathrm{p}}$ are the coordinates including both spatial and spin degrees of freedom for electrons and protons, respectively. For single-determinant methods, *e.g.*, HF and DFT, the wavefunction assumes the form of the following ansatz,

$$\Psi_{\mathrm{NEO}}(\boldsymbol{x}^{\mathrm{e}},\boldsymbol{x}^{\mathrm{p}};t)=\Phi^{\mathrm{e}}(\boldsymbol{x}^{\mathrm{e}};t)\Phi^{\mathrm{p}}(\boldsymbol{x}^{\mathrm{p}};t) \tag{5.2}$$

in which Φ^{e} and Φ^{p} are single Slater determinants for the electrons and protons.

By taking advantage of the product separable form of the wavefunction ansatz, eq. (5.1) can be written as two coupled differential equations that describe the motions of the electrons and protons:

$$\begin{aligned} i\hbar\frac{\partial}{\partial t}\boldsymbol{C}^{\mathrm{e}}(t)&=\boldsymbol{F}^{\mathrm{e}}(t)\boldsymbol{C}^{\mathrm{e}}(t)\\ i\hbar\frac{\partial}{\partial t}\boldsymbol{C}^{\mathrm{p}}(t)&=\boldsymbol{F}^{\mathrm{p}}(t)\boldsymbol{C}^{\mathrm{p}}(t) \end{aligned} \tag{5.3}$$

where $\boldsymbol{C}^{\mathrm{e}}(t)$ and $\boldsymbol{C}^{\mathrm{p}}(t)$ are the time-dependent orbital coefficients for the electrons and protons, respectively. $\boldsymbol{P}$ is the one-particle density matrix and $\boldsymbol{F}$ is the Fock/Kohn-Sham matrix, both in the orthonormal atomic orbital basis. Note that we will use primed notations

(*e.g.*, $\boldsymbol{F}'$ and $\boldsymbol{P}'$) for quantities in the non-orthogonal atomic orbital basis. In this chapter, the orthonormal basis is obtained with the Löwdin orthogonalization scheme.[175]

The Fock/Kohn-Sham matrices can be split into single- and multi-component contributions,

$$\begin{aligned} \boldsymbol{F}^{\mathrm{e}}(t) &= \boldsymbol{H}^{\mathrm{ee}}(t, \boldsymbol{P}^{\mathrm{e}}(t)) + \boldsymbol{H}^{\mathrm{ep}}(\boldsymbol{P}^{\mathrm{e}}(t), \boldsymbol{P}^{\mathrm{p}}(t)) \\ \boldsymbol{F}^{\mathrm{p}}(t) &= \boldsymbol{H}^{\mathrm{pp}}(t, \boldsymbol{P}^{\mathrm{p}}(t)) + \boldsymbol{H}^{\mathrm{pe}}(\boldsymbol{P}^{\mathrm{p}}(t), \boldsymbol{P}^{\mathrm{e}}(t)) \end{aligned} \tag{5.4}$$

The single-component contributions to the Fock/Kohn-Sham matrices are

$$\begin{aligned} \boldsymbol{H}^{\mathrm{ee}}(t, \boldsymbol{P}^{\mathrm{e}}(t)) &= \boldsymbol{H}^{\mathrm{e}}_{\mathrm{core}} + \boldsymbol{J}^{\mathrm{ee}}(\boldsymbol{P}^{\mathrm{e}}(t)) + \zeta \boldsymbol{K}^{\mathrm{ee}}(\boldsymbol{P}^{\mathrm{e}}(t)) + (1-\zeta)\boldsymbol{V}^{\mathrm{e}}_{xc}(\boldsymbol{P}^{\mathrm{e}}(t)) + \boldsymbol{V}^{\mathrm{e}}_{ext}(t) \\ \boldsymbol{H}^{\mathrm{pp}}(t, \boldsymbol{P}^{\mathrm{p}}(t)) &= \boldsymbol{H}^{\mathrm{p}}_{\mathrm{core}} + \boldsymbol{J}^{\mathrm{pp}}(\boldsymbol{P}^{\mathrm{p}}(t)) + \zeta \boldsymbol{K}^{\mathrm{pp}}(\boldsymbol{P}^{\mathrm{p}}(t)) + (1-\zeta)\boldsymbol{V}^{\mathrm{p}}_{xc}(\boldsymbol{P}^{\mathrm{p}}(t)) + \boldsymbol{V}^{\mathrm{p}}_{ext}(t) \end{aligned} \tag{5.5}$$

in which $\boldsymbol{H}_{\mathrm{core}}$ is the core Hamiltonian that includes the kinetic energy and the interaction with the classical nuclei. $\boldsymbol{J}^{\mathrm{ee(pp)}}$ and $\boldsymbol{K}^{\mathrm{ee(pp)}}$ are the Coulomb and HF exchange matrices, respectively, between electrons (protons). $\boldsymbol{V}^{\mathrm{e}}_{xc}$ and $\boldsymbol{V}^{\mathrm{p}}_{xc}$ are the electron-electron and proton-proton exchange-correlation potentials. ζ is a parameter that converts the Fock matrix between HF ($\zeta = 1$) and DFT ($\zeta = 0$), and $\boldsymbol{V}_{ext}(t)$ is the time-dependent external potential such as an electric field. The multi-component contributions to the Fock matrices are given by

$$\begin{aligned} \boldsymbol{H}^{\mathrm{ep}}(\boldsymbol{P}^{\mathrm{e}}(t), \boldsymbol{P}^{\mathrm{p}}(t)) &= -\boldsymbol{J}^{\mathrm{ep}}(\boldsymbol{P}^{\mathrm{e}}(t), \boldsymbol{P}^{\mathrm{p}}(t)) + (1-\zeta)\boldsymbol{V}^{\mathrm{ep}}_{c}(\boldsymbol{P}^{\mathrm{e}}(t), \boldsymbol{P}^{\mathrm{p}}(t)) \\ \boldsymbol{H}^{\mathrm{pe}}(\boldsymbol{P}^{\mathrm{p}}(t), \boldsymbol{P}^{\mathrm{e}}(t)) &= -\boldsymbol{J}^{\mathrm{pe}}(\boldsymbol{P}^{\mathrm{p}}(t), \boldsymbol{P}^{\mathrm{e}}(t)) + (1-\zeta)\boldsymbol{V}^{\mathrm{pe}}_{c}(\boldsymbol{P}^{\mathrm{p}}(t), \boldsymbol{P}^{\mathrm{e}}(t)) \end{aligned} \tag{5.6}$$

where $\boldsymbol{J}^{\mathrm{ep}}(\boldsymbol{J}^{\mathrm{pe}})$ is the classical Coulomb interaction between electrons and protons, and $\boldsymbol{V}^{\mathrm{ep}}_{c}(\boldsymbol{V}^{\mathrm{pe}}_{c})$ is the electron-proton correlation potential. Note that the terms $\boldsymbol{J}^{\mathrm{ep}}(\boldsymbol{J}^{\mathrm{pe}})$ and $\boldsymbol{V}^{\mathrm{ep}}_{c}(\boldsymbol{V}^{\mathrm{pe}}_{c})$ explicitly depend on *both* the time-dependent electronic and the protonic densities, and therefore these multi-component contributions introduce strong coupling and vibronic effects.

By multiplying $\boldsymbol{C}^{\mathrm{e}\dagger}(t)\left(\boldsymbol{C}^{\mathrm{p}\dagger}(t)\right)$ to the right of the upper (lower) equations in eq. (5.3),

and subtracting its adjoint, we arrive at the multicomponent Von Neumann's equation,

$$\begin{aligned} i\hbar\frac{\partial}{\partial t}\boldsymbol{P}^{\mathrm{e}}(t) &= [\boldsymbol{F}^{\mathrm{e}}(t,\boldsymbol{P}^{\mathrm{e}}(t),\boldsymbol{P}^{\mathrm{p}}(t)),\boldsymbol{P}^{\mathrm{e}}(t)] \\ i\hbar\frac{\partial}{\partial t}\boldsymbol{P}^{\mathrm{p}}(t) &= [\boldsymbol{F}^{\mathrm{p}}(t,\boldsymbol{P}^{\mathrm{p}}(t),\boldsymbol{P}^{\mathrm{e}}(t)),\boldsymbol{P}^{\mathrm{p}}(t)] \end{aligned} \tag{5.7}$$

It is important to note that the differential equations for the electron and proton density matrices do not evolve independently and are coupled together. The electron density matrix contributes to the proton Fock matrix through the electron-proton Coulomb potential and the electron-proton correlation potential in NEO-DFT, and the proton density matrix contributes to the electron Fock matrix through these same terms. Therefore, these two equations need to be solved simultaneously. In this chapter, eq. (6.2) is propagated in tandem with the modified midpoint unitary transformation (MMUT) algorithm (see the SI for more information),[3, 28] giving rise to the real-time time-dependent NEO formalism (RT-NEO-TDHF and RT-NEO-TDDFT).

The electric-dipole approximation in length gauge to the field-matter operator is invoked to simulate an external electric field. Given the time-dependent electronic and protonic one-particle densities, the time-dependent electronic and nuclear dipole moments can be computed as

$$D^{\mathrm{e}}_{\gamma}(t) = \mathrm{Tr}[\boldsymbol{P}'^{\mathrm{e}}(t)\cdot\boldsymbol{d}'^{\mathrm{e}}_{\gamma}] \tag{5.8}$$

$$D^{\mathrm{p}}_{\gamma}(t) = \mathrm{Tr}[\boldsymbol{P}'^{\mathrm{p}}(t)\cdot\boldsymbol{d}'^{\mathrm{p}}_{\gamma}] \tag{5.9}$$

where $\gamma \in \{x,y,z\}$ and $d^{\mathrm{e(p)}}_{\gamma,\mu\nu} = \langle\mu^{\mathrm{e(p)}}|r_{\gamma}|\nu^{\mathrm{e(p)}}\rangle$. Electronic (protonic) basis functions are denoted as $\mu^{\mathrm{e(p)}}$. The absorption cross section is computed as $\sigma(\omega) \propto \omega\sum_{i=x,y,z}\mathrm{Im}[\tilde{D}_i(\omega)]$, in which $\tilde{D}_i(\omega)$ is the Fourier transform of the time-dependent electron/proton dipole moment.

The RT-NEO-TDHF and RT-NEO-TDDFT algorithms and quantum dynamics are implemented in the Chronus Quantum open source package.[176] LR-NEO-TDHF and LR-NEO-TDDFT calculations were performed with a developer's version of Q-Chem,[177] which will be available in the Q-Chem 5.3 release. The B3LYP [178, 179, 180] functional was used in the DFT calculations, and the epc17-2 functional[170] was used to include the electron-proton correlation effects.

5.3 Spectroscopy

We first apply the RT-NEO-TDHF and RT-NEO-TDDFT methods to predict molecular spectra. The two test systems we choose are the FHF^- and HCN molecules. In these benchmark tests, only protons in addition to electrons are treated quantum mechanically, while the rest of the nuclei are frozen. Three quantum dynamical simulations were carried out, starting from the converged ground state NEO-HF or NEO-DFT wavefunction perturbed with three delta electric fields at $t = 0$ for the duration of one time-step with amplitude 1 mHartree/Å, polarized in the x, y, and z directions.

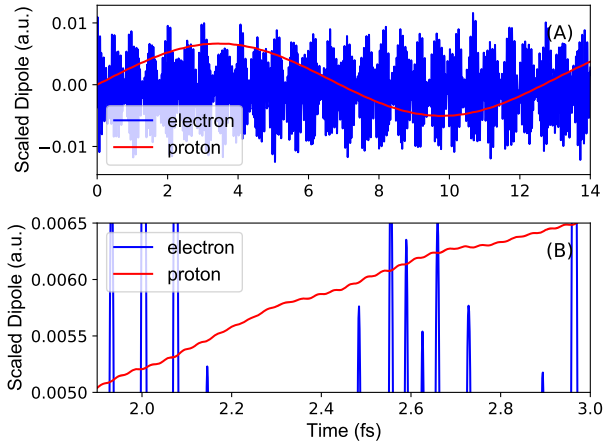

Figure 5.1: Electron and proton dipole moment evolution of RT-NEO-TDDFT for FHF^- for time from 0–14 fs(**A**) and 1.9–3 fs(**B**). Dipole moments are scaled by 10000 and 100 for protons and electrons respectively.

The time-evolutions of the electronic and protonic dipole moments of FHF^- obtained with the RT-NEO-TDDFT approach are plotted in fig. 5.1. Both the electronic and the protonic dipole moments can be seen to oscillate around their equilibrium values. As protons are much heavier than electrons, the protonic vibrational frequency is much lower than that of the electrons. A closer look reveals that the proton dipole moment contains high-frequency components modulated by the oscillations of the electronic dipole moment, as shown in the bottom part of fig. 5.1. These observations show direct evidence that the proton density

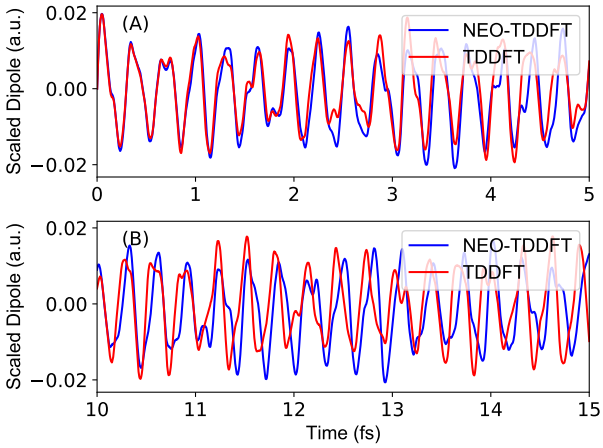

Figure 5.2: Comparison of the total dipole moment evolution between RT-NEO-TDDFT and RT-TDDFT for HCN molecule for short time duration (**A**) and long time duration (**B**).

responds to the change in electron density due to vibronic coupling.

The time evolutions of the total dipole moments of the HCN molecule predicted by the RT-NEO-TDDFT and RT-TDDFT[181, 64] methods are compared in fig. 5.2. It is worth noting that since the proton dipole fluctuations are much smaller than those of the electrons, the total dipole moment is dominated by the electronic component. In the short-time regime, the inclusion of proton motion does not change the dynamics of the total dipole moment significantly because the proton density change is negligible at short times. However, at longer propagation times, the total dipole moment obtained with RT-NEO-TDDFT yields noticeable differences compared to that from RT-TDDFT with a frozen proton, both in terms of frequencies and intensities. This again is due to the presence of electron-proton vibronic coupling.

The time-dependent protonic dipole moment gives rise to vibrational signatures associated with the protonic degrees of freedom. The predicted proton vibrational spectra are plotted in fig. 5.3 for HCN and FHF^-. For linear molecules such as HCN and FHF^-, there are four vibrational modes in total, but only three modes are active when the heavy nuclei are fixed. Furthermore, two among the three visible modes are degenerate, leading

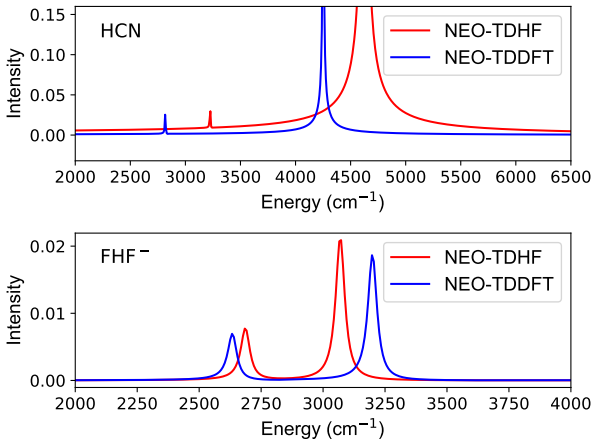

Figure 5.3: Calculated vibrational spectra of HCN (**Top**) and FHF^- (**Bottom**) with RT-NEO-TDHF and RT-NEO-TDDFT .

to only two distinct peaks in the spectrum. The peak positioned at higher energy arises from the stretching motion of the C-H and F-H bonds, and the other low-frequency peak corresponds to the degenerate pair of bending motions. In general, the vibrational frequencies predicted by RT-NEO-TDDFT are shifted by a few hundred cm^{-1} compared to those predicted by RT-NEO-TDHF. Although the results agree with corresponding linear response calculations, there is no uniform trend of the direction of shifting observed in the test systems. These differences can be attributed to the more accurate description of coupled electron-proton quantum dynamics provided by the electron-proton correlation functional in NEO-DFT.[170] At the asymptotic weak perturbation limit, spectra obtained from real-time simulations and linear response calculations should converge,[3] and this is indeed the case, as indicated by the comparison to results obtained with LR-TDHF and LR-TDDFT with the same basis sets and functionals. It is also worth noting that the proton vibrational frequencies are sensitive to both the electronic and nuclear basis sets. Increasing the size of the electronic and nuclear basis sets for the quantum proton has been shown to significantly lower the hydrogen bending frequency in HCN (see SI). [174, 182] The LR-TDDFT method has been benchmarked against a numerically accurate grid-based method,[182] suggesting

that the basis sets used in the current work are sufficient for qualitative agreement and, at the same time, allow for a clear interpretation of the computed spectra.

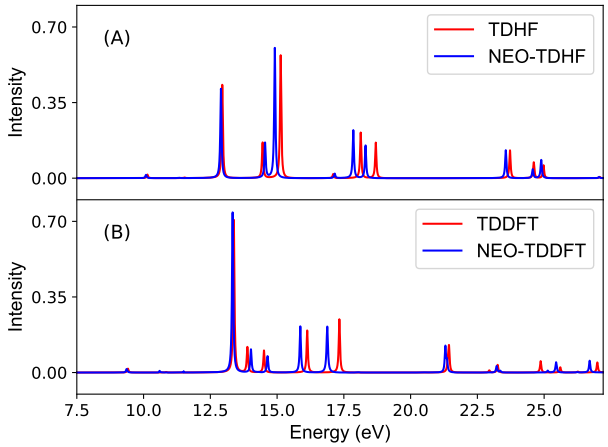

Figure 5.4: Calculated electronic spectra of the HCN molecule: (**A**) RT-NEO-TDHF and RT-TDHF, and (**B**) RT-NEO-TDDFT and RT-TDDFT.

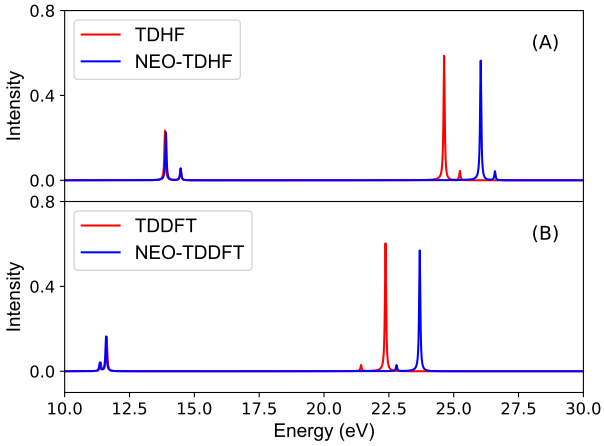

Figure 5.5: Calculated electronic spectra of FHF^- molecule: (**A**) RT-NEO-TDHF and RT-TDHF, and (**B**) RT-NEO-TDDFT and RT-TDDFT.

We now examine how nuclear quantum effects are manifested in the electronic spectrum. The predicted electronic spectra are plotted in fig. 5.4 for HCN and fig. 5.5 for FHF^-. In

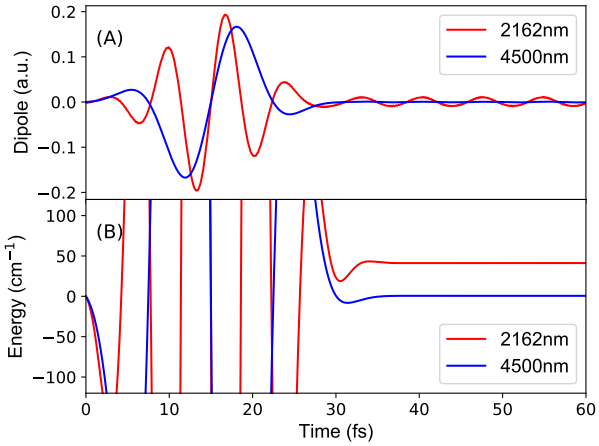

Figure 5.6: Total dipole (**A**) and energy (**B**) dynamics driven by laser fields with wavelengths of 2162 and 4500 nm.

both molecules, nuclear quantum effects modify the electronic spectrum in terms of both peak position (excitation energy) and peak intensity (oscillator strength). The non-Born-Oppenheimer vibronic mixing in the NEO approach gives rise to mixings of the electronic and protonic excitations and changes in transition densities, which result in changes in the excitation energies and oscillator strengths.

The lower electronic excitation energies are mostly unchanged, whereas higher energy excitations seem to be more affected by protonic quantum effects, as observed previously with the linear response NEO-TDDFT approach.[174, 182] This observation suggests that the electron-proton vibronic coupling becomes more important for the description of non-Born-Oppenheimer surfaces of higher-energy excited states. In addition to shifting the peak positions, nuclear quantum effects also slightly modify the peak intensity arising from variations in the transition densities.

The discussion above illustrates the fundamental characteristics of the RT-NEO approach from the perspective of linear absorption spectra. However, the unique strength of this approach lies in its capability to resolve ultrafast nonequilibrium chemical processes. For the first example, we investigate the ultrafast vibrational excitation driven by an electric

field pulse, *i.e.*, time-resolved infrared spectroscopy. Two different ∼30 fs laser pulses with 2162 nm and 4500 nm wavelengths are applied to drive the quantum dynamics of HCN (see fig. 5.6). The laser field is modelled using a sine function with a Gaussian envelope (see SI for details) and a maximum amplitude of 0.01 a.u. polarized along the bond axis.

The fundamental vibrational frequency of the CH stretching mode is predicted by RT-NEO-TDHF to be 2162 nm. When the driving field is off-resonant, the protonic dipole moment follows the field adiabatically. When the field is turned off, the system exhibits negligible energy absorption and much smaller proton dipole moment oscillations that are not visible in fig. 5.6. In contrast, when a resonant driving field is used, we observe a noticeable amount of energy absorption after the laser is turned off, and the proton dipole moment exhibits significant oscillations, as shown in fig. 5.6. This test demonstrates that the RT-NEO approach can be conveniently used to simulate time-resolved vibrational spectroscopy.

5.4 Excited State Intramolecular Proton Transfer Dynamics

For the second example, we use RT-NEO-TDDFT to simulate the excited state intramolecular proton transfer (ESIPT) in o-hydroxybenzaldehyde (oHBA). The ESIPT in oHBA has been studied extensively with both theoretical[183, 184] and spectroscopic [185] techniques. The potential energy surface predicted by TDDFT and coupled cluster methods show that the proton transfer occurs without any energy barrier on the S_1 ($\pi\pi^*$) excited state. This finding is corroborated by time-resolved photoelectron spectroscopy, which demonstrated that the proton transfer occurs in 50 fs.[185] The initial condition for the quantum dynamical simulations herein is prepared to simulate the vertical photoabsorption at $t = 0$. The excited electronic state is modelled by an electronic transition from the highest occupied molecular orbital (HOMO) to the electronic lowest unoccupied molecular orbital (LUMO), which gives rise to an $S_0 \rightarrow S_1$ excitation. In order to provide the dynamical flexibility to allow the proton to transfer on the excited state, two sets of nuclear and electronic basis functions are associated with the transferring hydrogen, with one set centered near the donor oxygen (O_D) and the other centered near the acceptor oxygen (O_A) (see SI for computational

details).

Two geometries are considered in the simulations: the ground state minimum energy structure and the restricted excited state structure. The restricted excited state geometry was obtained by optimizing the geometry on the excited state surface but fixing the H-O_D distance to the ground state value. Such a structure was used by Aquino *et al*[184] to investigate the importance of excited state structural relaxation on the proton transfer dynamics. The resulting structures show an O_D-O_A distance of 2.64 Å for the ground state geometry and 2.51 Å for the restricted excited state geometry. For both geometries, three proton basis function centers were utilized to enable the proton to transfer from the donor to the acceptor oxygen (see SI for more details).

The H-O_D and H-O_A distances obtained from the quantum dynamical simulations are plotted in fig. 6.6. Electronic vertical excitation gives rise to a nonequilibrium proton motion, as seen in fig. 6.6A. When the molecular backbone is frozen at the ground state geometry, only the bound H-O_D vibration can be observed, where the the H-O_D distance changes by up to +3% of the ground state equilibrium distance (fig. 6.6A). Thus, in the absence of excited state structural relaxation, proton transfer in oHBA is not a spontaneous process. As demonstrated by a previous study,[184] proton transfer is a multi-dimensional process with strong couplings between the transferring proton and other internal coordinates. Using the restricted excited state geometry as the initial condition, an ultrafast spontaneous proton transfer event is observed on the S_1 state (fig. 6.6B). Note that the observed reaction time of ∼8 fs does not include the time for the molecular geometry to relax on the excited state. This test showcases the capabilities of RT-NEO approaches for resolving excited state quantum dynamics and illustrates the importance of structural relaxation effects in excited state proton transfer. Moreover, a movie illustrating the time-dependent nonequilibrium density changes for the electrons and the quantum proton following photoexcitation highlights the intricate coupling between the electronic and nuclear quantum dynamics.

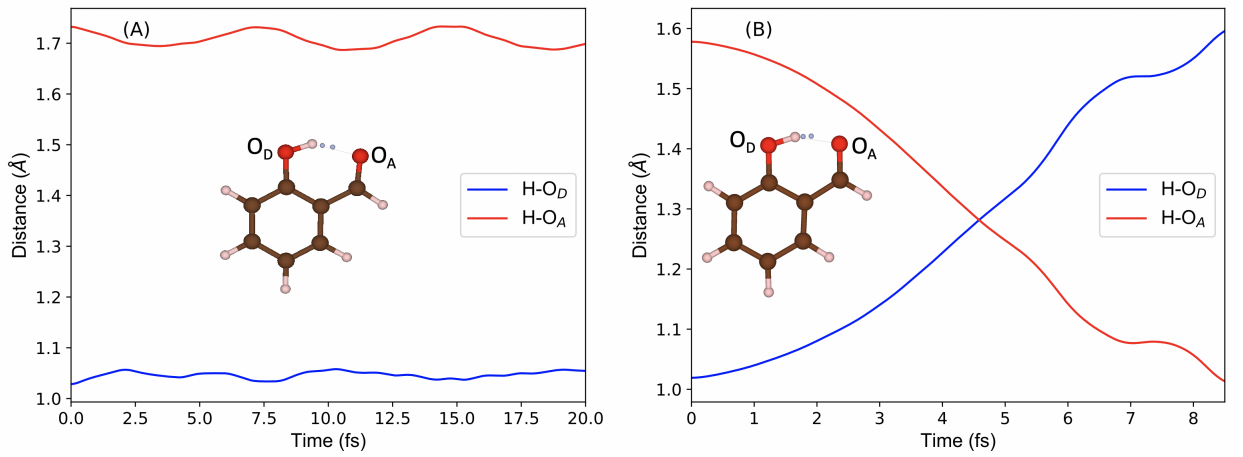

Figure 5.7: Distance from the transferring proton to the donor oxygen (O_D) and the acceptor oxygen (O_A) as a function of time for the ESIPT system with the optimized ground state structure (**A**) and the restricted optimized excited state structure (**B**).

5.5 Summary

This chapter presents the development of a new approach for simulating quantum dynamics that integrates the nuclear and electronic dynamics described by time-dependent Hartree-Fock or density functional theory within the nuclear-electronic orbital framework. We have demonstrated that RT-NEO is a powerful method that can resolve spectroscopic and dynamical properties of quantum mechanically coupled electrons and nuclei. Most importantly, this work lays the theoretical foundation of RT-NEO based quantum dynamical tools for simulating time-resolved nonlinear spectroscopies and nonadiabatic quantum dynamics.

Chapter 6

IMPLICITLY SOLVATED NUCLEAR ELECTRONIC ORBITAL DYNAMICS

This chapter combines the theory developed in the last chapter with the motivations from the first two chapters to model systems using a multiscale approach. In this chapter, the real-time NEO method from the last chapter is coupled with a time-dependent PCM solvent, and the effects of this embedding on spectroscopy and dynamics are examined.

6.1 Motivation

Nonadiabatic dynamic processes such as proton coupled electron transfer (PCET) and excited state intramolecular proton transfer (ESIPT) require careful treatment of the coupled nuclear and electronic quantum problems. At the same time, experimental studies of these processes are often performed in a solvent, and the solvation environment can strongly affect the dynamics of these processes.[186]

Of the many approaches used to account for coupled quantum nuclear and electronic structure,[139, 140, 143, 146, 147, 148, 150, 152, 153, 155, 187, 64, 141, 88] the nuclear-electronic orbital (NEO) approach provides an effective method for treating electrons and some select protons quantum mechanically. [165, 169, 188, 189, 190] The NEO approach naturally incorporates nuclear quantum effects, such as zero-point energy and quantized vibrational states. Furthermore, the NEO approach has recently been extended to allow for direct coupled propagation of the quantum electrons and protons.[188, 191] This real-time NEO (RT-NEO) approach has shown particular promise in the direct simulation of nonadiabatic processes such as PCET and ESIPT.

In order for these newly developed approaches to be applicable to understanding exper-

iments, the effects of solvation and chemical environment must also be taken into account. One of the most widely used methods to account for solvent effects is the polarizable continuum model (PCM).[8, 192, 43, 193] In the most common form of this model, the quantum mechanical molecule is placed within a uniform dielectric with the permittivity of the solvent, and the effects of solvation are captured through the polarization of this dielectric.[192, 193] PCM has been thoroughly studied, both in the time independent [19] and time dependent [194, 132, 195, 30] domains, and it has been shown to be a robust model for capturing solvent effects on the ground state and within dynamical processes.[193]

However, the effects of solvation on the NEO approach are yet unknown. In this chapter, NEO Hartree–Fock (NEO-HF) and NEO density functional theory (NEO-DFT) are coupled with PCM and the resulting phenomena are investigated. First, the theory required to couple these two formalisms is presented. Next, effects of solvation on the ground state properties of NEO-HF wavefunctions are analyzed through a case study of hydrogen cyanide in many different solvents. Solvation in time-dependent properties is then captured through the use of the RT-NEO formalism, and the resulting solvation effects on the electronic and vibrational spectrum of HCN is investigated. Finally, direct simulation of ESIPT in vacuum and in solvent is performed, demonstrating the significant effects solvation can have on these processes.

6.2 Theory

Both the theory of the NEO method[190, 188] and the theory of PCM[192, 193] are well described elsewhere. Here, we briefly review the equations necessary to couple these two models with an emphasis on the time dependent formulation. For time independent processes such as wavefunction optimization, the following equations reduce to time independent forms trivially.

The time-dependent NEO formalism for single-determinant methods takes the following product ansatz

$$\Psi_{NEO}(t) = \Phi_{\mathrm{e}}(t)\Phi_{\mathrm{p}}(t) \tag{6.1}$$

where Φ_{e} and Φ_{p} are Slater determinants for the electrons and protons, respectively. This ansatz leads to two coupled Von Neumann equations that determine the dynamics of the protons and the electrons

$$\begin{aligned} i\frac{\partial}{\partial t}\boldsymbol{P}^{\mathrm{e}}(t) &= [\boldsymbol{F}^{\mathrm{e}}(t, \boldsymbol{P}^{\mathrm{e}}(t), \boldsymbol{P}^{\mathrm{p}}(t)), \boldsymbol{P}^{\mathrm{e}}(t)] \\ i\frac{\partial}{\partial t}\boldsymbol{P}^{\mathrm{p}}(t) &= [\boldsymbol{F}^{\mathrm{p}}(t, \boldsymbol{P}^{\mathrm{p}}(t), \boldsymbol{P}^{\mathrm{e}}(t)), \boldsymbol{P}^{\mathrm{p}}(t)] \end{aligned} \tag{6.2}$$

where $\boldsymbol{P}^{\mathrm{x}}(t)$ is the time dependent density operator for the electrons (x = e) or protons, (x = p), and $\boldsymbol{F}^{\mathrm{x}}(t)$ is the time dependent Fock operator for each subsystem.

In order to couple a NEO wavefunction with a polarizable medium, one needs to account for the mutual polarization between the NEO quantum system and the classically polarizable system. This interaction is accounted for by introducing a solvent operator, $\boldsymbol{V}^{\mathrm{PCM}}(\boldsymbol{P}^{\mathrm{e}}(t), \boldsymbol{P}^{\mathrm{p}}(t))$, that is dependent on both the protonic and electronic time dependent density. This operator is directly added into the Fock matrices of both the electrons and the protons

$$\begin{aligned} \boldsymbol{F}^{\mathrm{e}}(t) &= \boldsymbol{F}^{\mathrm{e},0}(t, \boldsymbol{P}^{\mathrm{e}}(t), \boldsymbol{P}^{\mathrm{p}}(t)) - \boldsymbol{V}^{\mathrm{PCM}}(\boldsymbol{P}^{\mathrm{e}}(t), \boldsymbol{P}^{\mathrm{p}}(t)) \\ \boldsymbol{F}^{\mathrm{p}}(t) &= \boldsymbol{F}^{\mathrm{p},0}(t, \boldsymbol{P}^{\mathrm{p}}(t), \boldsymbol{P}^{\mathrm{e}}(t)) + \boldsymbol{V}^{\mathrm{PCM}}(\boldsymbol{P}^{\mathrm{e}}(t), \boldsymbol{P}^{\mathrm{p}}(t)) \end{aligned} \tag{6.3}$$

where $\boldsymbol{F}^{\mathrm{x},0}$ is the Fock matrix for either the electronic or protonic component in vacuum. The difference in sign originates from the opposite charge of electrons and protons. Taking the most common approach to solving the PCM equations, a boundary surface surrounding the molecule is defined and discretized into tesserae with apparent charges, q, and centers $\boldsymbol{\mathcal{R}}$. The solvent operator in the atomic orbital basis $(\mu, \nu, \dots)$ is then given by

$$V^{\mathrm{PCM}}_{\mu,\nu} = \sum_i \langle\mu| \frac{q_i(\boldsymbol{P}^{\mathrm{e}}(t), \boldsymbol{P}^{\mathrm{p}}(t))}{|\boldsymbol{r} - \boldsymbol{\mathcal{R}}_i|} |\nu\rangle \tag{6.4}$$

Solving for the apparent surface charge at each tessera, q_i, depends on the exact PCM formalism used. The differences and solutions for these different formalisms is given in detail elsewhere,[8] but the common elements between all formalisms is that the charge at each tessera depends both on the total charge density (electron, proton, and classical nuclei)

in the quantum mechanical region and on the charge of all other tesserae. Furthermore, the polarization of the cavity relies on the frequency dependent dielectric function, $\epsilon(\omega)$, of the solvent used. Directly accounting for this frequency dependence is possible, [195, 30] but it can be computationally expensive for long simulations and can be avoided when the absorption bands of the solvent and solute do not overlap significantly. Another approach is to partition the surface charge into "fast" and "slow" components - these correspond to the high-frequency electronic response and low-frequency orientational and vibrational response, respectively. [192]

$$q_i = q_i^{\text{slow}} + q_i^{\text{fast}} \tag{6.5}$$

For time independent problems, such as optimization of the ground state of a NEO wavefunction, both the fast and slow components are allowed to respond and optimize, and the total surface charge is determined by the static permittivity of the solvent, ϵ_0. For time dependent problems, such as real-time propagation of a NEO wavefunction, the fast component is allowed to respond instantaneously to the changes in electron and proton density with the high-frequency permittivity of the solvent, ϵ_∞, but the slow component is kept static for the duration of the simulation. When using this approach, the time dependence of the polarization of the cavity is solely through the fast component response to the time dependent density, not through an explicit equation of motion for the polarization of the cavity.

6.3 Ground State PCM-NEO

The time independent PCM-NEO-HF formalism is used to study the ground state properties of the HCN molecule in a variety of solvents. HCN has been well studied as a benchmark for NEO methods, and it is a well suited molecule for studying solvation, since it has a strong dipole moment that may be accentuated by solvation.

All calculations were performed in the Chronus Quantum open source electronic structure package.[196, 197] The cc-pVDZ basis set [198] was used for the electronic component, and

an even tempered 8s8p8d basis set [169] was used for the proton. The PCM equations were solved using the PCMSolver package [199] using the isotropic IEF-PCM formalism.

To investigate the interaction between solvation provided through PCM and NEO-HF, the ground state properties of HCN were calculated both using a classical proton and using the NEO approach. Each approach was placed in vacuum and PCM corresponding to the static permittivities of cyclohexane, tetrahydrofuran, acetonitrile, acetone, and water.

When placed in a solvent, the total energy of the whole system decreases for both the classical and NEO approaches, and the amount of stabilization of the system increases with increasing permittivity, as seen in fig. 6.1. Interestingly, the zero point energy, (ZPE) defined as the difference between the classical and NEO energies, increases as a function of permittivity as well.

Additionally, one can compare the change in molecular dipole moment as a function of solvent permittivity. In classical PCM electronic structure calculations, the total molecular dipole moment is expected to increase with solvent permittivity for polar molecules because the cavity stabilizes greater separation of charges within the quantum molecule through the surface charge.[192] As expected, this is observed for the HCN system with a classical proton, seen in fig. 6.2. However, a surprising result is observed for the HCN system using NEO; almost no change in molecular dipole moment is observed as a function of solvent permittivity. This can be explained by examining the expectation value for the proton position in the various solvents. While the position of the classical proton is fixed, the position of the proton is allowed to respond to the various solvation environments. As seen in fig. 6.2, the expectation value of the NEO proton position moves back towards the molecule, shortening the CH bond. This sort of optimization of proton position in the different solvent environments counteracts the expected increase in dipole moment, leading to an effectively stationary molecular dipole moment.

Both the decrease in CH bond and increase in ZPE can be explained by considering the effect of a molecular cavity with a surface charge surrounding the quantum proton. In a molecule with a terminal proton, such as HCN, the potential well acting on that proton is

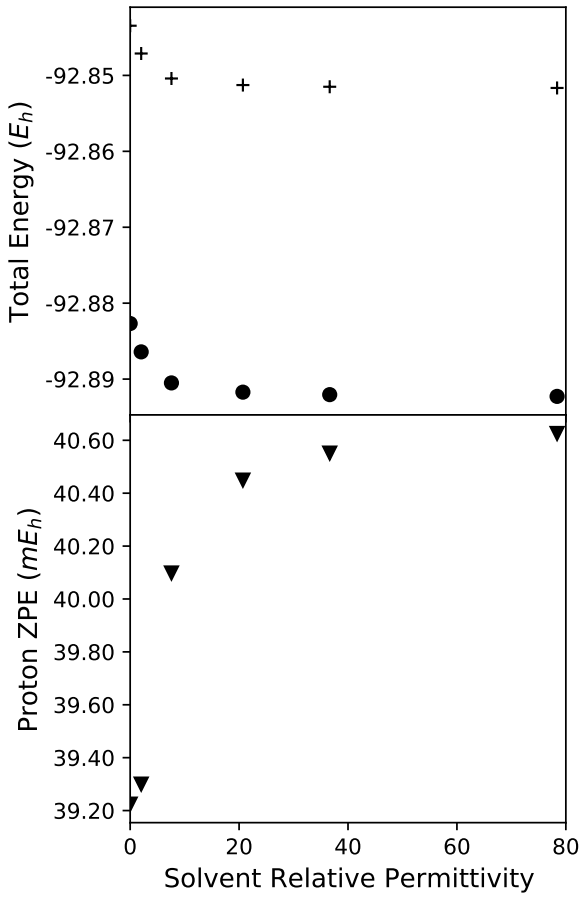

Figure 6.1: Energetics of HCN in a variety of solvents with a classical proton description (circles) and with a NEO protonic wavefunction (crosses). The protonic zero point energy is given with triangles.

rather asymmetric – repulsion steeply increases as the proton moves closer to the carbon than the optimal bonding position, but only gradually increases along the CH dissociation coordinate. When a solvent is introduced around the molecule, the potential along the dissociation coordinate increases, leading to a steeper potential well. This causes the expected value of the proton position to move toward the carbon, shortening the CH bond, and increases the zero point energy due to the steeper well.

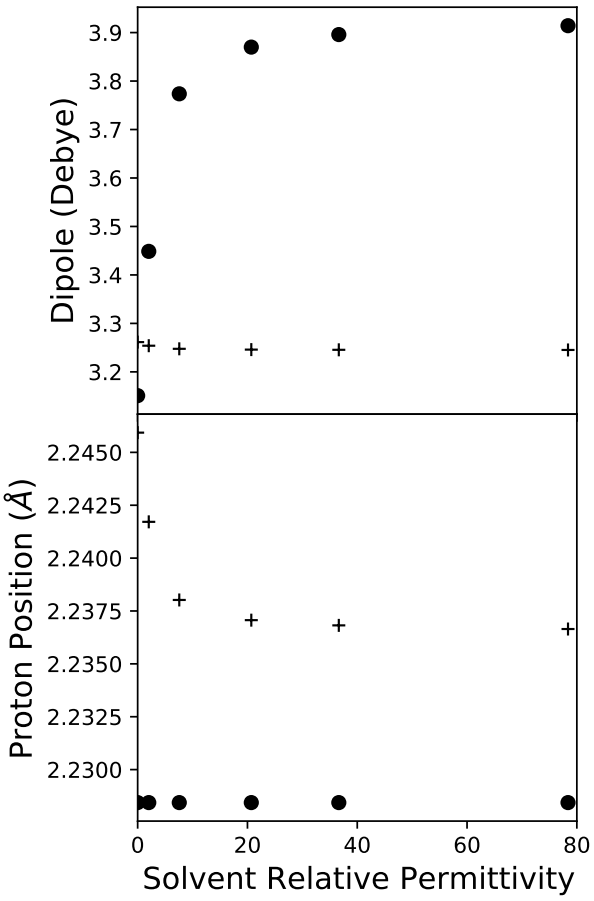

Figure 6.2: Total molecular dipole moment (top) and expected proton position (bottom) of HCN in a variety of solvents with a classical descripton (circles) and with a NEO protonic wavefunction (crosses).

6.4 Time Dependent PCM-NEO

The effect of solvation on the spectra of NEO-HF systems is investigated using the same HCN system as above. In this case study, only vacuum and water environments are considered. The spectrum is acquired by propagating three trajectories of the system corresponding to an initial electric field perturbation along each of the Cartesian coordinates. The linear absorption spectrum is calculated from the sum of the Fourier transforms of the time dependent

dipole moment along the same direction as the initial perturbation. [3, 191]

Both the classical spectra show solvent dependence, with the solvent dramatically affecting both excitation energy and intensity of all transitions, as seen in fig. 6.3. This is expected due to the changes to both the ground and excited states induced by the static polarized surface charges, and to a smaller extent, the dynamic response of the surface charge. However, the effects of the solvent on the spectrum of HCN modeled with NEO are significantly less dramatic. This can be explained by analogy to the ground state – solvatochromism can be qualitatively explained by understanding the dipole of both the ground and excited states. If the ground state has a larger dipole than the excited state, it will be relatively more stabilized by the solvent, increasing the excitation energy. The opposite occurs when the excited state has a larger dipole moment than the ground state. While this simplistic model can not describe all details of solvatochromism, it serves a useful framework for understanding the effects of solvent on the NEO electronic spectrum. Because the stabilization effects of the solvent on the molecular dipole moment are countered by the quantum treatment of the proton, the effects of the solvent on the electronic spectrum aren't as dramatic as in the classical case.

In contrast, the vibrational spectrum of HCN modeled with NEO demonstrates a strong solvent dependence. In HCN with the carbon and nitrogen fixed, three vibrational modes are active: one CH stretching mode and two CH bending modes. In fig. 6.4, the stretching mode is the higher energy mode, and the two bending modes are the lower energy peak. When placed in water, the energy of these transitions increases and the intensity decreases. Additionally, the stretch vibration increases in frequency much more than the bend vibrations. This can be understood with the changes to the potential energy surface discussed with the ground state. The surface charge introduces an additional potential along the CH dissociation coordinate, increasing the steepness of the potential well which increases the vibrational frequency of the stretch mode. However, the potential introduced orthogonal to the HCN bonding axis is symmetric and weaker on average than that along the HCN bonding axis. This gives only a small change in the potential along the HCN bending coordinates,

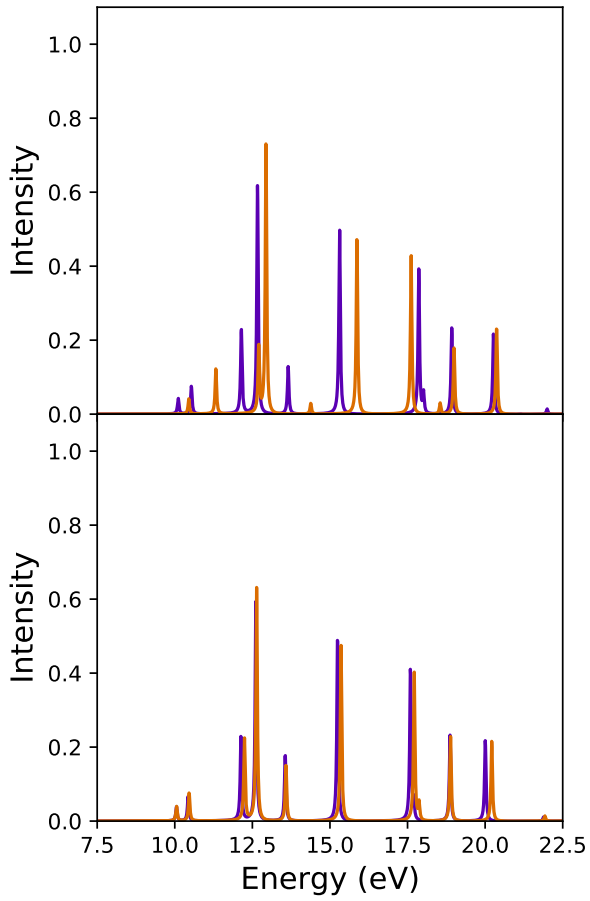

Figure 6.3: Electronic spectra for HCN with a classical proton (top) and using the NEO approach. (bottom) Solvatochromism is indicated by the changes between the vacuum (purple) and water solvated (orange) spectra.

leading to a much smaller change in vibrational frequency for the bend modes than for the stretch mode.

The real-time NEO approach has been demonstrated to be effective to simulate excited state intramolecular proton transfer, [188] (ESIPT) and this process can be modulated by the solvation environment of the molecule undergoing ESIPT. [200] Here, we present the ESIPT of o-hydroxybenzaldehyde (oHBA) simulated by RT-NEO-TDDFT in both vacuum and water. Because the ESIPT of oHBA has been studied by both experimental techniques

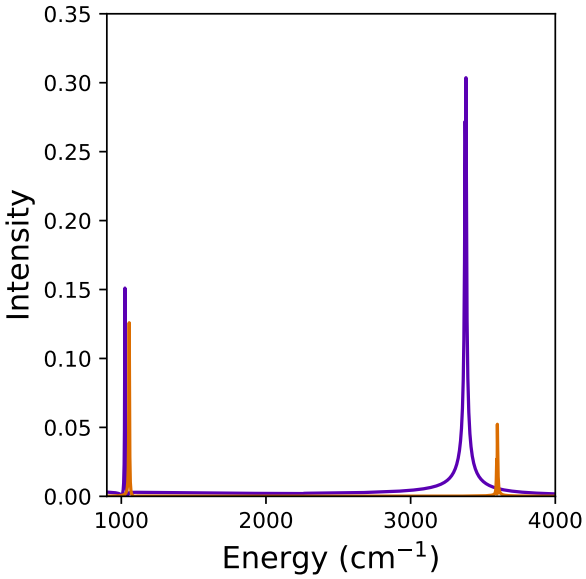

Figure 6.4: Vibrational spectra for HCN using the NEO approach in both vacuum (purple) and water. (orange)

and RT-NEO-TDDFT previously, it serves as a good gauge of the ability of PCM to capture the solvent modulation of proton transfer processes captured by the NEO approach.

In order to capture the ESIPT without motion of the heavy nuclei, one must begin from an excited state geometry. [188] The geometry used for this simulation was obtained from Aquino *et al.*[184] The cc-pVDZ basis set was used for the electrons, and a minimal, even-tempered sp basis was used for the proton. To provide enough flexibility along the proton transfer coordinate to capture the ESIPT, additional basis centers were added along the transfer path, shown in fig. 6.5. The B3LYP functional was used for electron correlation and exchange, and the epc17-2 functional was used for electron-proton correlation. The initial state was prepared by a HOMO-LUMO swap at prior to propagation.

The distances between the quantum proton and the donor and acceptor oxygens are shown in fig. 6.6 for simulations both in vacuum and in water. The proton crosses over to the acceptor oxygen approximately 5 fs after excitation in vacuum, however in water,

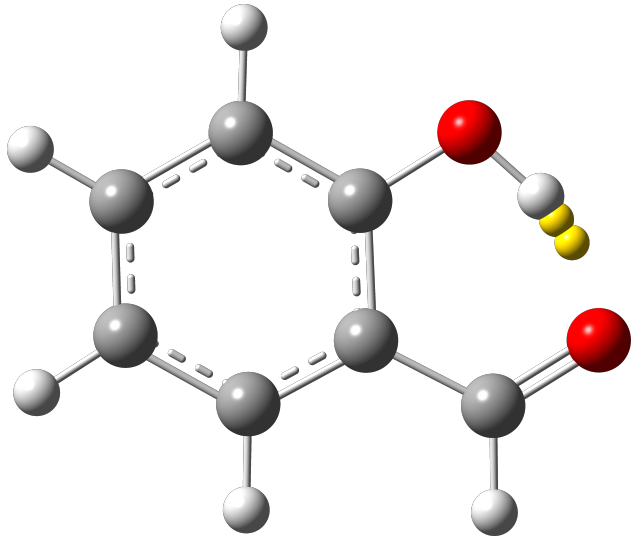

Figure 6.5: Excited state structure of oHBA. The additional basis centers are marked with yellow spheres.

this cross over occurs after only approximately 4 fs. This acceleration is primarily due to differences in the ground state; when neglecting the "fast" response of the solvent entirely and propagating only within the static field of the ground state PCM, the acceleration is still observed. It is likely that the the difference in initial proton position in vacuum and in water is responsible for the acceleration, since the HOMO-LUMO swap prepares a $\pi\pi^*$ antibonding state between the donor oxygen and proton. With a shorter OH bond, the initial repulsion is greater upon HOMO-LUMO swap, driving the transfer to occur faster.

6.5 Summary

In this chapter, the NEO approach was coupled with solvation modeled with PCM. The effects of this solvation are investigated on both ground state and time dependent properties. In both cases, solvation is shown to have a dramatic effect. Furthermore, the use of a NEO description of protons introduces novel effects of solvation compared to solvation of molecules with classical protons. Specifically, classically expected trends of increasing dipole moment and solvatochromism are complicated by the quantum nature of the proton and explanations

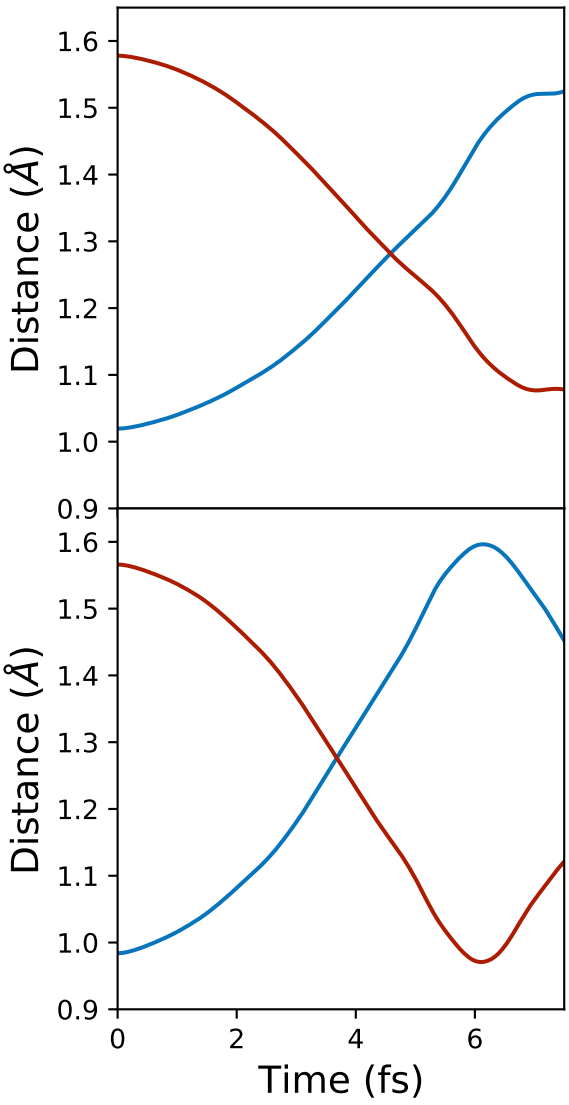

Figure 6.6: Excited state intramolecular proton transfer in oHBA in vacuum (top) and water (bottom). The distance between the expectation value of the transferring proton and the donor (blue) and acceptor (red) is given as a function of time.

of the effects of solvation must take this directly into account.

The approach to model solvation used in this chapter uses a continuum description of the solvent. This method offers some significant advantages, such as implicit integration over all

solvent degrees of freedom, but it also cannot model all processes important for solvation. In particular, hydrogen bonding between the solute and the solvent can be important for many processes, and this importance is only expected to increase for systems in which protons are described quantum mechanically. Further work will extend the polarizable coupling between NEO wavefunctions and their environments to solvent descriptions with explicit nuclear degrees of freedom, such as polarizable molecular mechanics. For solvents without hydrogen bonding to the solute, the current approach shows promise for modeling coupled electron-nuclear wavefunctions within a responsive environment. Additional further work will extend the equilibrium time-dependent solvation model used here for a direct equation of motion for the solvent.

BIBLIOGRAPHY

[1] Stefano Caprasecca, Sandro Jurinovich, Lucas Viani, Carles Curutchet, and Benedetta Mennucci. Geometry optimization in polarizable qm/mm models: The induced dipole formulation. *Journal of Chemical Theory and Computation*, 10(4):1588–1598, 2014.

[2] Attila Szabo and Neil S. Ostlund. *Modern Quantum Chemistry: Introduction to Advanced Electronic Structure Theory*. Dover Publications, Mineola, N.Y., 1996.

[3] Joshua J. Goings, Patrick J. Lestrange, and Xiaosong Li. Real-time time-dependent electronic structure theory. *Wiley Interdisciplinary Reviews: Computational Molecular Science*, 8(1):e1341, 2018.

[4] Alberto Castro, Miguel AL Marques, and Angel Rubio. Propagators for the time-dependent kohn–sham equations. *Journal of Chemical Physics*, 121(8):3425–3433, 2004.

[5] Chen Huang, Michele Pavone, and Emily A Carter. Quantum mechanical embedding theory based on a unique embedding potential. *Journal of Chemical Physics*, 134(15):154110, 2011.

[6] Emil Proynov. Optimized effective potentials at a glance: The effective exchange potential of becke–johnson applied to molecules. *Theoretical Chemistry Accounts*, 135(11):248, 2016.

[7] Frederick R Manby, Martina Stella, Jason D Goodpaster, and Thomas F Miller III. A simple, exact density-functional-theory embedding scheme. *Journal of Chemical Theory and Computation*, 8(8):2564–2568, 2012.

[8] Jacopo Tomasi, Benedetta Mennucci, and Roberto Cammi. Quantum mechanical continuum solvation models. *Chemical Reviews*, 105(8):2999–3094, 2005.

[9] Anthony Stone. *The Theory of Intermolecular Forces*. Oxford University Press, 2013.

[10] Arieh Warshel, Mitsunori Kato, and Andrei V Pisliakov. Polarizable force fields: History, test cases, and prospects. *Journal of Chemical Theory and Computation*, 3(6):2034–2045, 2007.

[11] Csaba Daday, Carles Curutchet, Adalgisa Sinicropi, Benedetta Mennucci, and Claudia Filippi. Chromophore—protein coupling beyond nonpolarizable models: Understanding absorption in green fluorescent protein. *Journal of Chemical Theory and Computation*, 11(10):4825–4839, 2015.

[12] Koji Ando. A stable fluctuating-charge polarizable model for molecular dynamics simulations: Application to aqueous electron transfers. *Journal of Chemical Physics*, 115(11):5228–5237, 2001.

[13] Mark S Gordon, Mark A Freitag, Pradipta Bandyopadhyay, Jan H Jensen, Visvaldas Kairys, and Walter J Stevens. The effective fragment potential method: A qm-based mm approach to modeling environmental effects in chemistry. *Journal of Physical Chemistry A*, 105(2):293–307, 2001.

[14] E. Boulanger and W. Thiel. Solvent boundary potentials for hybrid qm/mm computations using classical drude oscillators: A fully polarizable model. *Journal of Chemical Theory and Computation*, 8:4527–4538, 2012.

[15] Nanna Holmgaard List, Jógvan Magnus Haugaard Olsen, and Jacob Kongsted. Excited states in large molecular systems through polarizable embedding. *Physical Chemistry Chemical Physics*, 18(30):20234–20250, 2016.

[16] Lasse Jensen, Per-Olof Åstrand, and Kurt V Mikkelsen. Molecular mechanics interaction models for optical electronic properties. *Journal of Computational Theoretical Nanoscience*, 6(2):270–291, 2009.

[17] Piet Th. van Duijnen and Marcel Swart. Molecular and Atomic Polarizabilities: Thole's Model Revisited. *Journal of Physical Chemistry A*, 102(14):2399–2407, 1998.

[18] Wolfgang Hackbusch. *Integral Equations: Theory and Numerical Treatment.* Birkhauser Verlag, 1995.

[19] E Cances, Benedetta Mennucci, and J Tomasi. A new integral equation formalism for the polarizable continuum model: Theoretical background and applications to isotropic and anisotropic dielectrics. *Journal of Chemical Physics*, 107(8):3032–3041, 1997.

[20] Zilvinas Rinkevicius, Jaime AR Sandberg, Xin Li, Mathieu Linares, Patrick Norman, and Hans Ågren. Hybrid complex polarization propagator/molecular mechanics method for heterogeneous environments. *Journal of Chemical Theory and Computation*, 12(6):2661–2667, 2016.

[21] Benedetta Mennucci, Roberto Cammi, and Jacopo Tomasi. Excited states and solvatochromic shifts within a nonequilibrium solvation approach: A new formulation of the integral equation formalism method at the self-consistent field, configuration interaction, and multiconfiguration self-consistent field level. *Journal of Chemical Physics*, 109(7):2798–2807, 1998.

[22] Roberto Cammi, Luca Frediani, Benedetta Mennucci, Jacopo Tomasi, Kenneth Ruud, and Kurt V. Mikkelsen. A second-order, quadratically convergent multiconfigurational self-consistent field polarizable continuum model for equilibrium and nonequilibrium solvation. *Journal of Chemical Physics*, 117:13–26, 2004.

[23] MA Aguilar. Separation of the electric polarization into fast and slow components: A

comparison of two partition schemes. *Journal of Physical Chemistry A*, 105(45):10393–10396, 2001.

[24] R E Stratmann, G E Scuseria, and M J Frisch. An Efficient Implementation of Time-dependent Density-functional Theory for the Calculation of Excitation Energies of Large Molecules. *Journal of Chemical Physics*, 109:8218–8224, 1998.

[25] Andreas Dreuw and Martin Head-gordon. Single-Reference ab Initio Methods for the Calculation of Excited States of Large Molecules. *Sciences-New York*, pages 4009–4037, 2005.

[26] Patrick J. Lestrange, Phu D. Nguyen, and Xiaosong Li. Calibration of energy-specific tddft for modeling k-edge xas spectra of light elements. *Journal of Chemical Theory and Computation*, 11:2994–2999, 2015.

[27] Alessio Petrone, Joshua J. Goings, and Xiaosong Li. Quantum confinement effects on optical transitions in nanodiamonds containing nitrogen vacancies. *Physical Review B*, 94:165402, 2016.

[28] Xiaosong Li, Stanley M. Smith, Alexei N. Markevitch, Dmitri A. Romanov, Robert J. Levis, and H. Bernhard Schlegel. A time-dependent hartree-fock approach for studying the electronic optical response of molecules in intense fields. *Physical Chemistry Chemical Physics*, 7:233–239, 2005.

[29] Wenkel Liang, Craig T. Chapman, and Xiaosong Li. Efficient first-principles electronic dynamics. *Journal of Chemical Physics*, 134(18):184102, 2011.

[30] Feizhi Ding, David B. Lingerfelt, Benedetta Mennucci, and Xiaosong Li. Time-dependent Non-equilibrium Dielectric Response in QM/Continuum Approaches. *Journal of Chemical Physics*, 142(3):034120, 2015.

[31] Silvio Pipolo, Stefano Corni, and Roberto Cammi. Equation of motion for the sovent polarization apparent charges in the polarizable continuum model: Application to time-dependent ci. *Journal of Chemical Physics*, 146:064116–064124, 2017.

[32] Silvio Pipolo and Stefano Corni. Real-time description of the electronic dynamics for a molecule close to a plasmonic nanoparticle. *Journal of Physical Chemistry C*, 120:28774–28781, 2016.

[33] Feizhi Ding, Benjamin E. Van Kuiken, Bruce E. Eichinger, and Xiaosong Li. An efficient method for calculating dynamical hyperpolarizabilities using real-time time-dependent density functional theory. *Journal of Chemical Physics*, 138:064104, 2013.

[34] W. Wislicenus. Ueber die isomerie der formylphenylessigester. *Liebigs Annalen der Chemie*, 291:147–216, 1896.

[35] H. Stobbe. Studien über tautomerie, insbesondere an einem semicyklischen 1,3-diketon der pentamethylenreihe. *Liebigs Annalen der Chemie*, 326:347–370, 1903.

[36] Christian Reichardt. *Solvents and Solvent Effects in Organic Chemistry*. VCH Publishers, Weinheim, 1988.

[37] J. F. Coetzee and C. D. Ritchie. *Solute-Solvent Interactions*, volume 1 and 2. Dekker, New York, 1969 and 1976.

[38] M. H. Abraham, P. L. Grellier, J. L. M. Abboud, R. M. Doherty, and R. W. Taft. Solvent effects in organic chemistry - recent developments. *Canadian Journal of Chemistry*, 66:2673–2686, 1988.

[39] E. S. Amis. *Solvent Effects on Reaction Rates and Mechanisms*. Academic Press, New York, 1966.

[40] E. S. Amis. *Solvent Effects on Chemical Phenomena*, volume 1. Academic Press, New York, 1973.

[41] M. H. Abraham. Solvent effects on reaction rates. *Pure and Applied Chemistry*, 57:1055–1064, 1985.

[42] K. A. Connors. *Chemical Kinetics - The Study of Reaction Rates in Solution*. VCH Publishers, Weinheim, 1990.

[43] Jacopo Tomasi and Maurizio Persico. Molecular interactions in solution: An overview of methods based on continuous distributions of the solvent. *Chemical Reviews*, 94(7):2027–2094, 1994.

[44] CJ Cramer and DG Truhlar. Implicit solvation models: Equilibria, structure, spectra, and dynamics. *Chemical Reviews*, 99(8):2161–2200, 1999.

[45] A Klamt. The cosmo and cosmo–rs solvation models. *WIREs Comput. Mol. Sci.*, 1(5):699–709, 2011.

[46] B. Mennucci. Modeling environment effects on spectroscopies through qm/classical models. *Physical Chemistry Chemical Physics*, 15:6583–6594, 2013.

[47] J. Gao. Hybrid quantum and molecular mechanics simulations: An alternative to solvent effects in organic chemistry. *Accounts of Chemical Research*, 29:298–305, 1996.

[48] H. Lin and D. G. Truhlar. Qm/mm: What have we learned, where are we, and where do we go from here? *Theoretical Chemistry Accounts*, 117:185–199, 2006.

[49] H. M. Senn and W. Thiel. Qm/mm methods for biomolecular systems. *Angewandte Chemie*, 48:1198–1229, 2009.

[50] P. N. Day, J. H. Jensen, M. S. Gordon, S. P. Webb, W. J. Stevens, M. Krauss, D. Garmer, H. Basch, and D. Cohen. An effective fragment method for modeling solvent effects in quantum mechanical calculations. *Journal of Chemical Physics*, 105:1968–1986, 1996.

[51] V. Kairys and J. H. Jensen. Qm/mm boundaries across covalent bonds: A frozen localized molecular orbital-based approach for the effective fragment potential method. *Journal of Physical Chemistry A*, 104:6656–6665, 2000.

[52] Carles Curutchet, Aurora Muñoz-Losa, Susanna Monti, Jacob Kongsted, Gregory D. Scholes, and Benedetta Mennucci. Electronic Energy Transfer in Condensed Phase Studied by a Polarizable QM/MM Model. *Journal of Chemical Theory and Computation*, 5(7):1838–1848, 2009.

[53] Stefano Caprasecca, Sandro Jurinovich, Louis Lagardère, Benjamin Stamm, and Filippo Lipparini. Achieving linear scaling in computational cost for a fully polarizable mm/continuum embedding. *Journal of Chemical Theory and Computation*, 11(2):694–704, 2015.

[54] Y. Mao, O. Demerdash, M. Head-Gordon, and T. Head-Gordon. Assessing ion-water interactions in the amoeba force field using energy decomposition analysis of electronic structure calculations. *Journal of Chemical Theory and Computation*, 12:5422–5437, 2016.

[55] Daniele Loco, Étienne Polack, Stefano Caprasecca, Louis Lagardère, Filippo Lipparini, Jean-Philip Piquemal, and Benedetta Mennucci. A qm/mm approach using the amoeba polarizable embedding: From ground state energies to electronic excitations. *Journal of Chemical Theory and Computation*, 12(8):3654–3661, 2016.

[56] S. W. Rick, S. J. Stuart, and B. J. Berne. Dynamical fluctuating charge force fields: Application to liquid water. *Journal of Chemical Physics*, 101:6141–6156, 1994.

[57] S. W. Rick and B. J. Berne. Dynamical fluctuating charge force fields: The aqueous solvation of amides. *Journal of the American Chemical Society*, 118:672–679, 1996.

[58] F. Lipparini and V. Barone. Polarizable force fields and polarizable continuum model:

A fluctuating charges/pcm approach. 1. theory and implementation. *Journal of Chemical Theory and Computation*, 7:3711–3724, 2011.

[59] Filippo Lipparini, Chiara Cappelli, and Vincenzo Barone. Linear response theory and electronic transition energies for a fully polarizable qm/classical hamiltonian. *Journal of Chemical Theory and Computation*, 8(11):4153–4165, 2012.

[60] A. H. Steindal, K. Ruud, L. Frediani, K. Aidas, and J. Kongsted. Excitation energies in solution: The fully polarizable qm/mm/pcm method. *Journal of Physical Chemistry B*, 115:3027–3037, 2011.

[61] S. Juronovich, C. Curutchet, and B. Mennucci. The fenna-matthews-olson protein revisited: A fully polarizable (td) dft/mm description. *ChemPhysChem*, 15:3194–3204, 2014.

[62] C. Curutchet, V. I. Novoderezhkin, J. Kongsted, A. Muñoz-Losa, R. van Grondelle, G. D. Scholes, and B. Mennucci. Energy flow in the cryptophyte pe545 antenna is directed by bilin pigment conformation. *Journal of Physical Chemistry B*, 117:4263–4273, 2013.

[63] Xiaojing Wu, Jean-Marie Teuler, Fabien Cailliez, Carine Clavaguéra, Dennis R Salahub, and Aurélien de la Lande. Simulating Electron Dynamics in Polarizable Environments. *Journal of Chemical Theory and Computation*, page DOI:10.1021/acs.jctc.7b00251, 2017.

[64] Christine M. Isborn, Xiaosong Li, and John C. Tully. TDDFT Ehrenfest dynamics: Collisions between atomic oxygen and graphite clusters. *Journal of Chemical Physics*, 126:134307, 2007.

[65] Joshua J. Goings, Joseph M. Kasper, Franco Egidi, Shichao Sun, and Xiaosong Li. Real time propagation of the exact two component time-dependent density functional theory. *Journal of Chemical Physics*, 145(10):104107, 2016.

[66] B. T. Thole. Molecular Polarizabilities Calculated with a Modified Dipole Interaction. *Chemical Physics*, 59(3):341–350, 1981.

[67] J. Wang, P. Cieplak, J. Li, T. Hou, R. Luo, and Y. Duan. Development of polarizable models for molecular mechanical calculations i: Parameterization of atomic polarizability. *Journal of Physical Chemistry B*, 115:3091–3099, 2011.

[68] M. Maroncelli and G. R. Fleming. Picosecond solvation dynamics of coumarin 153: The importance of molecular aspects of solvation. *Journal of Chemical Physics*, 86:6221–6239, 1987.

[69] J. E. Lewis and M. Maroncelli. On the (uninteresting) dependence of the absorption and emission transition moments of coumarin 153 on solvent. *Chemical Physics Letters*, 282:197–203, 1998.

[70] S. A. Kovalenko, J. Ruthmann, and N. P. Ernsting. Ultrafast stokes shift and excited-state transient absorption of coumarin 153 in solution. *Chemical Physics Letters*, 271:40–50, 1997.

[71] M. L. Horng, J. A. Gardecki, A. Papazyan, and M. Maroncelli. Subpicosecond measurements of polar solvation dynamics: Coumarin 153 revisited. *Journal of Physical Chemistry*, 99:17311–17337, 1995.

[72] P. V. Kumar and M. Maroncelli. Polar solvation dynamics of polyatomic solutes: Simulation studies in acetonitrile and methanol. *Journal of Chemical Physics*, 103:3038–3059, 1995.

[73] L. Reynolds, J. A. Gardecki, S. J. V. Frankland, M. L. Horng, and M. Maroncelli. Dipole solvation in nondipolar solvents: Experimental studies of reorganization energies and solvation dynamics. *Journal of Physical Chemistry*, 100:10337–10354, 1996.

[74] R. J. Cave and Jr. E. W. Castner. Time-dependent density functional theory investigation of the ground and excited states of coumarins 102, 152, 153, and 343. *Journal of Physical Chemistry A*, 106:12117–12123, 2002.

[75] Roberto Improta, Vincenzo Barone, Giovanni Scalmani, and Michael J. Frisch. A state-specific polarizable continuum model time dependent density functional theory method for excited state calculations in solution. *Journal of Chemical Physics*, 125(5):054103, 2006.

[76] A. Mühlpfordt, R. Schanz, N. P. Ernsting, V. Farztdinov, and S. Grimme. Coumarin 153 in the gas phase: Optical spectra and quantum chemical calculations. *Physical Chemistry Chemical Physics*, 1:3209–3218, 1999.

[77] Y. Kurashige, T. Nakajima, S. Kurashige, K. Hirao, and Y. Nishikitani. Theoretical investigation of the excited states of coumarin dyes for dye-sensitized solar cells. *Journal of Physical Chemistry A*, 111:5544–5548, 2007.

[78] B. O'Regan and M. Grätzel. A low-cost, high-efficiency solar cell based on dye-sensitized colloidal tio$_2$ films. *Nature*, 353:737–740, 1991.

[79] Carlo Adamo and Vincenzo Barone. Toward reliable density functional methods without adjustable parameters: The PBE0 model. *Journal of Chemical Physics*, 110(13):6158–6170, 1999.

[80] P. C. Hariharan and J. A. Pople. The influence of polarization functions on molecular orbital hydrogenation energies. *Theoretica Chimica Acta*, 28(3):213–222, 1973.

[81] Michelle M. Francl, William J. Pietro, Warren J. Hehre, J. Stephen Binkley, Mark S. Gordon, Douglas J. DeFrees, and John A. Pople. Self-consistent molecular orbital methods. XXIII. A polarization-type basis set for second-row elements. *Journal of Chemical Physics*, 77(7):3654–3665, 1982.

[82] D. Jacquemin, A. Planchat, C. Adamo, and B. Mennucci. Td-dft assessment of functionals for optical 0-0 transitions in solvated dyes. *Journal of Chemical Theory and Computation*, 8:2359–2372, 2012.

[83] R. Improta, V. Barone, and F. Santoro. Ab initio calculations of absorption spectra of large molecules in solution: Coumarin 153. *Angewandte Chemie*, 119:409–412, 2007.

[84] Wendy D. Cornell, Piotr Cieplak, Christopher I. Bayly, Ian R. Gould, Kenneth M. Merz, David M. Ferguson, David C. Spellmeyer, Thomas Fox, James W. Caldwell, and Peter A. Kollman. A Second Generation Force Field for the Simulation of Proteins, Nucleic Acids, and Organic Molecules. *Journal of the American Chemical Society*, 117(19):5179–5197, 1995.

[85] J. M. Wang, P. Cieplak, and P. A. Kollman. How well does a restrained electrostatic potential (resp) model perform in calculating conformational energies of organic and biological molecules? *Journal of Computational Chemistry*, 21:1049–1074, 2000.

[86] V. Hornak, R. Abel, A. Okur, B. Strockbine, A. Roitberg, and C. Simmerling. Comparison of multiple amber force field and development of improved protein backbone parameters. *Proteins*, 65:712–725, 2006.

[87] Adam Bruner, Daniel LaMaster, and Kenneth Lopata. Accelerated Broadband Spectra Using Transition Dipole Decomposition and Padé Approximants. *Journal of Chemical Theory and Computation*, 12(8):3741–3750, 2016.

[88] Joshua J. Goings, David B. Lingerfelt, and Xiaosong Li. Can quantized vibrational effects be obtained from Ehrenfest mixed quantum-classical dynamics? *Journal of Physical Chemistry Letters*, 7(24):5193–5197, 2016.

[89] Franco Egidi, Shichao Sun, Joshua J. Goings, Giovanni Scalmani, Michael J. Frisch, and Xiaosong Li. Two-component non-collinear time-dependent spin density functional

theory for excited state calculations. *Journal of Chemical Theory and Computation*, 13(6):2591–2603, 2017.

[90] S. Caprasecca, C. Curutchet, S. Juronovich, and B. Mennucci. Polchat: A polarisation-consistent charge fitting tool. Molecolab Tools. 2014-2017 molecolab.dcci.unipi.it/tools.

[91] M. J. Frisch, G. W. Trucks, H. B. Schlegel, G. E. Scuseria, M. A. Robb, J. R. Cheeseman, G. Scalmani, V. Barone, G. A. Petersson, H. Nakatsuji, X. Li, M. Caricato, A. V. Marenich, J. Bloino, B. G. Janesko, R. Gomperts, B. Mennucci, H. P. Hratchian, J. V. Ortiz, A. F. Izmaylov, J. L. Sonnenberg, D. Williams-Young, F. Ding, F. Lipparini, F. Egidi, J. Goings, B. Peng, A. Petrone, T. Henderson, D. Ranasinghe, V. G. Zakrzewski, J. Gao, N. Rega, G. Zheng, W. Liang, M. Hada, M. Ehara, K. Toyota, R. Fukuda, J. Hasegawa, M. Ishida, T. Nakajima, Y. Honda, O. Kitao, H. Nakai, T. Vreven, K. Throssell, J. A. Montgomery, Jr., J. E. Peralta, F. Ogliaro, M. J. Bearpark, J. J. Heyd, E. N. Brothers, K. N. Kudin, V. N. Staroverov, T. A. Keith, R. Kobayashi, J. Normand, K. Raghavachari, A. P. Rendell, J. C. Burant, S. S. Iyengar, J. Tomasi, M. Cossi, J. M. Millam, M. Klene, C. Adamo, R. Cammi, J. W. Ochterski, R. L. Martin, K. Morokuma, O. Farkas, J. B. Foresman, and D. J. Fox. Gaussian Development Version Revision I.10++. Gaussian Inc., Wallingford CT 2016.

[92] Takeshi Yanai, David P Tew, and Nicholas C Handy. A New Hybrid Exchange–Correlation Functional Using the Coulomb-Attenuating Method (CAM-B3lyp). *Chemical Physics Letters*, 393(1):51–57, 2004.

[93] Riccardo Guareschi, Omar Valsson, Carles Curutchet, Benedetta Mennucci, and Claudia Filippi. Electrostatic Versus Resonance Interactions in Photoreceptor Proteins: The Case of Rhodopsin. *Journal of Physical Chemistry Letters*, 7(22):4547–4553, 2016.

[94] Dario Polli, Piero Altoé, Oliver Weingart, Katelyn M. Spillane, Cristian Manzoni, Daniele Brida, Gaia Tomasello, Giorgio Orlandi, Philipp Kukura, Richard A. Mathies,

Marco Garavelli, and Giulio Cerullo. Conical Intersection Dynamics of the Primary Photoisomerization Event in Vision. *Nature*, 467(7314):440–443, 2010.

[95] Judy E. Kim, Michael J. Tauber, and Richard A. Mathies. Wavelength Dependent Cis-Trans Isomerization in Vision. *Biochemistry*, 40(46):13774–13778, 2001.

[96] Remedios González-Luque, Marco Garavelli, Fernando Bernardi, Manuela Merchán, Michael A. Robb, and Massimo Olivucci. Computational Evidence in Favor of a Two-State, Two-Mode Model of the Retinal Chromophore Photoisomerization. *Proceedings of the National Academy of Sciences*, 97(17):9379–9384, 2000.

[97] Luis Manuel Frutos, Tadeusz Andruniów, Fabrizio Santoro, Nicolas Ferré, and Massimo Olivucci. Tracking the Excited-State Time Evolution of the Visual Pigment with Multiconfigurational Quantum Chemistry. *Proceedings of the National Academy of Sciences*, 104(19):7764–7769, 2007.

[98] R. Cammi, S. Corni, B. Mennucci, and J. Tomasi. Electronic excitation energies of molecules in solution: State specific and linear response methods for nonequilibrium continuum solvation models. *Journal of Chemical Physics*, 122(10):104513, 2005.

[99] S. Corni, R. Cammi, B. Mennucci, and J. Tomasi. Electronic excitation energies of molecules in solution within continuum solvation models: Investigating the discrepancy between state-specific and linear-response methods. *Journal of Chemical Physics*, 123(13):134512, 2005.

[100] Bernd Lunkenheimer and Andreas Köhn. Solvent effects on electronically excited states using the conductor-like screening model and the second-order correlated method adc(2). *Journal of Chemical Theory and Computation*, 9(2):977–994, 2013.

[101] Tobias Schwabe. General theory for environmental effects on (vertical) electronic excitation energies. *Journal of Chemical Physics*, 145(15):154105, 2016.

[102] Marco Caricato, Benedetta Mennucci, and Jacopo Tomasi. Solvent Polarity Scales Revisited: a ZINDO-PCM Study of the Solvatochromism of Betaine-30. *Molecular Physics*, 104(5-7):875–887, 2006.

[103] Aleksandr V. Marenich, Christopher J. Cramer, Donald G. Truhlar, Ciro A. Guido, Benedetta Mennucci, Giovanni Scalmani, and Michael J. Frisch. Practical computation of electronic excitation in solution: Vertical excitation model. 2:2143–2161, 2011.

[104] Arieh Warshel. Multiscale Modeling of Biological Functions: From Enzymes to Molecular Machines (Nobel Lecture). *Angewandte Chemie*, 53(38):10020–10031, 2014.

[105] Elizabeth Brunk and Ursula Rothlisberger. Mixed Quantum Mechanical/Molecular Mechanical Molecular Dynamics Simulations of Biological Systems in Ground and Electronically Excited States. *Chemical Reviews*, 115(12):6217–6263, 2015.

[106] Eliot Boulanger and Jeremy N Harvey. QM/MM Methods for Free Energies and Photochemistry. *Current Opinions in Structural Biology*, 49:72–76, 2018.

[107] Mark S Gordon, Dmitri G Fedorov, Spencer R Pruitt, and Lyudmila V Slipchenko. Fragmentation Methods: A Route to Accurate Calculations on Large Systems. *Chemical Reviews*, 112(1):632–672, 2012.

[108] Jiali Gao, Donald G Truhlar, Yingjie Wang, Michael J M Mazack, Patrick Löffler, Makenzie R Provorse, and Pavel Rehak. Explicit Polarization: A Quantum Mechanical Framework for Developing Next Generation Force Fields. *Accounts of Chemical Research*, 47(9):2837–2845, 2014.

[109] Christian B Nielsen, Ove Christiansen, Kurt V Mikkelsen, and Jacob Kongsted. Density Functional Self-Consistent Quantum Mechanics/Molecular Mechanics Theory for Linear and Nonlinear Molecular Properties: Applications to Solvated Water and Formaldehyde. *Journal of Chemical Physics*, 126(15):154112–18, 2007.

[110] Jacek Dziedzic, Yuezhi Mao, Yihan Shao, Jay Ponder, Teresa Head-Gordon, Martin Head-Gordon, and Chris-Kriton Skylaris. TINKTEP: A Fully Self-Consistent, Mutually Polarizable QM/MM Approach Based on the AMOEBA Force Field. *Journal of Chemical Physics*, 145(12):124106–19, 2016.

[111] Xiaojing Wu, Jean-Marie Teuler, Fabien Cailliez, Carine Clavaguéra, Dennis R Salahub, and Aurélien de la Lande. Simulating electron dynamics in polarizable environments. *Journal of Chemical Theory and Computation*, 13(9):3985–4002, 2017.

[112] Jógvan Magnus Olsen, Kestutis Aidas, and Jacob Kongsted. Excited States in Solution through Polarizable Embedding. *Journal of Chemical Theory and Computation*, 6(12):3721–3734, 2010.

[113] Quansong Li, Benedetta Mennucci, Michael A Robb, Lluís Blancafort, and Carles Curutchet. Polarizable QM/MM Multiconfiguration Self-Consistent Field Approach with State-Specific Corrections: Environment Effects on Cytosine Absorption Spectrum. *Journal of Chemical Theory and Computation*, 11(4):1674–1682, 2015.

[114] Riccardo Guareschi, Omar Valsson, Carles Curutchet, Benedetta Mennucci, and Claudia Filippi. Electrostatic versus Resonance Interactions in Photoreceptor Proteins: The Case of Rhodopsin. *Journal of Physical Chemistry Letters*, 7(22):4547–4553, 2016.

[115] Daniele Loco, Francesco Buda, Johan Lugtenburg, and Benedetta Mennucci. The Dynamic Origin of Color Tuning in Proteins Revealed by a Carotenoid Pigment. *Journal of Physical Chemistry Letters*, 9:2404–2410, 2018.

[116] Morten S Nørby, Olav Vahtras, Patrick Norman, and Jacob Kongsted. Assessing frequency-dependent site polarisabilities in linear response polarisable embedding. *Molecular Physics*, 115(1-2):39–47, 2017.

[117] Oliviero Andreussi, Stefano Corni, Benedetta Mennucci, and Jacopo Tomasi. Radiative

and Nonradiative Decay Rates of a Molecule Close to a Metal Particle of Complex Shape. *Journal of Chemical Physics*, 121(20):10190–13, 2004.

[118] Sinisa Vukovic, Stefano Corni, and Benedetta Mennucci. Fluorescence Enhancement of Chromophores Close to Metal Nanoparticles. Optimal Setup Revealed by the Polarizable Continuum Model. *Journal of Physical Chemistry C*, 113(1):121–133, 2009.

[119] Hanning Chen, Jeffrey M McMahon, Mark A Ratner, and George C Schatz. Classical Electrodynamics Coupled to Quantum Mechanics for Calculation of Molecular Optical Properties: a RT-TDDFT/FDTD Approach. *Journal of Physical Chemistry C*, 114(34):14384–14392, 2010.

[120] S. M. Morton, D. W. Silverstein, and L. Jensen. Theoretical studies of plasmonics using electronic structure methods. *Chemical Reviews*, 111:3962–3994, 2011.

[121] Rubén Esteban, Andrei G Borisov, Peter Nordlander, and Javier Aizpurua. Bridging Quantum and Classical Plasmonics with a Quantum-Corrected Model. *Nature Chemistry*, 3:825, 2012.

[122] Liang-Yan Hsu, Wendu Ding, and George C Schatz. Plasmon-Coupled Resonance Energy Transfer. *Journal of Physical Chemistry Letters*, 8(10):2357–2367, 2017.

[123] Ignat Harczuk, Olav Vahtras, and Hans Ågren. Frequency-dependent force fields for qmmm calculations. *Physical Chemistry Chemical Physics*, 17(12):7800–7812, 2015.

[124] A. Mayer, Ph Lambin, and P-O Åstrand. An electrostatic interaction model for frequency-dependent polarizability: Methodology and applications to hydrocarbons and fullerenes. *Nanotechnology*, 19(2):025203, 2007.

[125] Greta Donati, Andrew Wildman, Stefano Caprasecca, David B. Lingerfelt, Filippo Lipparini, Benedetta Mennucci, and Xiaosong Li. Coupling real-time time-dependent density functional theory with polarizable force field. *Journal of Physical Chemistry Letters*, 8(21):5283–5289, 2017.

[126] Laurence D. Barron. *Molecular Light Scattering and Optical Activity*. Cambridge University Press, 2004.

[127] John David Jackson. *Classical Electrodynamics*. John Wiley & Sons, 1975.

[128] Marco Caricato, Francesca Ingrosso, Benedetta Mennucci, and Jacopo Tomasi. A time-dependent polarizable continuum model: Theory and application. *Journal of Chemical Physics*, 122(15):154501, 2005.

[129] John R Taylor. *Classical Mechanics*. University Science Books, 2005.

[130] Christine M. Isborn and Xiaosong Li. Modeling the doubly excited state with time-dependent hartree–fock and density functional theories. *Journal of Chemical Physics*, 129(20):204107, 2008.

[131] Bruce W. Shore. *The Theory of Coherent Atomic Excitation*. John Wiley & Sons, 1990.

[132] Phu Nguyen, Feizhi Ding, Sean A. Fischer, Wenkel Liang, and Xiaosong Li. Solvated first-principles excited state charge transfer dynamics with time-dependent polarizable continuum model and solvent dielectric relaxation. *Journal of Physical Chemistry Letters*, 3:2898–2904, 2012.

[133] Vadim M Farztdinov, Roland Schanz, Sergey A Kovalenko, and Nikolaus P Ernsting. Relaxation of optically excited p-nitroaniline: Semiempirical quantum-chemical calculations compared to femtosecond experimental results. *The Journal of Physical Chemistry A*, 104(49):11486–11496, 2000.

[134] S.A. Kovalenko, R. Schanz, V.M. Farztdinov, H. Hennig, and N.P. Ernsting. Femtosecond relaxation of photoexcited para-nitroaniline: Solvation, charge transfer, internal conversion and cooling. *Chemical Physics Letters*, 323(3-4):312–322, 2000.

[135] Leandro Martínez, Ricardo Andrade, Ernesto G Birgin, and José Mario Martínez. Packmol: A package for building initial configurations for molecular dynamics simulations. *Journal of Computational Chemistry*, 30(13):2157–2164, 2009.

[136] Chengteh Lee, Weitao Yang, and Robert G Parr. Development of the colle-salvetti correlation-energy formula into a functional of the electron density. *Physical Review B*, 37(2):785, 1988.

[137] A. D. Becke. Density-functional thermochemistry. iii. the role of exact exchange. *Journal of Chemical Physics*, 98:5648, 1993.

[138] Anthony K Rappé, Carla J Casewit, KS Colwell, William A Goddard III, and WM Skiff. UFF, a full periodic table force field for molecular mechanics and molecular dynamics simulations. *Journal of the American Chemical Society*, 114(25):10024–10035, 1992.

[139] J. W. Negele. The mean-field theory of nuclear structure and dynamics. *Reviews of Modern Physics*, 54:913, 1982.

[140] Xiaosong Li, John C. Tully, H. Bernhard Schlegel, and Michael J. Frisch. Ab initio Ehrenfest dynamics. *Journal of Chemical Physics*, 123(8):084106, 2005.

[141] Feizhi Ding, Joshua J. Goings, Hongbin Liu, David B. Lingerfelt, and Xiaosong Li. Ab initio two-component Ehrenfest dynamics. *Journal of Chemical Physics*, 143:114105, 2015.

[142] X. Andrade, A. Castro, D. Zueco, J. L. Alonso, P. Echenique, F. Falceto, and Á. Rubio. Modified ehrenfest formalism for efficient large-scale ab initio molecular dynamics. *Journal of Chemical Theory and Computation*, 5:728–742, 2009.

[143] J. C. Tully. Trajectory surface hopping approach to nonadiabatic molecular collisions: The reaction of h+ with d_2. *Journal of Chemical Physics*, 55:562, 1971.

[144] J. C. Tully. Molecular dynamics with electronic transitions. *Journal of Chemical Physics*, 93:1061, 1990.

[145] S. Hammes-Schiffer and J. C. Tully. Proton transfer in solution: Molecular dynamics with quantum transitions. *Journal of Chemical Physics*, 101:4657, 1994.

[146] Joseph E. Subotnik, Amber Jain, Brian Landry, Andrew Petit, Wenjun Ouyang, and Nicole Bellonzi. Understanding the surface hopping view of electronic transitions and decoherence. *Annual Review of Physical Chemistry*, 67:387–417, 2016.

[147] L. Wang, A. Akimov, and O. V. Prezhdo. Recent progresses in surface hopping: 2011-2015. *Journal of Physical Chemistry Letters*, 7:2100–2112, 2016.

[148] M. Ben-Nun, J. Quenneville, and T. J. Martínez. Ab initio multiple spawning: Photochemistry from first principles quantum molecular dynamics. *Journal of Physical Chemistry A*, 104(22):5161–5175, 2000.

[149] B. F. E. Curchod and T. J. Martínez. Ab initio nonadiabatic quantum molecular dynamics. *Chemical Reviews*, 118:3305–3336, 2018.

[150] B. Mignolet and B. F. E. Curchod. Excited-state molecular dynamics triggered by light pulses-*Ab Initio* multiple spawning vs trajectory surface hopping. *Journal of Physical Chemistry A*, 123:3582–3591, 2019.

[151] B. Mignolet and B. F. E. Curchod. A walk through the approximations of *ab initio* multiple spawning. *Journal of Chemical Physics*, 148:134110, 2018.

[152] M. H. Beck, A. Jäckle, G. A. Worth, and H.-D. Meyer. The multiconfiguration time-dependent hartree (MCTDH) method: A highly efficient algorithm for propagating wavepackets. *Physical Review*, 324:1–105, 2000.

[153] H. Wang and M. Thoss. Multilayer formulation of the multiconfiguration time-dependent hartree theory. *Journal of Chemical Physics*, 119:1289, 2003.

[154] E. J. Heller. Time-dependent approach to semiclassical dynamics. *Journal of Chemical Physics*, 62:1544, 1975.

[155] E. J. Heller. Guided gaussian wave packets. *Accounts of Chemical Research*, 39:127–134, 2006.

[156] My Hang V. Huynh and Thomas J. Meyer. Proton-coupled electron transfer. *Chemical Reviews*, 107:5004–5064, 2007.

[157] Sharon Hammes-Schiffer. Proton-coupled electron transfer: Moving together and charging forward. *Journal of the American Chemical Society*, 137:8860–8871, 2015.

[158] Hiroyuki Tamura, Miquel Huix-Rotllant, Irene Burghardt, Yoann Olivier, and David Beljonne. First-principle quantum dynamics of singlet fission: Coherent versus thermally activated mechanisms governed by molecular π stacking. *Physical Review Letters*, 115:107401, 2015.

[159] K. Miyata, Y. Kurashige, K. Watanabe, T. Sugimoto, S. Takahashi, S. Tanaka, J. Takeya, T. Yanai, and Y. Matsumoto. Coherent singlet fission activated by symmetry breaking. *Nature Chemistry*, 9:983–989, 2017.

[160] Peter L. Walters and Nancy Makri. Quantum-classical path integral simulation of ferrocene-ferrocenium charge transfer in liquid hexane. *Journal of Physical Chemistry Letters*, 6:4959–4965, 2015.

[161] M. Vacher, M. J. Bearpark, M. A. Robb, and J. Pedro Malhado. Electron dynamics upon ionization of polyatomic molecules: Coupling to quantum nuclear motion and decoherence morgane. *Physical Review Letters*, 118:083001, 2017.

[162] Qian Wang and K. Domen. Particulate photocatalysts for light-driven water splitting: Mechanisms, challenges, and design strategies. *Chemical Reviews*, Article ASAP, 2019.

[163] Gregory D. Scholes, Graham R. Fleming, Alexandra Olaya-Castro, and Rienk van Grondelle. Lessons from nature about solar light harvesting. *Nature Chemistry*, 3:763–774, 2011.

[164] H. Seo, A. L. Falk, P. V. Klimov, K. C. Miao, G. Galli, and D. D. Awschalom. Quantum decoherence dynamics of divacancy spins in silicon carbide. 7:12935, 2016.

[165] Simon P. Webb, Tzvetelin Iordanov, and Sharon Hammes-Schiffer. Multiconfigurational nuclear-electronic orbital approach: Incorporation of nuclear quantum effects in electronic structure calculations. *Journal of Chemical Physics*, 117:4106, 2002.

[166] Michael V. Pak and Sharon Hammes-Schiffer. Electron-proton correlation for hydrogen tunneling systems. *Physical Review Letters*, 92:103002, 2004.

[167] Chet Swalina, Michael V. Pak, Arindam Chakraborty, , and Sharon Hammes-Schiffer. Explicit dynamical electron-proton correlation in the nuclear-electronic orbital framework. *Journal of Physical Chemistry A*, 110:9983–9987, 2006.

[168] Arindam Chakraborty, Michael V. Pak, and Sharon Hammes-Schiffer. Development of electron-proton density functionals for multicomponent density functional theory. *Physical Review Letters*, 101:153001, 2008.

[169] Yang Yang, Kurt R. Brorsen, Tanner Culpitt, Michael V. Pak, and Sharon Hammes-Schiffer. Development of a practical multicomponent density functional for electron-proton correlation to produce accurate proton densities. *Journal of Chemical Physics*, 147:114113, 2017.

[170] Kurt R. Brorsen, Yang Yang, and Sharon Hammes-Schiffer. Multicomponent density functional theory: Impact of nuclear quantum effects on proton affinities and geometries. *Journal of Physical Chemistry Letters*, 8:3488–3493, 2017.

[171] C. Swalina, M. V. Pak, and S. Hammes-Schiffer. Alternative formulation of many-body perturbation theory for electron-proton correlation. *Chemical Physics Letters*, 404:394–399, 2005.

[172] Fabijan Pavošević, Tanner Culpitt, and Sharon Hammes-Schiffer. Multicomponent coupled cluster singles and doubles theory within the nuclear-electronic orbital framework. *Journal of Chemical Theory and Computation*, 15:338–347, 2019.

[173] Fabijan Pavošević and Sharon Hammes-Schiffer. Multicomponent equation-of-motion coupled cluster singles and doubles: Theory and calculation of excitation energies for positronium hydride. *Journal of Chemical Physics*, 150:161102, 2019.

[174] Yang Yang, Tanner Culpitt, and Sharon Hammes-Schiffer. Multicomponent time-dependent density functional theory: Proton and electron excitation energies. *Journal of Physical Chemistry Letters*, 9:1765–1770, 2018.

[175] Xiaosong Li, John M. Millam, Gustavo E. Scuseria, Michael J. Frisch, and H. Bernhard Schlegel. Density matrix search using direct inversion in the iterative subspace as a linear scaling alternative to diagonalization in electronic structure calculations. *Journal of Chemical Physics*, 119:7651, 2003.

[176] D. B. Williams-Young, A. Petrone, S. Sun, T. F. Stetina, P. Lestrange, C. E. Hoyer, D. R. Nascimento, L. Koulias, A. Wildman, J. Kasper, and *et al.* The chronus quantum software package. e1436, 2019.

[177] Yihan Shao, Zhengting Gan, Evgeny Epifanovsky, Andrew T.B. Gilbert, Michael Wormit, Joerg Kussmann, Adrian W. Lange, Andrew Behn, Jia Deng, Xintian Feng, and *et al.* Advances in molecular quantum chemistry contained in the q-chem 4 program package. *Molecular Physics*, 113(2):184–215, 2015.

[178] C. Lee, W. Yang, and R. G. Parr. Development of the colle-salvetti correlation-energy formula into a functional of the electron density. *Physical Review B*, 37(2):785, 1988.

[179] A. D. Becke. Density-functional exchange-energy approximation with correct asymptotic behavior. *Physical Review A*, 38(6):3098, 1988.

[180] Axel D. Becke. A New Inhomogeneity Parameter in Density-Functional Theory. *Journal of Chemical Physics*, 109(6):2092, 1998.

[181] Xiaosong Li and John C. Tully. Ab initio time-resolved density functional theory for lifetimes of excited adsorbate states at metal surfaces. *Chemical Physics Letters*, 439(1-3):199–203, 2007.

[182] Tanner Culpitt, Yang Yang, Fabijan Pavošević, Zhen Tao, and Sharon Hammes-Schiffer. Enhancing the applicability of multicomponent time-dependent density functional theory. *Journal of Chemical Physics*, 150(20):201101, 2019.

[183] S. Scheiner. Theoretical studies of excited state proton transfer in small model systems. *Journal of Physical Chemistry A*, 104:5898–5909, 2000.

[184] A. J. A. Aquino, H. Lischka, and C. Hättig. Excited-state intramolecular proton transfer: A survey of tddft and ri-cc2 excited-state potential energy surfaces. *Journal of Physical Chemistry A*, 109:3201–3208, 2005.

[185] S. Lochbrunner, T. Schultz, M. Schmitt, J. P. Shaffer, M. Z. Zgierski, and A. Stolow. Dynamics of excited-state proton transfer systems via time-resolved photoelectron spectroscopy. *Journal of Chemical Physics*, 114:2519, 2001.

[186] Sharon Hammes-Schiffer and Alexander V Soudackov. Proton-coupled electron transfer in solution, proteins, and electrochemistry. *Journal of Physical Chemistry B*, 112(45):14108–14123, 2008.

[187] Sean A. Fischer, Craig T. Chapman, and Xiaosong Li. Surface hopping with Ehrenfest excited potential. *Journal of Chemical Physics*, 135(14):144102, 2011.

[188] L. Zhao, Z. Tao, F. Pavošević, A. Wildman, S. Hammes-Schiffer, and X. Li. Real-time time-dependent nuclear-electronic orbital approach: Dynamics beyond the born-oppenheimer approximation. *Journal of Physical Chemistry Letters*, 11:4052–4058.

[189] F. Pavošević, Z. Tao, T. Culpitt, L. Zhao, X. Li, and S. Hammes-Schiffer. Frenquency and time domain nuclear-electronic orbital equation-of-motion coupled cluster methods: Combination bands and electronic-protonic double excitations. *Journal of Physical Chemistry Letters*, 11:6435–6442, 2020.

[190] F. Pavošević, T. Culpitt, and S. Hammes-Schiffer. Multicomponent quantum chemistry: Integrating electronic and nuclear quantum effects via the nuclear-electronic orbital method. *Chemical Reviews*, 120:4222–4253, 2020.

[191] Xiaosong Li, Niranjan Govind, Christine Isborn, A. Eugene DePrince, and Kenneth Lopata. Real-time time-dependent electronic structure theory. *Chemical Reviews*, 120(18):9951–9993, 2020.

[192] Benedetta Mennucci and Roberto Cammi. *Continuum Solvation Models in Chemical Physics: from Theory to Applications*. John Wiley & Sons, 2008.

[193] Benedetta Mennucci. Polarizable continuum model. *Wiley Interdisciplinary Reviews: Computational Molecular Science*, 2(3):386–404, 2012.

[194] Wenkel Liang, Craig T. Chapman, Feizhi Ding, and Xiaosong Li. Modeling ultrafast solvated electronic dynamics using time-dependent density functional theory and polarizable continuum model. *Journal of Physical Chemistry A*, 116(8):1884–1890, 2012.

[195] Stefano Corni, Silvio Pipolo, and Roberto Cammi. Equation of motion for the solvent polarization apparent charges in the polarizable continuum model: Application to real-time tddft. *Journal of Physical Chemistry A*, 119(21):5405–5416, 2015.

[196] Xiaosong Li, David Williams-Young, Edward F. Valeev, Alessio Petrone, Shichao Sun, Torin Stetina, and Joesph Kasper. Chronus quantum, beta 2 version, 2018. http://www.chronusquantum.org.

[197] David B Williams-Young, Alessio Petrone, Shichao Sun, Torin F Stetina, Patrick Lestrange, Chad E Hoyer, Daniel R Nascimento, Lauren Koulias, Andrew Wildman, Joseph Kasper, Joshua J. Goings, Feizhi Ding, A. Eugene DePrince III, Edward F. Valeev, and Xiaosong Li. The chronus quantum (chronusq) software package. *Wiley Interdisciplinary Reviews: Computational Molecular Science*, page e1436, 2019.

[198] Thom H. Dunning. Gaussian basis sets for use in correlated molecular calculations. I. the atoms boron through neon and hydrogen. *Journal of Chemical Physics*, 90:1007, 1988.

[199] `PCMSolver`, an open-source library for the polarizable continuum model electrostatic problem, written by R. Di Remigio, L. Frediani and contributors (see http://pcmsolver.readthedocs.io/).

[200] Sebastião J Formosinho and Luís G Arnaut. Excited-state proton transfer reactions ii. intramolecular reactions. *Journal of Photochemistry and Photobiology*, 75(1):21–48, 1993.